



Evaluation Techniques for Determining the Reflectivity, Specularity, and Figure of Solar Mirrors

J. W. Griffin
M. A. Lind
L. D. Philipp

Pacific Northwest Laboratory
Richland, Washington

Prepared under Subcontract No. XP-9-8366-1
for the



SERI

Solar Energy Research Institute

A Division of Midwest Research Institute

1617 Cole Boulevard
Golden, Colorado 80401

Operated for the
U.S. Department of Energy
under Contract No. EG-77-C-01-4042

Printed in the United States of America
Available from:

National Technical Information Service
U.S. Department of Commerce

5285 Port Royal Road
Springfield, VA 22161

Price:

Microfiche \$3.00

Printed Copy \$6.50

NOTICE

This report was prepared as an account of work sponsored by the United States Government. Neither the United States nor the United States Department of Energy, nor any of their employees, nor any of their contractors, subcontractors, or their employees, makes any warranty, express or implied, or assumes any legal liability or responsibility for the accuracy, completeness or usefulness of any information, apparatus, product or process disclosed, or represents that its use would not infringe privately owned rights.

SERI/TR-98366-1
UC CATEGORY: UC-62

EVALUATION TECHNIQUES FOR DETERMINING
THE REFLECTIVITY, SPECULARITY
AND FIGURE OF SOLAR MIRRORS

J. W. GRIFFIN
M. A. LIND
L. D. PHILIPP

PACIFIC NORTHWEST LABORATORY
RICHLAND, WASHINGTON

APRIL 1980

PREPARED UNDER SUBCONTRACT
NO. XP-9-8366-1

FOR THE
Solar Energy Research Institute

A Division of Midwest Research Institute

1617 Cole Boulevard
Golden, Colorado 80401

Prepared for the
U.S. Department of Energy
Contract No. EG-77-C-01-4042

SERI TECHNICAL MONITOR:
P. A. ROBERTS


PREFACE

This report is intended as a primer for those persons interested in the optical evaluation of heliostat mirrors. A cursory review of the current options for measuring the reflectance, specularity and figure of mirrors is presented. The extension of both traditional and novel optical laboratory techniques to field applications is also discussed.

The authors conclude that while the presently available techniques are invaluable for laboratory testing of moderately sized optical components, they offer no immediate solution to the problem of quality assessment of large solar optics. This is due to the difficulty in altering the techniques to accommodate large optics either because of physical limitation or financial constraints. In general, the spatial resolution capabilities of the available techniques are either too stringent (i.e., interferometry) or too coarse for meaningful results. However, it is felt that eventually viable techniques will evolve based directly or indirectly on concepts presented in this document.



P. A. Roberts, Technical Monitor
Solar Energy Research Institute



M. A. Lind, Principal Investigator
Pacific Northwest Laboratory

CONTENTS

	<u>Page</u>
PREFACE	iii
LIST OF FIGURES.	vii
LIST OF TABLES	ix
I. INTRODUCTION	1
Objectives of Report	1
Solar Power Systems	2
Point-Focus Distributed-Receiver Systems	2
Point-Focus Central-Receiver System	2
Fixed-Mirror Distributed-Focus System	2
Line-Focus Distributed-Receiver Tracking-Collector System	3
Line-Focus Distributed-Receiver Tracking-Receiver System	3
Line-Focus Central-Receiver System	3
Low Concentration Nontracking System	3
Reflectors for Solar Power Systems	4
Quality Evaluation Parameters for Heliostat Mirrors	5
II. TECHNIQUES FOR EVALUATION OF MIRROR PARAMETERS	9
Transmittance and Reflectance	9
Definition	10
Theory	11
Techniques for Solar Transmittance and Reflectance Evaluation	13
Laboratory Measurements	13
Portable Reflectometers for Measurement of Hemispherical Solar Reflectivity	17
Portable Reflectometer for Measurement of Specular Solar Reflectivity	19
Specularity	21
Definition	21

CONTENTS (Cont'd.)

	<u>Page</u>
Theory of Optical Transfer Function and Modulation	
Transfer Function Techniques	22
Techniques for Specularity Evaluation	24
Fourier Transform Method	24
Bi-Directional Reflectometer Technique	28
Beam Characterization System (BCS)	30
Image Characterization System	37
Extension of Specularity Assessment Techniques	40
Figure	41
Definition	42
Techniques of Figure Error Evaluation	43
Laser Ray Trace	43
Moiré Fringe Analysis	51
Image Evaluation	55
Schlieren Method	58
Mechanical Techniques	58
Optical Profilometer	61
Beam Characterization System	71
Interferometry	67
<i>Newton Interferometer</i>	67
<i>Multiple Beam Interferometers</i>	71
<i>Holographic Interferometry</i>	76
<i>Speckle Techniques</i>	81
Extension of Figure Assessment Techniques	86
III. CONCLUSIONS	89
IV. RECOMMENDATIONS	93
REFERENCES	95

LIST OF FIGURES

<u>Figure</u>	<u>Page</u>
1. Typical Reflector Construction and Scattering Parameters	5
2. Characteristics of the Three Main Categories of Solar Reflector Materials	6
3. Dual Beam Spectrophotometers	14
4. Mirror Configuration in the Reference Position and Mirror Configuration in the Sample Position	15
5. Bi-Directional Reflectometer	16
6. Schematic of Willey Alpha Meter Reflectometer	18
7. Schematic Diagram of Portable Reflectometer	20
8. Planar Imaging System	22
9. Fourier Transform Specularity Analysis Apparatus and Mathematical Representation of Fourier Transform System	25
10. Practical Integral Fourier Transform System	27
11. Bi-Directional Reflectometer Instrument for Measuring Specularity	29
12. Bi-Directional Reflectometer Incorporating Spherical Mirror Optics	31
13. Reflectometer for Specularity Evaluation of Stretched Membrane Reflectors	32
14. Beam Characterization System	34
15. Electronic System for Forward Gazing BCS	35
16. Pointing Accuracy Mode of BCS	36
17. Image Characterization System	38
18. Electronic Evaluation System for ICS	39
19. Laser Ray Trace Instrument for Glass Flatness Measurements	44

LIST OF FIGURES (Cont'd.)

	<u>Page</u>
20. Laser Ray Trace Instrument for Analysis of Parabolic Surfaces	45
21. Illustration of Slope and Sag Error	46
22. Laser Ray Trace Apparatus for Measurement of Slope and Sag Errors in Parabolic Concentrators	47
23. Geometry for Sag Error Calculation	49
24. Optical Inspection System for Evaluation of Figure Error in Large Parabolic Mirror Facets	50
25. Containment Contour for Focal Spots Generated by Three Large Parabolic Facets	51
26. Experimental Arrangement for Specular Surface Contour Generation by the Oblique Shadow Method	53
27. Moiré Fringe Apparatus for Generation of Surface Contour on Diffusely Reflecting Objects	54
28. Experimental Arrangement for Mirror Figure Analysis by Image Evaluation	56
29. Image Evaluation Technique Utilizing Collimated Illumination	57
30. Schlieren System for Evaluation of Mirror Figure and Specularity	59
31. Spherometer for Measuring Surface Curvature of Spherical Mirrors	60
32. Fiber-Optic Proximity Gauges	62
33. Calibration Curves for Fiber-Optic and Fiber-Optic/Lens Proximity Gauges	62
34. Scanning Optical Profilometer	64
35. Optical Triangulation Profilometer (Spatial Detection Method)	65
36. Optical Triangulation Profilometer (Temporal Detection Method)	66
37. Optical Arrangement for Observation of Newton Fringes	68
38. Fringe Formation Due to Wedge Air Gap Between Optical Flats	68

LIST OF FIGURES (Cont'd.)

	<u>Page</u>
39. Fringes Formed by Air Gap Between Spherical Surface and Optical Flat	69
40. Configuration of Newton's Fringes for Various Test Surface Geometries	70
41. Twyman-Green Interferometer	72
42. Analysis of Glass Plate with Twyman-Green Interferometer	72
43. Laser Illuminated Fizeau Interferometer	74
44. Modification of Fizeau Interferometer for Analysis of Phase Objects	74
45. Sheared Wavefront Geometry	76
46. Parallel Plate Interferometer for Evaluation of Concave Mirrors	77
47. Parallel Plate Interferometer for Evaluation of Phase Objects	77
48. Interferogram Produced by a Wavefront Exhibiting Primary Spherical Aberration	78
49. Modified Twyman-Green Interferometer for Holographic Evaluation of Concave Mirrors	78
50. Foucault Knife Edge Test for Evaluation of Holographically Reconstructed Wavefront	79
51. Interferometric Evaluation of Holographically Reconstructed Wavefront	80
52. Experimental Arrangement for Production of Real-Time Holographic Interferograms	80
53. Experimental Arrangement for Study of Speckle Distribution in Image Planes of a Plano-Convex Lens	82
54. Speckle Patterns in the Paraxial, Marginal, Least Confusion, and Defocused Planes for Three Diffuser Spot Sizes	83
55. Experimental Configuration for Mirror Figure Evaluation by Speckle Photography	85

LIST OF TABLES

<u>Table</u>	<u>Page</u>
1. Typical Values for Transmission and Reflection Coefficients of Uncoated Optical Materials	12
2. Solar Reflectance Values for Glass to Metal and Air to Metal Interfaces	13
3. Contour Intervals for Given Grating Pitches and Illumination Incidence Angle	55

I. INTRODUCTION

The rapid appearance of prototype solar and solar hybrid power plant designs has resulted in an urgent need for a figure of merit for reflector performance. While techniques exist for characterization of mirror reflectance, methods for evaluating specularly (scatter due to microstructure nonuniformity and figure (slope error) are not clearly defined. Consequently, comparisons of mirror facets rely heavily on qualitative judgment rather than quantitative measurements.

In an effort to alleviate this dilemma, a study was undertaken to collect and develop mirror evaluation techniques and if possible to quantify previously qualitative tests. Mirror specularly and figure were considered the most desirable mirror performance parameters to quantify since transmittance and reflectance are readily adapted from routine laboratory procedures. While specularly is also readily determined in the optics laboratory, extension of the techniques to solar mirror facet characterization in the field is not straightforward. It also appears that mirror figure evaluation will require relatively innovative approaches due to the lack of quantization of this parameter in the past.

The evaluation of transmittance, reflectance, specularly, and figure for heliostat quality assurance may well require three discrete procedures. However, candidate techniques which measure two or more parameters simultaneously (or with slight modifications, consecutively) may be most desirable from the point of view of the economics of cost and time.

A. Objectives of Report

The objectives of this report are twofold: 1) to collect and report mirror evaluation techniques relevant to the determination of reflectivity, specularly and figure parameters for heliostat mirror facets, and 2) to evaluate and report on the applicability and feasibility of these techniques to the heliostat mirror quality assurance problem.

This report is not intended to be an exhaustive compendium of optical shop methods since in many cases these techniques are impracticable for

evaluation of large surface elements of relatively poor optical quality. More exhaustive accounts of described mirror evaluation techniques are to be found in the noted references.

B. Solar Power Systems

The overall design configuration of the solar power facility will usually determine the constraints on reflector quality. For this reason an overview of some of the solar facility concepts and operating configurations is presented in order to illustrate the diversity of the mirror configuration and bring the mirror characterization problem into perspective. For a detailed and varied summary of the options for small power systems applications, the reader is referred to Laity, 1978.

a. Point-Focus Distributed-Receiver Systems. The point-focus distributed-receiver system is composed of a field of parabolic dish collectors, each equipped with its own receiver. The parabolic concentrators are fabricated from curved reflective gore elements or plane mirror facets. Concentrator focal lengths range from 5 to 15 m with diameters of 10 to 20 m (45°-90° included rim angle). Either a Stirling or Brayton cycle heat engine may be mounted on each receiver, or the receiver may be used to generate steam for a Rankine cycle power plant centrally located within the collector field.

b. Point-Focus Central-Receiver System. In the point-focus central-receiver system, incident solar energy is reflected from a field of heliostats to a tower mounted receiver. The heliostat facets are planar or near planar with lateral dimensions ranging from 5 to 15 feet. The effective focal length is temperature dependent and may range from 30 m to ∞ (flat). The 5 MW test facility at Albuquerque and the proposed 10 MWe Barstow power plant are of this configuration.

c. Fixed-Mirror Distributed-Focus System. In the fixed-mirror distributed-focus system, a large stationary fixed focus spherical mirror focuses incident solar energy on a cone-shaped receiver. Array diameter may vary from 10 to 100 m with effective focal lengths of 10 to 50 m. The working fluid (water/steam) is pumped through the receiver and absorbs the incident solar

energy. The thermal energy is transferred to a turbine-generator system via an insulated piping network. The receiver is boom mounted on a dual axis mount to allow tracking of the sun's motion.

d. Line-Focus Distributed-Receiver Tracking-Collector System. In the line-focus distributed-receiver tracking-collector system, the collector field is composed of parabolic troughs each equipped with its own receiver through which the heat transfer fluid is pumped to absorb incident solar thermal energy. Trough segments may vary from 1 to 5 m in length with widths from 0.5 to 2 m. Focal lengths range from 0.5 to 2 m (approximately 90° rim angle). The collectors track on one axis.

e. Line-Focus Distributed-Receiver Tracking-Receiver System. In the line-focus distributed-receiver tracking-receiver system the collector field is composed of fixed troughs each producing a sharp line focus. Reflector elements are similar to those described above for the line-focus distributed-receiver tracking-collector system. The receiver intercepts and tracks this line focus via circular arc translation. A heat transfer fluid is pumped through the receiver to absorb the incident energy.

f. Line-Focus Central-Receiver System. In the line-focus central-receiver configuration a field of tracking parabolic trough collectors mounted in parallel rows focus incident solar energy on a centrally located, tower mounted, line receiver. While the reflector trough segments have similar dimensions as those described for the two previous systems, the effective focal lengths are much longer (i.e., less surface curvature) to allow radiation concentration onto an extended receiver.

g. Low Concentration Nontracking System. The low concentration non-tracking configuration utilizes low concentration collectors (such as the CPC or V-trough) interfaced with vacuum tube receivers to heat an organic working fluid to approximately 450°F. The organic liquid is routed via insulated pipelines to supply thermal energy for a Rankine-cycle power plant.

The above examples illustrate the complexities of the heliostat evaluation problem. First, the spatial dimensions of the reflective elements generally exceed sizes which would prove amenable to conventional optical testing

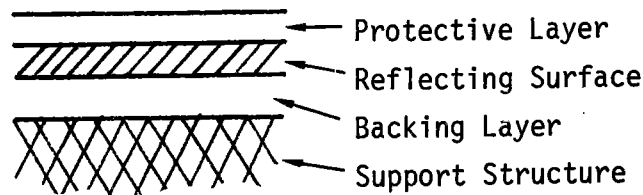
techniques. Secondly, the range of reflector figure ($0.5 \text{ m} \leq \text{focal length} \leq \infty$) dictates the use of a variety of test configurations (e.g., mirror gore evaluation for point focus distributed receiver applications will almost certainly demand a different evaluation method than that utilized for nearly flat ($200 \text{ m} \leq \text{focal length} \leq \infty$) facets to be implemented in point focus central receiver systems). Finally, the optical evaluation techniques proposed for heliostat mirror analysis should be field applicable. Field evaluation is generally a severe constraint for conventional optical testing. Innovative schemes will probably be necessary to evaluate the optical quality of these solar mirrors.

C. Reflectors for Solar Power Systems (Pettit, 1978)

The parameters relevant to solar mirror quality are largely determined by the techniques and materials utilized in their construction. Consequently, each construction component will either enhance or degrade mirror performance depending on its compatibility with the overall mirror design.

A practical solar reflector may consist of multiple sandwiched layers: typically, an outer protective layer, the reflecting surface, a backing protective layer, and a support substrate which maintains the mirror figure. Each of these layers will influence the overall optical performance of the mirror. These effects are summarized in Figure 1.

Present solar reflector materials can be grouped into three main categories; silvered glass (second surface), metallized plastic films and polished sheet aluminum. The performance characteristics and production considerations of these three categories are summarized in Figure 2. Each class of materials has its own advantages and disadvantages. Actual materials selection for a given heliostat field is usually determined by cost-performance trade-off. Thus the lower performance materials may be viable if their cost is low enough. The key to implementing the trade-off study is an accurate determination of the optical performance of the material, not only initially, but as a function of environmental exposure.



Protective Layer:

- Absorption in the material
- Specularity losses from scattering caused by processing limitations
- Figure limitations caused by surface undulations and parallelism

Reflecting Surface:

- Hemispherical reflectance of the layer
- Scattering due to surface roughness

Backing Layer:

- Scattering losses due to surface roughness
- Figure losses due to the lamination techniques

Support Structure:

- Figure imperfections

FIGURE 1. Typical Reflector Construction and Optical Considerations

D. Quality Evaluation Parameters for Heliostat Mirrors

The primary concern of heliostat quality assurance is maximization of the solar radiant energy density at the power system collectors. The problem is to determine the fraction of incident energy that may be actually directed onto the receiver surface for a given solar irradiance distribution. This requires that a relation be established between the spatial and spectral power distribution of the reflected flux and the spatial and spectral distribution of the incident solar flux.

SILVERED GLASS

REFLECTANCE

- Evaporated, Chem. Deposited Silver:
 $R_s \approx 95-97\%$
- Absorption in Glass (Fe^{+2} @ 1 micron)
 - Low iron glass
 - Thin glass
 - Control oxidation state of $Fe(Fe^{+3})$

SPECULARITY

- Typically $\sigma \leq 0.5$ mrad
- Index Variation (Composition)
- Thickness Variations
- Surface Slope Errors
 - Sheet, Float, Fusion

ENVIRONMENTAL

- Good Abrasion Resistance
- UV Resistance
- Silver Adhesion; Edge Protection
- Corrosion (Moisture Plus Dirt)

METALLIZED PLASTIC FILMS

- Vacuum Deposited Ag ($R_s \approx 95\%$) Al ($R_s \approx 88\%$)
- Absorption in IR (≤ 1 micron)

- Surface Texture Metallized Surface
- Scattering Within Film
- Laminating Parameters (adhesive, substrate)
Obtained $\sigma \leq 1.0$ mrad (3M FEK - 163)

- Poor Abrasion Resistance
- Possible UV Degradation
- Moisture Penetration
- Static Charge

POLISHED ALUMINUM SHEET

- Typical of Aluminum: $R_s(2\pi) \approx 85\%$
- Anodized Protection Film

- Surface Roughness (Polishing Technique)
- Anodized Film
- Orientation Dependence
- 5-15% loss at 17 mrad

- Good Abrasion Resistance
- Good UV Stability

FIGURE 2. Characteristics of the Three Main Categories of Solar Reflector Materials (Pettit, 1978)

One obvious solution to this problem is to construct a prototype heliostat and measure the spatial and spectral composition of the radiation directed into a simulated receiver aperture. An overall figure of merit for the heliostat could then be determined. Although this approach may be a viable option, it is encumbered by practical cost limitations. A more realistic scenario is to measure in the laboratory the relevant optical parameters for reflector components. These parameters could then be used to calculate the integrated performance of a mirror surface. One set of parameters that could be used is spectral hemispherical transmittance and/or reflectance, specularity, and mirror figure.

The spectral hemispherical transmittance and reflectance should be specified in the wavelength range of primary solar irradiance (300-3000 nm). When weighted by the terrestrial solar spectral irradiance distribution (TSSID) at a particular geographic location and time, these parameters provide an indication of the maximum performance to be expected from the mirror.

Specularity is a measure of the angular spread or divergence of an existing beam resulting when an incident collimated beam is either transmitted through or reflected from a material. Specularity is generally a weak function of wavelength and incident angle. The scattering distribution may be unfolded or deconvoluted to produce information on the microstructure smoothness of the reflecting surface. The specularity parameter provides the heliostat designer with an established relationship between maximum theoretical solar flux at the receiver aperture and that which can actually be attained for a reflector with perfect geometry.

Mirror figure usually requires prototype heliostat mockup for evaluation. Mirror figure error refers to the deviation of the mirror surface geometry from that desired. As macrostructure surface inhomogeneities and mechanical stability play an important role in integral heliostat performance, the figure of the mirror should be measured under actual dynamic operating conditions including thermal variation, wind loading, and orientation.

II. TECHNIQUES FOR EVALUATION OF MIRROR PARAMETERS

The ensuing discussion is an overview of mirror evaluation techniques deemed to be applicable to the heliostat characterization problem. While the techniques discussed have for the most part proven successful primarily in laboratory environments they may also be adaptable for field use.

At a large solar power installation (e.g., a central-receiver distributed-collector facility) a knowledge of the optical condition of each concentrator or reflector is desirable. Transmittance, reflectance, specularity, and figure would be desirable information for each point on the reflector surface. Ideally, these parameters would be ascertained by an inspection system which does not contact the reflector surface and the gathered data would be stored for comparison with previous or theoretical values. If feasible, the inspection system should be capable of real-time analysis so that the effect of active wind loading, dust accumulation, etc., could be observed and monitored. This would allow plant operators near real time feedback for cleaning or replacement scenarios for individual heliostat facets.

These are ambitious goals that probably circumvent the reality of time, manpower and fiscal constraints. While these limitations will probably dictate practical solutions, the intent of this report is to generate a "shopping list" of optical evaluation alternatives which provide reasonable satisfaction of the stated goals and to suggest areas which could provide solutions.

A. Transmittance and Reflectance

The accurate determination of transmittance and reflectance of candidate superstrates for heliostat mirrors is necessary prior to consideration of the material for usage. These parameters are time- and environment-dependent. Techniques for evaluation of reflectance of second surface mirrors indirectly measure superstrate absorption although results are still reported as "percent reflection". Likewise transmittance measurements are not necessarily a true indicator of glass absorption since reflections and scattering are present at the sample boundaries. To alleviate these ambiguities, the following definition has been adopted.

1. Definition

Transmittance is defined as the ratio of light flux transmitted through a material to the total incident flux. The transmittance value may refer to specular or diffuse transmittance and in general varies with angle of incidence and wavelength of the light. Reflectance (also termed reflection coefficient or reflectivity) is the ratio of the light flux reflected from a surface to the total incident flux and generally exhibits wavelength and angular dependence.

Transmittance and reflectivity measurements may take two forms: hemispherical and specular. In hemispherical transmittance measurements all transmitted energy in the hemisphere, defined by the rear sample normal (2π), is collected and compared with the incident intensity. In hemispherical reflectance measurements, all light energy reflected into the hemisphere, defined by the front surface normal, is collected for the ratio determination. In specular transmittance or reflectance measurements only the light flux transmitted or reflected into a predetermined solid angle ($\Delta\Omega$) is admitted by the detector aperture and recorded. This solid angle is sometimes user definable depending on the instrumentation and measurement technique, but usually subtends an angle between 10 and 25 milliradians.

Reflectance and transmittance measurements performed on solar materials are often solar weighted. Solar weighting has its basis in the wavelength dependence of the TSSID. This wavelength dependence has been experimentally determined by many experimenters, but the commonly utilized ones are those of Moon (1940) and NASA.^(a)

The solar weighted value for a wavelength dependent variable, $Z(\lambda)$, (e.g., transmittance or reflectance) is denoted as Z' and is defined as

$$Z' = \frac{\int_{\lambda_1}^{\lambda_2} Z(\lambda) G(\lambda) d\lambda}{\int_{\lambda_1}^{\lambda_2} G(\lambda) d\lambda} \quad (1)$$

(a) "Terrestrial Photovoltaic Measurement Procedures," ERDA/NASA/1022-77/16, NASA TM 73702.

where $G(\lambda)$ is the solar irradiance value at λ . For the discrete case

$$Z' = \frac{\sum_i Z_i(\lambda) A_i(\lambda)}{\sum_i A_i(\lambda)} \quad (2)$$

where $A_i(\lambda)$ is the area under the solar insolation segment utilized for weighting the experimental data point at λ , and i denotes the segment number. The solar weighted parameter is then termed the solar transmittance or solar reflectance. For details on the implications of selecting a particular TSSID or weighting procedure, the reader is referred to Lind, 1980.

2. Theory

The solar transmittance of an uncoated dielectric material is primarily determined by boundary reflections at the air to glass interfaces and impurity absorption within the material. The air/dielectric boundary condition predicts a first surface reflection given by

$$R_1 = \left(\frac{1-n}{1+n} \right)^2 \quad (3)$$

which for soda lime glass with an index of 1.52 calculates to be 0.0426. If one considers multiple reflections from the first and second surfaces of the dielectric, and atomic/molecular absorption in the volume, the total reflectance for uncoated material is given by

$$R = \frac{R_1 (1 + \chi^2 - 2R_1)}{1 - R_1^2 \chi^2} \quad (4)$$

where χ is the internal transmittance of the sample given by

$$\chi = \exp \left(- \sum_i \alpha_i C_i \ell \right). \quad (5)$$

α_i and C_i are the molar absorptivity and molar concentration of the i^{th} species and ℓ is the sample thickness. Since $T + R = 1$, the transmittance is given by

$$T = \frac{(1-R_1)^2 \chi}{1-R_1^2 \chi^2} \quad (6)$$

As a basis for comparison, calculated values of reflectance and transmittance for nonabsorbing glasses calculated from Equations 4 and 6 appear in Table 1. These values represent the theoretical values achievable without special surface treatment (e.g., coating).

TABLE 1. Typical Values for Transmission and Reflection Coefficients of Uncoated Optical Materials

	<u>Fused Silica</u>	<u>Soda Lime</u>	<u>Quartz</u>
n	1.4600	1.5200	1.5500
R ₁	0.0350	0.0426	0.0465
R	0.0676	0.0817	0.0889
T	0.9324	0.9183	0.9111

For the case of second surface mirrors where the back surface has a metallic film coating, the reflectance is given by

$$R = \frac{R_1 + \chi^2 R_m - 2R_1 \chi^2 R_m}{1 - \chi^2 R_m R_1} \quad (7)$$

where R_m is the glass to metal interface reflectance which is either calculable from the complex dielectric functions for the base metals or measurable in the laboratory. Calculated solar weighted values of R_m (Pettit, 1978) for three metals appear in Table 2. The reflectance of the base metal is included for comparison. Note that the base metal reflectance exceeds the glass to metal interface reflectance by several percent.

Insertion of the appropriate values into Equation 7 indicates that the maximum theoretical values of second surface mirror reflectance for nonabsorbing glass differ only slightly from those of the glass to metal interface.

TABLE 2. Solar Reflectance Values for Glass to Metal and Air to Metal Interfaces

<u>Metal</u>	<u>Reflectance Metal to Air</u>	<u>Reflectance Metal to Glass</u>
Ag	0.98	0.97
Al	0.92	0.88
Au	0.85	0.82

3. Techniques for Solar Transmittance and Reflectance Evaluation

The following discussion is a survey of existing techniques for the evaluation and monitoring of heliostat mirror solar transmittance and reflectance. In all probability instrumentation and techniques utilized for field measurement of these parameters will be based upon these laboratory methods.

a. Laboratory Measurements. The most common laboratory instrument for the measurement of transmittance is the dual beam spectrophotometer schematically depicted in Figure 3. Samples cut to appropriate size are placed in the sample beam and generally the reference beam is left unobstructed (air reference) for specular transmittance measurements. Most dual beam instruments may also be modified to measure specular reflectance.

Hemispherical transmittance and reflectance measurements utilizing spectrophotometers require the use of an integrating sphere to collect the scattered radiation over 2π steradians. In the case of transmittance measurements, the unaltered reference beam and the attenuated sample beam illuminate separate barium sulfate or Halon reference surfaces which scatter the incident light into the integrating sphere. The resulting diffuse illumination is detected by a photomultiplier or lead sulfide detector depending on the wavelength region of interest. For hemispherical reflectance measurements one of the reference standards is replaced with the reflective surface and the measurement performed as above. This instrumentation is particularly adaptable to computer operation and digital data acquisition. Such a technique facilitates solar weighting of the data.

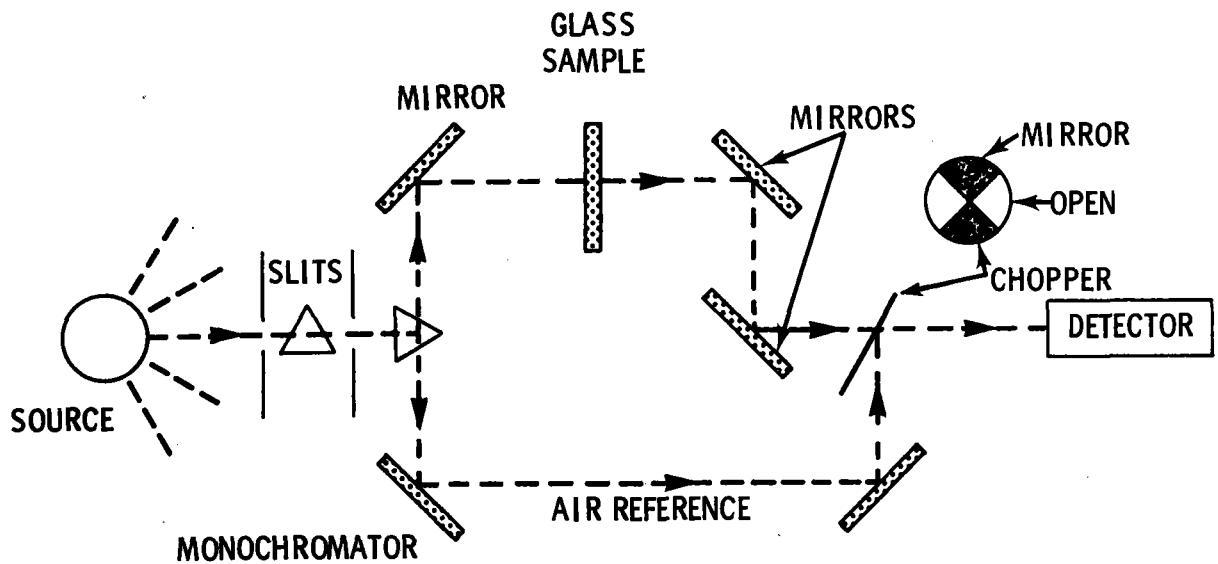


FIGURE 3. Dual Beam Spectrophotometers (Bauer, 1978)

The integrating sphere technique is especially well-suited for measurement of diffuse reflecting surfaces. When specular surfaces are measured special care must be taken to characterize the sphere. Large errors (5%) are possible. To avoid such errors it is desirable to employ a specular reference standard such as is available from NBS.

A direct measurement of the absolute reflectivity of highly specular mirrors is possible using a Strong "V-W" optical accessory available on some spectrophotometers. The optical arrangement is shown in Figure 4. The theory of operation is as follows. Suppose the reflectivity of the three mirrors shown in Figure 4a are M_1 , M_2 and M_3 . The intensity of the output beam I_0 is related to the intensity of the input beam I_i by the relation

$$I_{0r} = I_i M_1 M_3 M_2 \quad (8)$$

Similarly with the same mirrors rearranged as in Figure 4b. The output intensity is

$$I_{0s} = I_i M_1 R M_2 = I_i M_1 M_3 M_2 R^2. \quad (9)$$

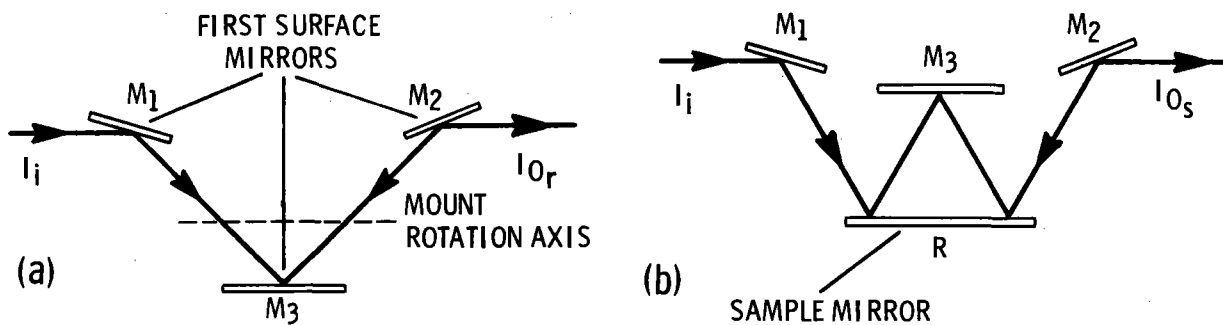


FIGURE 4. Mirror Configuration in the Reference Position (a) and Mirror Configuration in the Sample Position (b)

Assuming the input intensity is the same in both cases a ratio of the two signals yields

$$\frac{I_{0s}}{I_{0r}} = R^2 \text{ or } R = \sqrt{\frac{I_{0s}}{I_{0r}}} \quad (10)$$

which is the absolute reflectivity of the sample under test. Although conceptually easy to understand, the technique is difficult to employ in practice. Alignment and beam divergence are critical factors affecting accuracy.

It is believed that typical laboratory accuracies for specular transmittance and reflectance are on the order of 1% to 5% (Coleman et al., 1977). This accuracy should be compared with the 0.2% obtainable at the National Bureau of Standards for similar measurements. Diffuse hemispherical reflectance is also measured to 0.2% at NBS; however, diffuse transmittance usually cannot be determined more accurately than 5% (Coleman et al., 1977). While many laboratories are capable of 1% measurements (sufficient for the screening of solar materials), such accuracies are not sufficient for short time span definitive aging studies.

Another useful instrument for laboratory measurements of specular reflectance is the bi-directional reflectometer. A schematic of this device appears in Figure 5. The unit consists of a source section composed of a filtered radiation source (tungsten lamp, xenon arc, etc.) with collimating optics, a

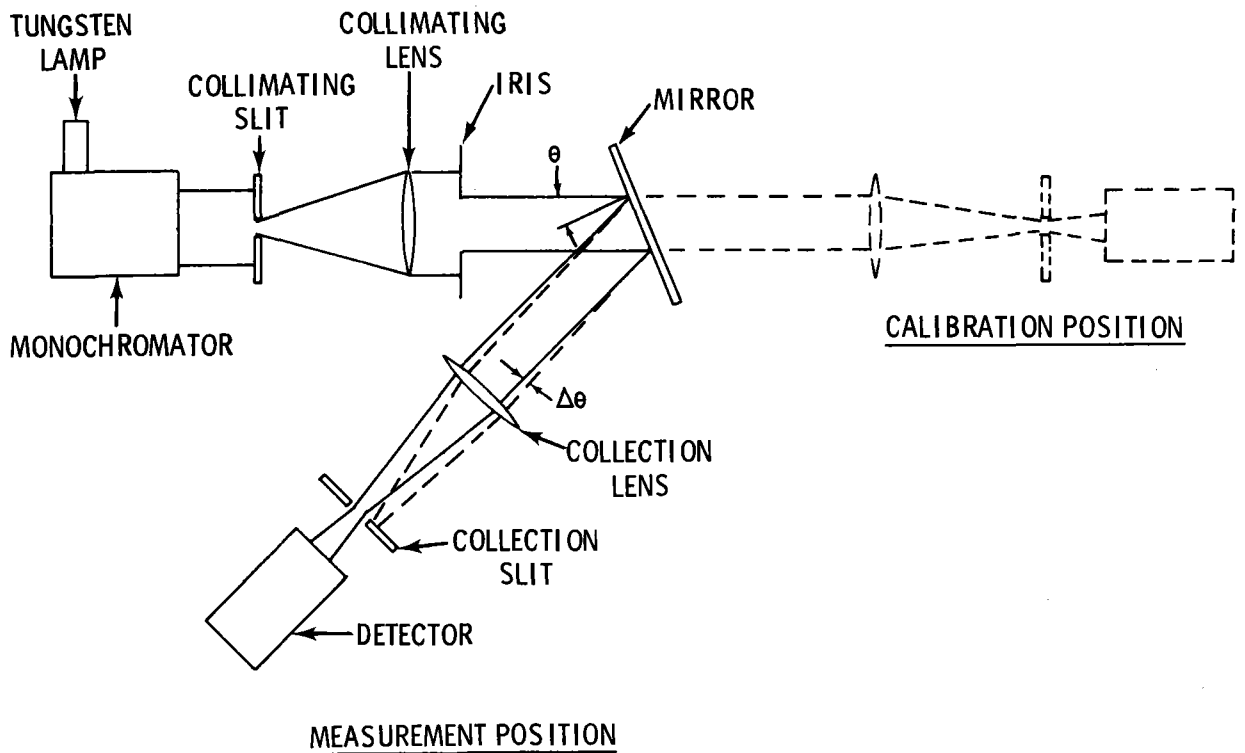


FIGURE 5. Bi-Directional Reflectometer (Pettit, 1977)

sample stage, and a collection section containing focusing optics and the detector. Both source and detector arms are adjustable allowing measurement of the angular dependence of the specular reflectivity. Calibration is accomplished via a standard reflectivity surface or straight-through measurement. The wavelength dependence of the reflectance may be determined by appropriate choice of notch filters in the illumination and collection heads, by coupling the collected light via fiber optics to a monochromator equipped with photomultiplier, or by interposing a monochromator between the continuum source and the collimation optics (Pettit, 1977b).

Although the instruments discussed above are proven for in-laboratory analysis of solar reflector materials, extension of these techniques to the quality assurance of heliostat mirrors presents problems. The most practical limitations are the maximum acceptable sample size, and the fraction of surface

area sampled in the measurement. The above instruments are excellent for samples measuring less than several inches square but will not generally accept larger surfaces. Also the fraction of the area actually sampled is small, necessitating repeated measurements over the sample surface for accurate analysis. (This problem could possibly be alleviated in the bi-directional reflectometer by use of large aperture optics such as spherical and parabolic mirrors, although such an instrument may prove unwieldy).

b. Portable Reflectometers for Measurement of Hemispherical Solar Reflectivity. Two manufacturers of portable solar reflectometers were identified during the course of this investigation. These vendors are Gier Dunkle Instruments Incorporated, Santa Monica, California, and Willey Corporation, Melbourne, Florida.

The Gier Dunkle Solar Reflectometer (Model MS-251) is a portable optical device capable of determining the solar reflectance (or absorptance) of planar, opaque reflectors for normal incidence illumination. To accomplish this, the normal hemispherical reflectance is averaged over the spectral radiance distribution of a filtered xenon lamp source. The xenon lamp spectrum roughly approximates an extraterrestrial solar irradiance spectrum^(a) resulting in a measured reflectance equivalent to an air mass zero (Moon, 1940) solar averaged reflectance.

The Willey Alpha Meter (Model 2150) is a portable optical instrument utilized for determination of normal incidence solar reflectivity (or absorptance) of planar, opaque materials. The reflectometer head is composed of an elliptical radiation collector coated with white reflecting paint, a source imaging lens, a sample measurement port, and a silicon detector. A schematic representation of the device appears in Figure 6. The active detector area (either Si or PbS) is illuminated by the collector wall and is screened from direct reflected sample radiation. The reflectometer light source is a Kodak Carousel projector lamp. Two types of lamps are commonly used; (1) a Sylvania type DFW tungsten coil filament lamp or (2) a GE Quartzline ELH tungsten

(a) "Compact Arc Lamps", Product Bulletin CA0624, Conrad-Hanovia, Inc., Newark, NJ.

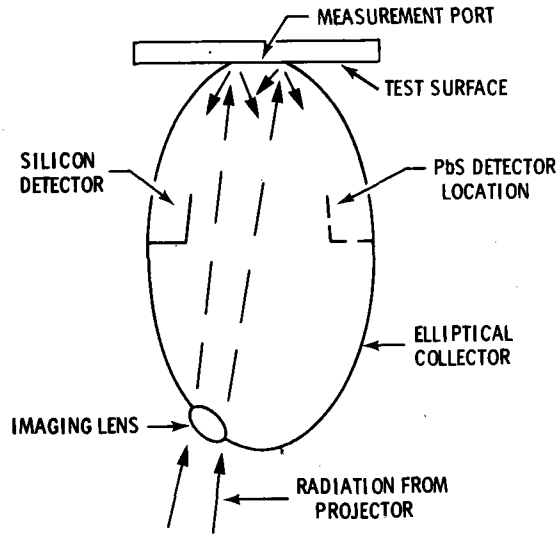


FIGURE 6. Schematic of the Willey Alpha Meter Reflectometer (Pettit, 1977)

halogen lamp mounted in an ellipsoidal reflector. The infrared blocking mirror mounted between the illumination lenses in the projector housing is removed prior to performing measurements. The measurement procedure is similar to that of the Gier Dunkle solar reflectometer. The zero baseline reading I_0 is established with the measurement port uncovered, and the 100 percent reading, I_{100} , with a $MgCO_3$ standard over the port. The fractional reflectivity is then given by

$$R_s = (I_s - I_0) / (I_{100} - I_0) \quad (11)$$

An evaluation of the accuracy of the two instruments has been performed for measurement of solar absorptance by Pettit (1977b). The solar absorptance of black chrome coatings (absorptance range of 0.85 to 0.96) was measured over the wavelength range 350 nm to 2500 nm with a Beckman DK-2A Spectroreflectometer with a stated accuracy of ± 0.01 absorptance units. For the Gier Dunkle Solar Reflectometer the average deviation of the absorptance values was ± 0.013 absorptance units, which is within the measurement accuracy of the data. The maximum deviation from the air mass zero value was 0.03 absorptance

units. The same standard samples were evaluated using the Willey instrument. The absorptance results for both lamps were found to be consistently higher than the correct values. For the ELH lamp the largest error measured was 0.11 absorptance units while the largest error measured for the DFW lamp was 0.08 absorptance units. This anomaly is a result of the limited spectral extent of the two lamps utilized for sample illumination.

The utility of these two instruments for reflectivity evaluation of heliostat mirrors is presently unknown; however, the techniques and optical configurations of these devices could well provide a starting point for design of a prototype specialized instrument. While the instruments at present may prove technically sound, it is suggested that prototype instruments incorporating similar operating principles be developed. Improvement features would include: 1) tailoring of the source spectrum to more closely approximate the air mass 1.5 spectrum; 2) addition of provisions for measuring specular reflectance; 3) increased portability allowing more diversified instrument orientation; 4) provision for allowing narrow spectral bandwidth measurements; and 5) increased sampling area capability.

c. Portable Reflectometer for Measurement of Specular Solar Reflectivity.

Freese (1978) describes the development of a portable specular reflectometer for field measurements of solar mirror materials. The design is based on modification of a conventional laboratory reflectometer.^(a) A schematic of the instrument appears in Figure 7.

The device consists of a conventional reflectometer mounted on a vertical positioning stage, the baseplate of which is fitted with soft felt backing to allow support of the instrument on the surface to be analyzed. The reflectometer section may be tilted about two orthogonal axes. The source arm contains a tungsten filament lamp, filter (350-750 nm passband), focusing lens, source aperture, collimating lens, and beam aperture. Beam divergence is 5.0 mrad. The collection arm is composed of a collection lens, aperture, filter (for attenuation of scattered ambient light), and silicon detector.

(a) "Instrumentation Manual for Gamma Scientific Model 191 Reflectometer," Gamma Scientific Inc., San Diego, CA.

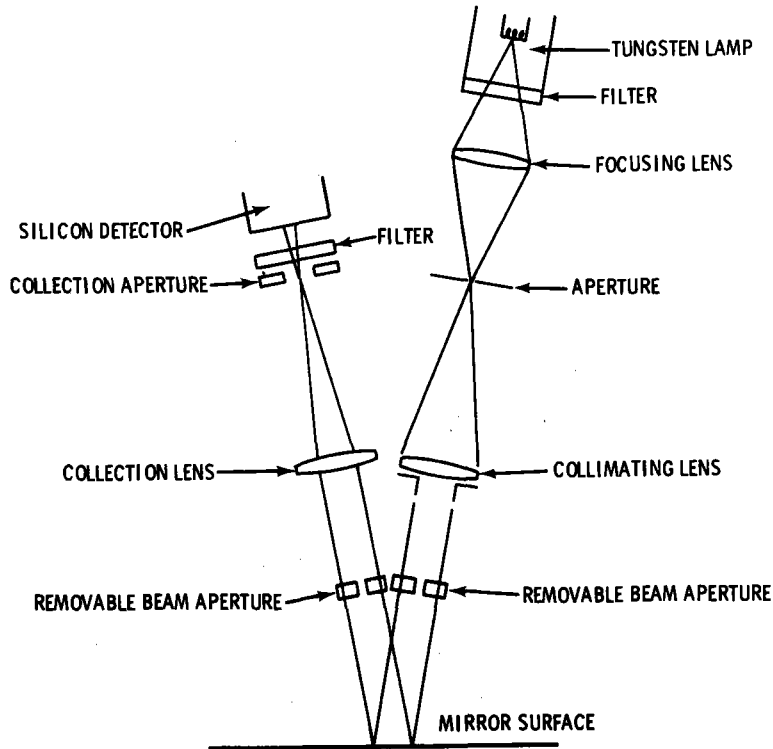


FIGURE 7. Schematic Diagram of Portable Reflectometer (Freese, 1978)

The reflectometer is calibrated with an aluminized quartz flat which has been calibrated by the National Bureau of Standards as having reflectance R_{STD} . The detector output is noted with this mirror in place and the standard replaced with the mirror to be analyzed. The reflectivity of the sample mirror is then given by

$$R_{Sample} = R_{STD} (I_{Sample}/I_{STD}) \quad (12)$$

If discrete wavelength measurements of reflectivity are desired, notch filters of appropriate wavelength could be inserted into both the source and collection arms. The device requires precise alignment and lengthy data acquisition times are required since the sampled area is small.

B. Specularity

In some respects specularity measurement devices are similar to those used to measure specular solar reflectivity. All techniques to be described examine an optical image that has been modified or modulated by the mirror under test. Since the term specularity is usually linked closely with the instrumentation used to make the measurement, it requires careful definition.

1. Definition

If a collimated (i.e., angular beam divergence equal to zero) beam of light is made to fall incident onto a small area of a mirror and upon reflection possesses a beam divergence differing from zero the mirror is said to have specularity error. The distinction is made here between specularity error and figure error (discussed later) on the basis of spatial frequency of the mirror inhomogeneity. Specularity error is a result of relatively high spatial frequency variations in the shape of the reflective surface (<cm dimensions). Specularity error may be due to the manufacturing or extrusion technique, material inclusions (bubbles, dirt, etc.) or mode of metallic layer deposition.

Specularity error produces an angular dependence of reflected beam intensity for a given incidence angle. In the case of commercially available mirror materials detailed experimental analysis has indicated that the angular dependence of the reflected beam profile may be accurately predicted by either a single normal (Gaussian) distribution or the sum of two normal distributions (Pettit et al., 1979). For the case of the single normal distribution two parameters are required to specify the specular reflectance properties; the solar averaged hemispherical reflectance, R_s , and the dispersion σ_R which specifies the angular width of the reflected beam. An expression for the solar averaged reflectance at angle $\Delta\theta$ from the specular direction is then

$$R_s(\Delta\theta) = \frac{R_s}{2\pi\sigma_R^2} e^{-\left(\frac{\Delta\theta^2}{2\sigma_R^2}\right)} \quad (13)$$

(Pettit et al., 1979). The root mean square (RMS) width of the reflected beam is given by $\langle \Delta\theta^2 \rangle^{1/2} = \sqrt{2} \sigma_R$. If it is necessary to describe the reflected beam angular reflectance profile by the sum of two normal distributions, the corresponding relation is

$$R_s(\Delta\theta) = \frac{R_1}{2\pi\sigma_{R_1}^2} e^{-\left(\frac{\Delta\theta^2}{2\sigma_{R_1}^2}\right)} + \frac{R_2}{2\pi\sigma_{R_2}^2} e^{-\left(\frac{\Delta\theta^2}{2\sigma_{R_2}^2}\right)} \quad (14)$$

with the normalization constraint $R_s = (R_1 + R_2)$.

2. Theory - Optical Transfer Function and Modulation Transfer Function Techniques

Consider a planar imaging system as depicted in Figure 8. If $I_0(x,y)$ is the object plane irradiance distribution at point x,y , then the radiant flux emitted by surface element $dx dy$ is $I_0(x,y) dx dy$. Due to diffraction at the lens aperture, aberrations and scattering, the imaged point will not appear as a delta function any longer but will in general display a Gaussian character (actually a Bessel function).

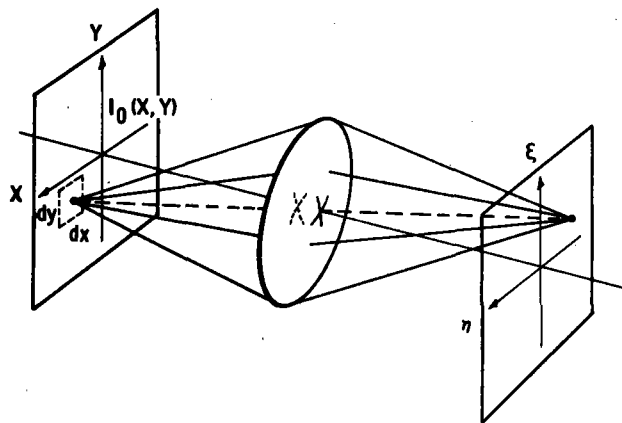


FIGURE 8. Planar Imaging System (Hecht and Zajac, 1974)

This modified radiant flux distribution in the image plane may be mathematically expressed by the point spread function $S(x,y;\epsilon,\eta)$. The flux density at the image point can then be expressed as

$$dI_I(\epsilon,\eta) = S(x,y;\epsilon,\eta)I_0(x,y)dx dy \quad (15)$$

The image intensity may be reconstructed as the sum of the modified object point function in the case of incoherent illumination or

$$I_I(\epsilon,\eta) = \iint_{-\infty}^{\infty} I_0(x,y) S(x,y;\epsilon,\eta)dx dy . \quad (16)$$

For an aberration-free, diffraction-limited optical system $S(x,y;\epsilon,\eta)$ corresponds to the diffraction figure of a point source (Airy disc). The point spread function is also termed the impulse response function since it has the same functional form as that exhibited for a δ -function ($I_0(x,y) = A\delta(x-x_0)\delta(y-y_0)$) input.

In summary, the image can be expressed as the convolution of the point spread function and the object irradiance, i.e.,

$$I_I(\epsilon,\eta) = I_0(x,y) \otimes S(x,y) . \quad (17)$$

The unnormalized optical transfer function (OTF $\equiv T$) is defined as the Fourier transform (F) of the point spread function or

$$T(k_\epsilon, k_\eta) \equiv F \{S(x,y)\} . \quad (18)$$

The optical transfer function may be expressed as the product of two additional functions, i.e.,

$$T(k_\epsilon, k_\eta) = M(k_\epsilon, k_\eta) \exp i\phi(k_\epsilon, k_\eta) \quad (17)$$

where $M(k_\epsilon, k_\eta)$ is termed the unnormalized modulation transfer function and $\phi(k_\epsilon, k_\eta)$ is the phase transfer function.

The concept of the point spread function and the optical transfer function is the basis for several possible techniques for the evaluation of heliostat mirror specularity discussed below.

3. Techniques for Specularity Evaluation

The current techniques for mirror specularity evaluation do not differ appreciably from those used for imaging optics e.g., lenses and spherical or parabolic mirrors. The technique involves the inspection of the image of a precise source target formed by the optical element under test. In the case of plane mirrors the reflective surface is interposed between object and image planes and imaging is performed by auxiliary optical elements. The mirror surface under test is therefore, said to modulate the object function. In the following sections, several techniques are discussed which utilize this concept.

a. Fourier Transform Method. The Fourier transforming characteristic of lenses may be exploited to allow determination of the scattering parameters for optical materials in particular mirrors. Such a technique is described by Lind, et al. (1978). The optical system necessary for Fourier transform specularity analysis appears in Figure 9a. The experimental apparatus consists of a light source, collimation lens (for sample illumination), scattering sample, and collection lens (Fourier transforming lens). The entire system may be schematically represented as in Figure 9b with the notation from Lind, et al. (1978). In this representation $\psi(x,y;s_1)$ is the input wave function, $f(x,y)$ is the aperture function in the P_1 plane, $g(c,d)$ is the reflection/transmission function of the mirror/glass under investigation, P_2 and P_4 are the lens planes, and finally, $h(m,n)$ is the resultant image plane amplitude distribution. For this system $h(m,n)$ is given by

$$h(m,n) = - \lambda^2 f^2 \iint_{P_1} \iint_{P_3} \left\{ \psi(x,y;s_1) f(x,y) \exp \left[-j \frac{k}{f} (xc + yd) \right] \times \right. \\ \left. xg(c,d) \exp \left[-j \frac{k}{f} (cm + dn) \right] dx dy dc dd \right\}. \quad (20)$$

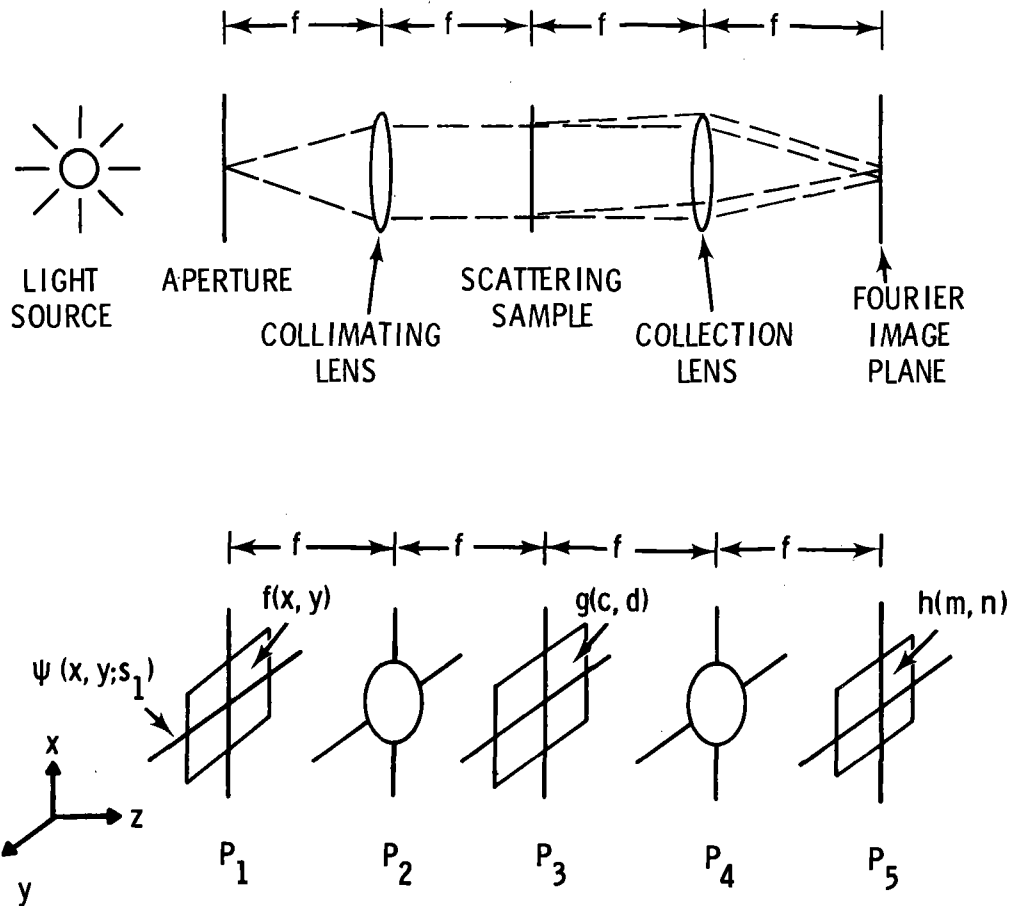


FIGURE 9. (a) Fourier Transform Specularity Analysis Apparatus and (b) Mathematical Representation of Fourier Transform System

If the aperture function can be approximated by a two-dimensional delta (δ) function and the input illumination is a plane wave, the relation simplifies to

$$h(m, n) = K \iint_{P_3} g(c, d) \exp \left[-j \frac{k}{F} (cm + dn) \right] dc dd . \quad (21)$$

For the stated assumptions the amplitude distribution at the image plane is the exact Fourier transform of the reflection/transmission function, $g(c, d)$.

Note that K is a complex constant which equals $\frac{1}{j f \lambda}$ when the separation distances P_3-P_4 and P_4-P_5 equal the focal length of the transforming lens. Calculation of intensities, $h(m,n)xh^*(m,n)$, removes the imaginary nature of the coefficient.

Some general characteristics of the Fourier technique of scattering sample analysis are apparent. One-dimensional (grating type) inhomogeneities in the sample volume are exhibited as linear intensity dispersions about the optical axis in the Fourier plane. Likewise two-dimensional striations manifest themselves as multiple intensity dispersions. Random noise has the effect of lowering contrast of the spatial details in the Fourier plane.

If one realizes that the scattered light displacement, Δr , for a lens of focal length f in the Fourier plane can be expressed as

$$\Delta r \approx f \Delta \theta_{\text{scatter}}, \quad (22)$$

a more quantitative analysis of the specularity of the optical surface is possible. This allows mapping of the angular scattering distribution given the optical geometry and the Fourier intensity distribution.

For more detailed information about the scattering function of the material, several intensity sampling techniques are possible. These are 1) one-dimensional sampling, 2) two-dimensional sampling, and 3) integral sampling.

In one-dimensional sampling, the intensity distribution along a single axis (perpendicular to the optical axis) in the Fourier plane is sampled. Detectors utilized have included small aperture scanning detectors and linear diode arrays (Hampton, et al. 1978). Resolution limit is determined by the aperture size or the dimensions of the array elements. For isotropically scattering materials the technique produces useful results; however, such is not the case for anisotropic scatterers. Detector alignment is important as minute displacement of the detector from the optical axis produces inconsistent data. The principal advantage of the one-dimensional mode is the ease of data manipulation and analysis as compared with a multidimensional technique.

Two-dimensional analysis allows intensity measurements over the entire Fourier plane. A system using two-dimensional detectors is less susceptible to alignment errors and to extraneous scattering caused by anisotropic samples. Detectors which have been used in this experimental configuration include photographic film, a mechanically scanned small aperture detector, conventional raster scan vidicons, and two-dimensional diode arrays. The lengthy processing time required of photographic film eliminates its use in a real-time system; however, the vidicon and diode array allow nearly real-time intensity contour mapping. The advantage of the photographic system however, is the inherent spatial resolution which is large compared to raster devices (limited raster spacing) or array detectors (limited pixel size).

The limited spatial resolution and restricted dynamic range of the above techniques suggests the use of one- and two-dimensional integral methods. A practical two-dimensional system appears in Figure 10. A beam block is utilized to reduce the intensity of the specularly transmitted or reflected beam at the Fourier plane. The beam block also establishes the minimum detectable scattering angle. Maximum detectable scattering angle is established by the phototube diameter, its distance from the Fourier plane and the diameter of the Fourier transform lens. Samples which scatter in the mrad and sub-mrad range may be analyzed with appropriate beam blocks. While quantization and angular scattering distributions are obtainable with this experimental setup, the technique is most suited to the screening of high specularity solar reflectors and substrates.

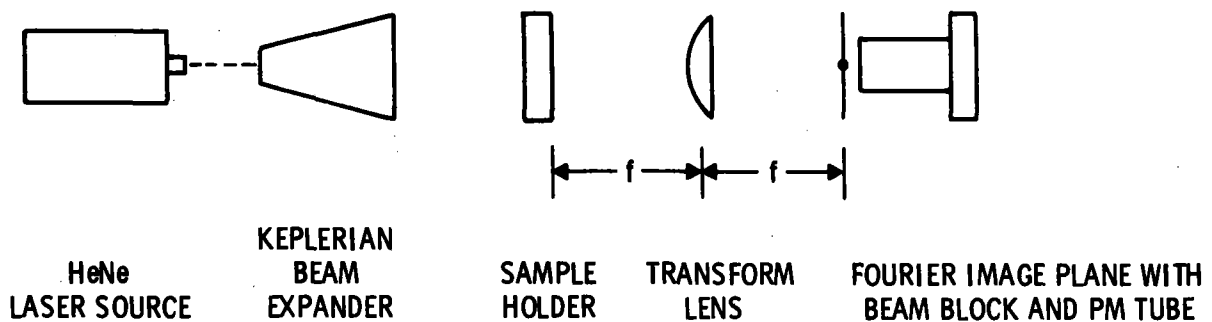


FIGURE 10. Practical Integral Fourier Transform System

The analysis of highly specular optical components with the above systems produces a Fourier transform intensity distribution of low dispersion. That is to say when the test sample inhomogeneities are represented by relatively low spatial frequencies, their Fourier components are difficult to resolve from the diffraction limited illumination spot. Calculations were performed (Lind et al., 1978) to determine the necessary beam block size for elimination of this spot from the detection system. For practical optical systems, 98% of the focused diffraction limited spot can be easily contained within 0.4 mrad.

As a final point, Lind, et al. (1978) state that the optical apparatus is insensitive to misalignment of planar samples (parallel sides) when used for transmission specular measurements. Samples with nonparallel faces will produce off-axis specular components producing an apparent dispersion in the Fourier plane consistent with nonzero spatial frequency inhomogeneities. Therefore care should be exercised in the evaluation of samples with suspected nonparallel faces.

b) Bi-Directional Reflectometer Technique. A variation on the Fourier transform technique utilizing a laboratory bi-directional reflectometer is described by Pettit (1977b). A schematic of the device appears in Figure 11. The collimation optics is composed of a tungsten lamp, monochromator, bilateral slit, collimating lens, and a variable iris diaphragm. Illumination beam divergence is 1.0 mrad perpendicular to the slit length. Divergence parallel to the slit axis is approximately 6 mrad. The collimation optics is rigidly mounted on an arm which rotates about the mirror mounting platform. The collection arm consists of a lens, bilateral slit, and detector. The collecting lens is located so as to image the collimating slit onto the collecting aperture. Since the collection slit is nearly six times the length of the collimation slit image, radiation scattered to an angular deviation of 36 mrad in the longitudinal direction is detected. This consideration is included in the data analysis algorithm.

For equal collimating and collecting slit width and appropriate specular reflection arm position only the specular portion of the reflected illumination is incident on the detector. If the collection slit width is increased,

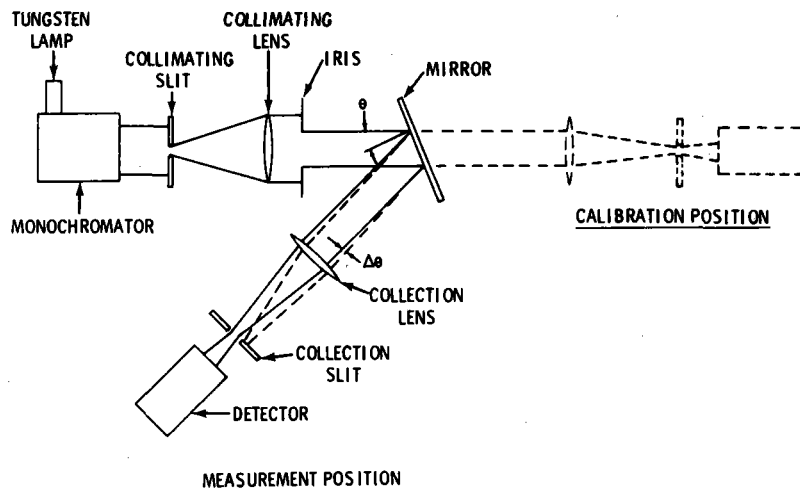


FIGURE 11. Bi-Directional Reflectometer Instrument for Measuring Specularity

portions of the nonspecular component are incident onto the detector surface allowing mapping of the angular distribution of the reflected beam. This is an integral procedure for which the 100% value has been previously established by swinging the collection arm to intercept the undeviated (no sample) illumination beam. The reflected beam intensity distribution may be determined for angular deviations ranging from 1 to 17 mrad. The functional form of the angular scattering distribution is then calculated using the ratio of detector output (at a given slit setting) to the 100% baseline output.

In this system, as in the previously described Fourier transform system, the collection lens (transform lens) must be of sufficient diameter to enable collection of all scattered radiation.

Sources of error include variation of detector response over the collection slit area ($\pm 1\%$) and electronic instability of source and detector electronics ($\pm 0.3\%$). The reported accuracy over a wavelength range of 400-900 nm is $\pm 1.0\%$. Details and justification of the data analysis algorithm appear in Pettit (1977b).

A version of the bi-directional reflectometer which incorporates spherical mirrors has been utilized by Sheldahl Inc. for the analysis of tensional plastic film reflectors.^(a) A schematic of the test apparatus appears in Figure 12. The collimation and imaging optics consist of a pair of matched 4-1/2-inch diameter spherical telescope mirrors. The illumination source is a tungsten ribbon lamp. Diaphragms are utilized to form an annular beam extending from a 0.625-inch radius inner edge to a 1-inch radius outer edge. Specularity determination is accomplished with a variable iris positioned in front of the entrance port of a photodetector equipped integrating sphere. A tabulation of relative beam intensity versus iris diameter provides an indication of the reflected beam divergence. For instrument calibration the detector telescope can be positioned for line-of-sight observation of the source pinhole.

A reflectometer for specularity evaluation of stretched membrane reflectors has been reported by Zeltner (1977). A schematic of the device appears in Figure 13. To establish the incident beam angle the source yoke (composed of M3, lens, and M4) is rotated about its vertical axis. Then the entire source head assembly is rotated about a common axis in order to align the reflected beam with the detector aperture. Rather than utilizing an adjustable iris, the detector acceptance angle is established by a set of fixed diameter entrance apertures. Intensity calibration is performed by direct measurement of the source beam energy. To accomplish this the sample and holder are removed and the source yoke is rotated to 90° incidence. The beam then passes through the source head and is focused into the integrating sphere. This allows establishment of incident beam energy and instrument introduced beam divergence.

c) Beam Characterization System (BCS). A novel approach to the problem of mirror specularity evaluation is the beam characterization system (also called forward gazing system) described by King (1979), and currently under use at the Central Receiver Test Facility (CRTF). A schematic of the configuration appears in Figure 14. The experimental system allows inspection of the

(a) "Solar Power Array for the Concentration of Energy," Sheldahl, Inc., 31 July 1974. Available NTIS, PB-236-247.

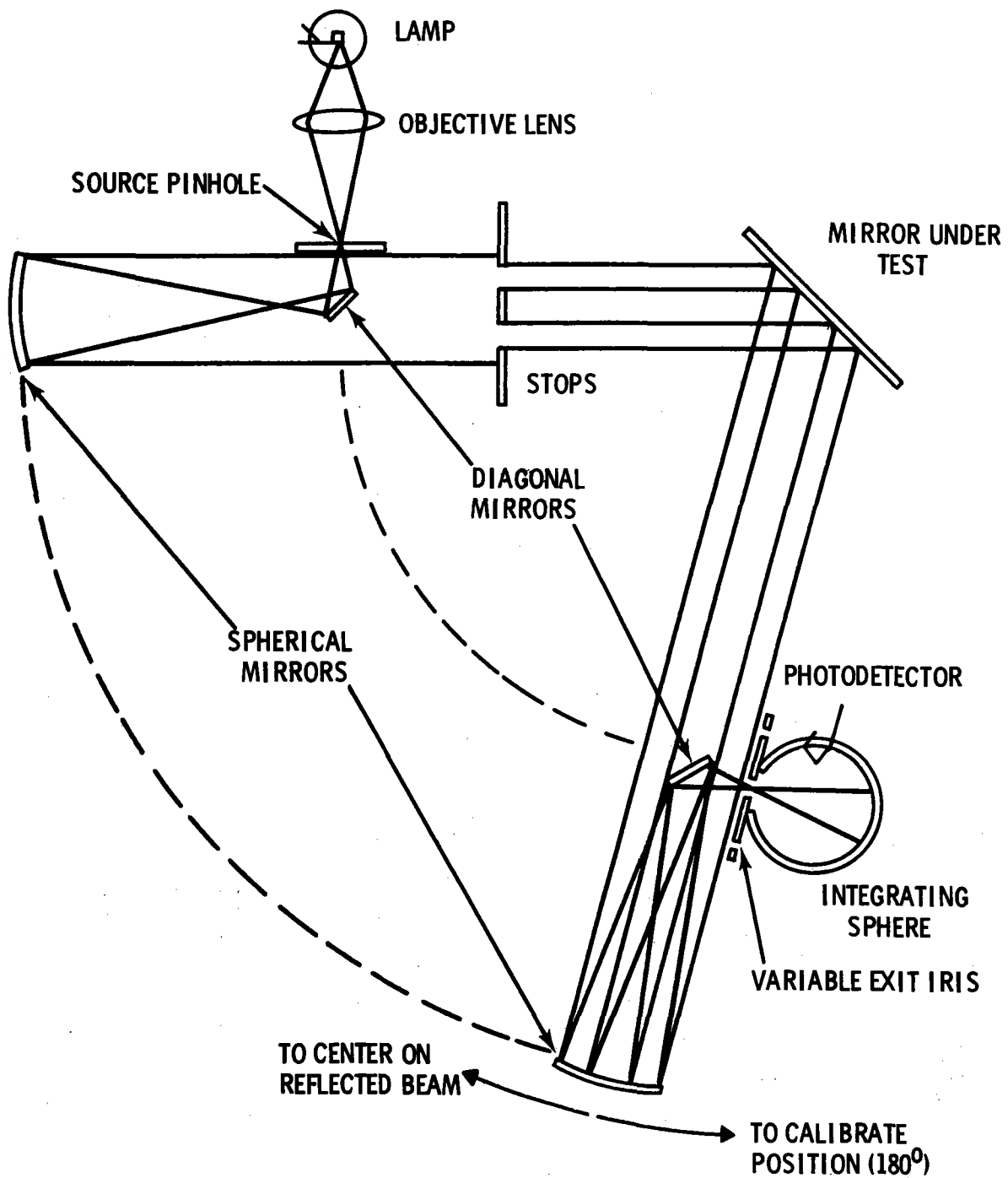


FIGURE 12. Bi-Directional Reflectometer Incorporating Spherical Mirror Optics (Sheldahl, 1974)

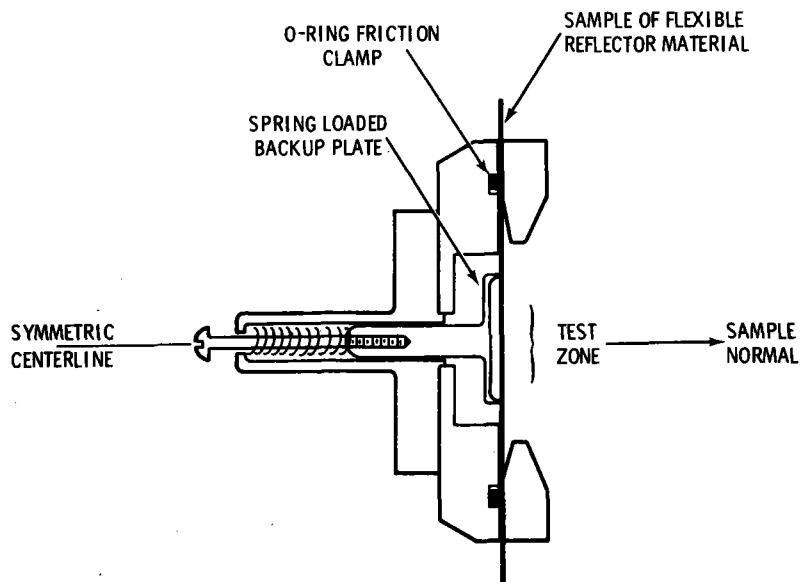
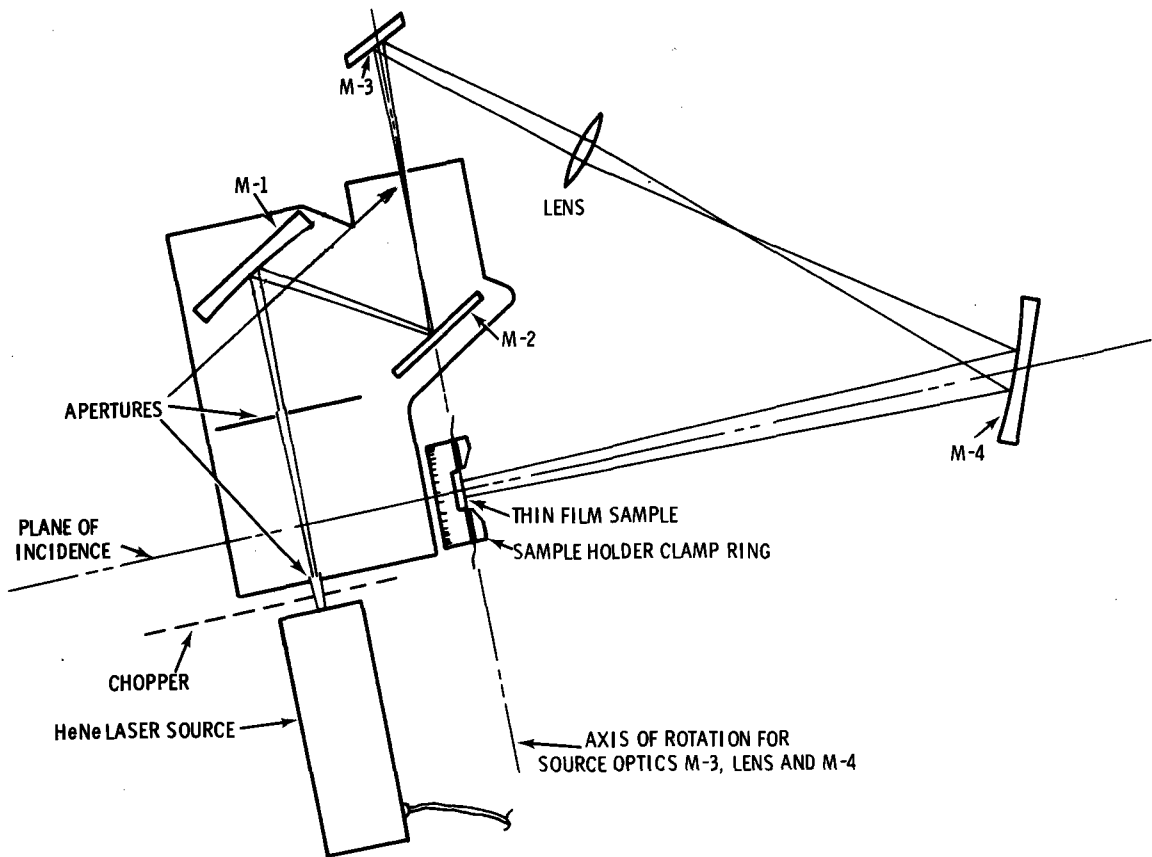


FIGURE 13. Reflectometer for Specularity Evaluation of Stretched Membrane Reflectors (Zeltner, 1977)

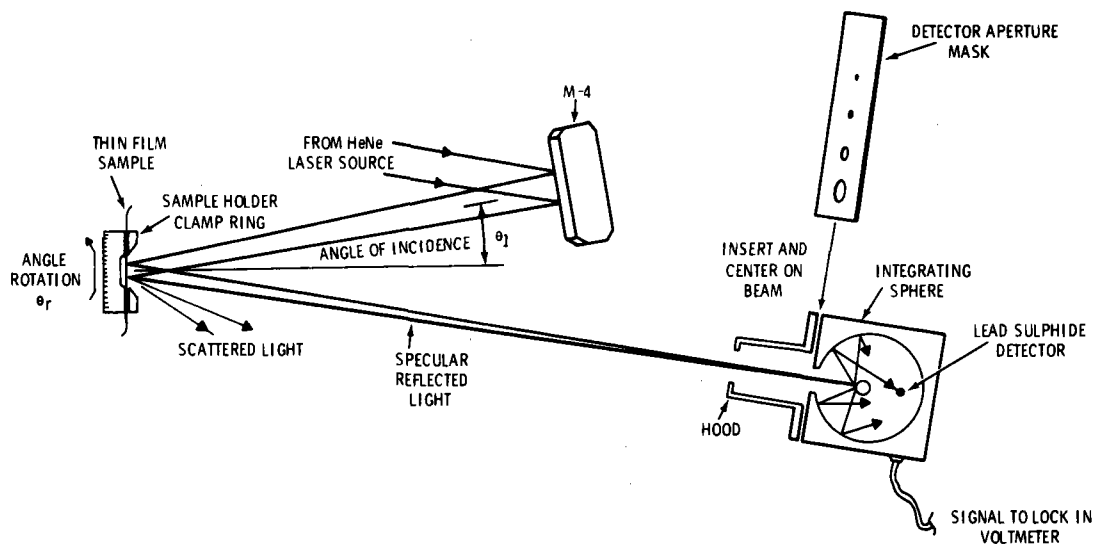


FIGURE 13. (Continued)

solar intensity distribution incident on a target screen at the collector focus. Analysis of this spatial intensity distribution allows quality assessment of the aggregate beam formed by each component heliostat. Specularity error is manifested as a deviation of the focused spot geometry from that of a theoretical result of the calculated sunshape. The observed beam divergence is actually a convolution of figure and specularity errors and the de-convolution of these components is not a straightforward exercise and in fact may not be possible.

The data acquisition and analysis system used in the BCS is schematically represented in Figure 15. The basic output is a 256 by 256 matrix of heat flux (W/cm^2) values. With computer support and data analysis, flux level plots, beam centroid location, total beam power, and percent of beam power versus radius from beam centroid are calculable. The BCS may also be utilized for pointing accuracy testing. This may be accomplished by recording centroid location versus time or by mounting a laser in the heliostat proper and observing the beam position on a coordinate grid as in Figure 16.

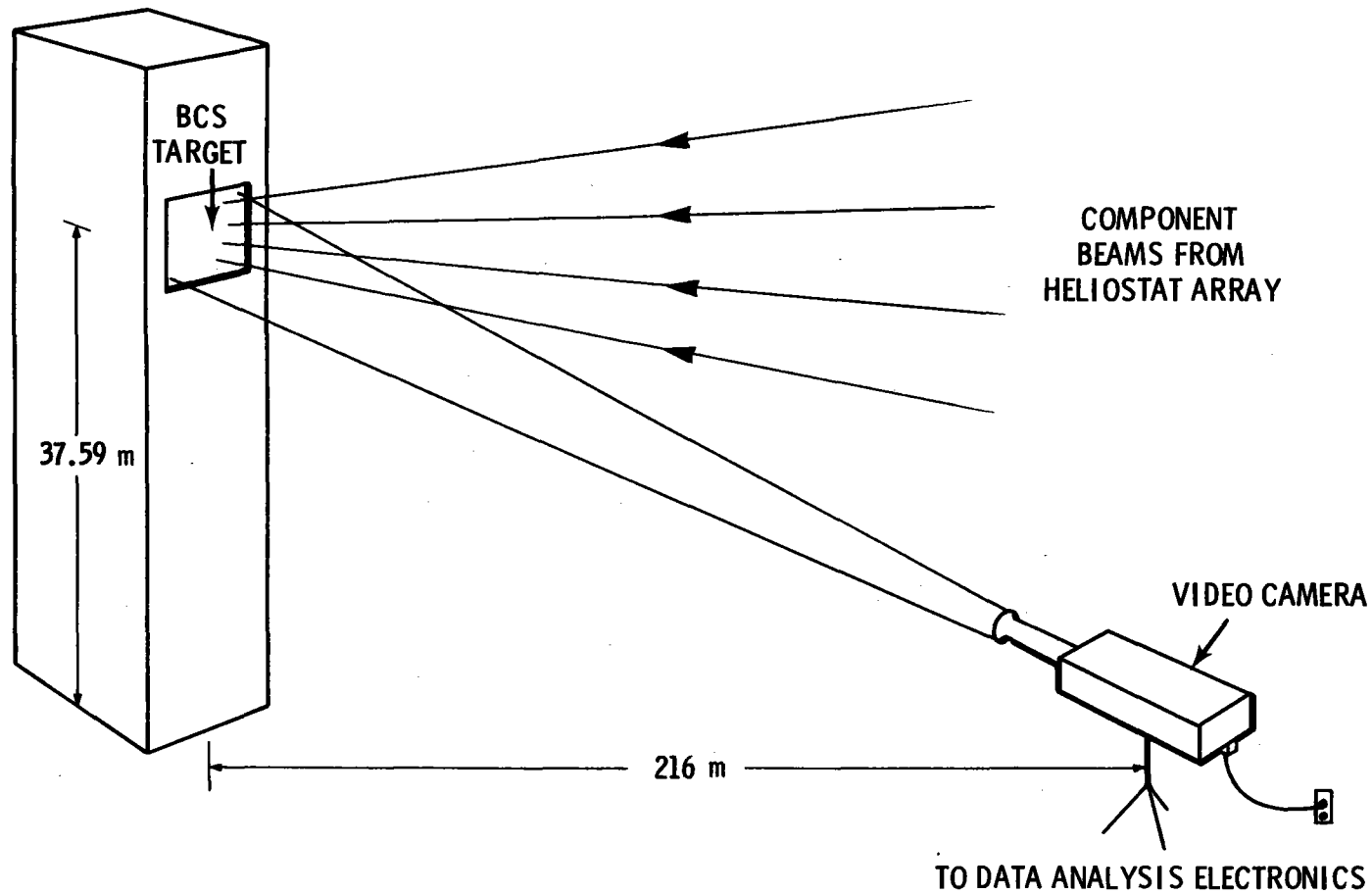


FIGURE 14. Beam Characterization System (BCS) (King, 1979)

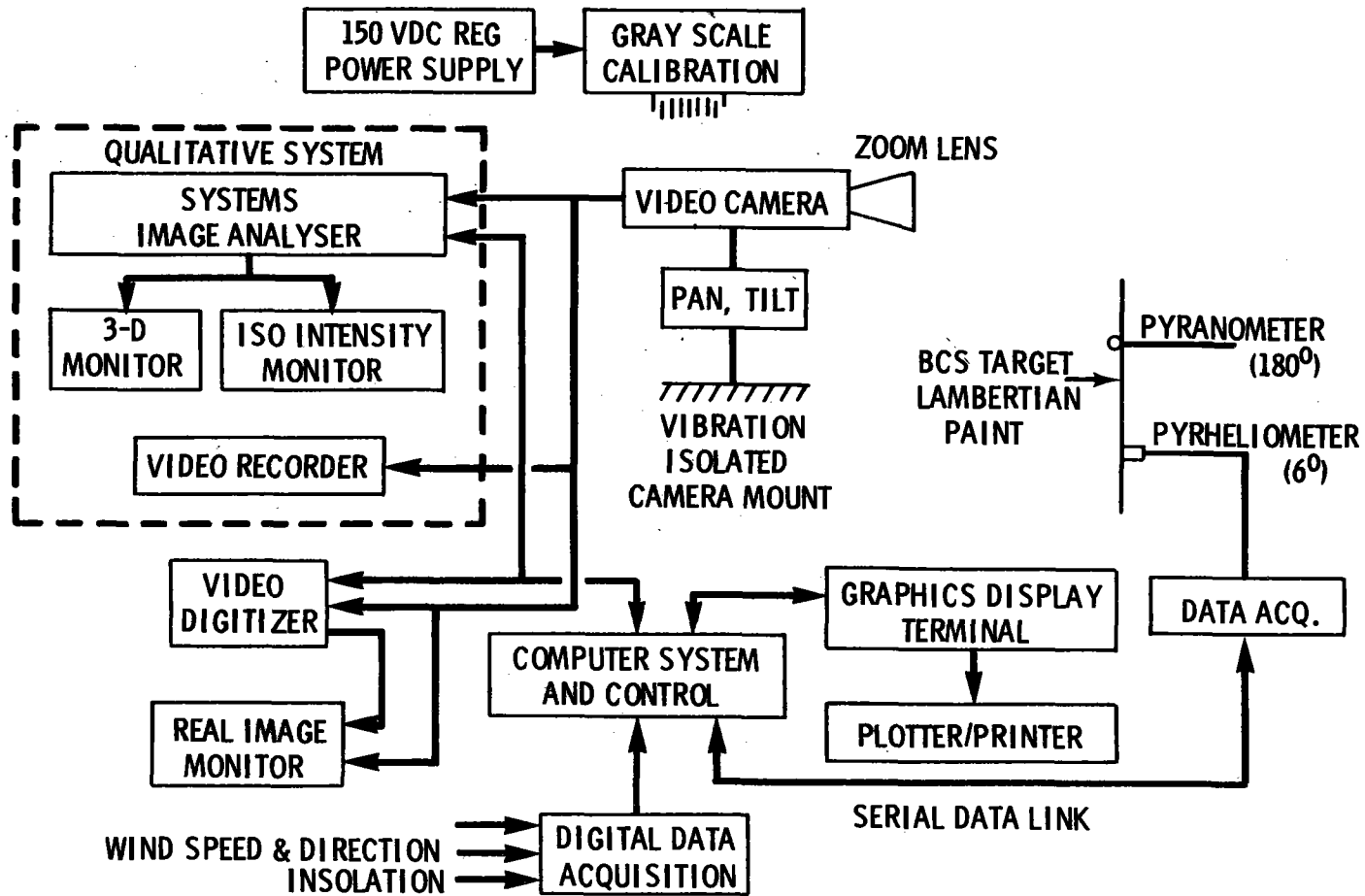


FIGURE 15. Electronic System for Forward Gazing BCS (King, 1979)

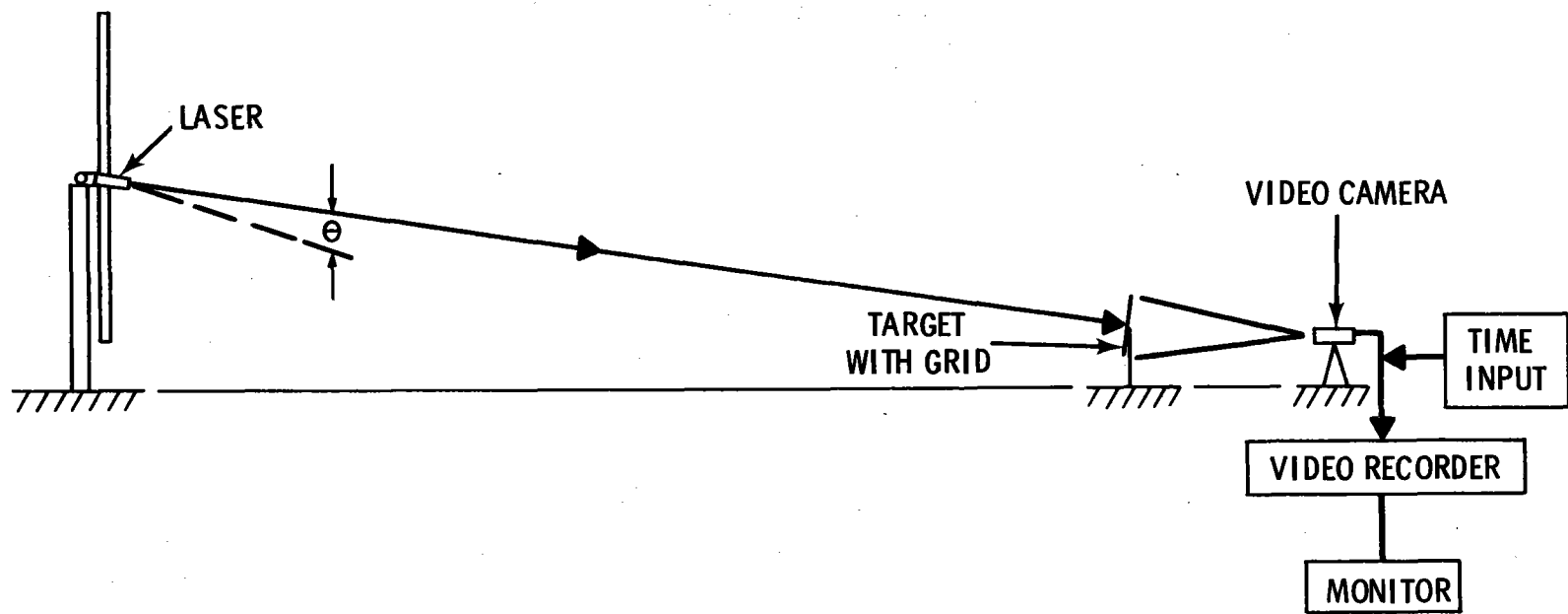


FIGURE 16. Pointing Accuracy Mode of BCS (King, 1979)

The inherent drawback of any forward gazing system is the lack of specific specular information obtainable by observation of the focused beam intensity profile (spot of confusion). In this technique the primary quality criterion is minimum spot size. If the heliostat field produces a beam size larger than the requisite, one or more heliostats are not conforming to specular tolerance, but the propagator of the defect is not ascertained. An additional complication is the difficulty of separating the image defects due to specular error from those arising from figure error. Even more basic is the unfolding of these mirror defects from image aberrations caused by characteristic optical aberrations of the heliostat field optical system. For example, spherical aberration and astigmatism will also be contributors to the overall solar image defect. The deconvolution of all of these aberration factors to actually determine the remaining anomaly attributable to specular error will require an in-depth theoretical analysis.

d) Image Characterization System. A variation on the forward gazing system (BCS) described above is the backward gazing system or image characterization system (ICS) described by Brumleve (1979). A schematic of the system configuration appears in Figure 17. In the ICS, rather than viewing the heliostat beam on a target, the camera is positioned in the target plane and gazes backward along the optical axis at the heliostat. The camera then sees a modified solar image which has been modulated by the mirror reflective characteristics.

The associated electronic data handling/analysis system for the ICS appears in Figure 18. In the measurement procedure the television camera is first pointed directly at the sun to allow recording of the reference source image. The limb darkening of the sun is enhanced by the interposition of a band pass filter allowing the resulting intensity variation to be correlated with angular deviation from the central ray. The solar image is then color coded by a video analysis unit to represent a source target in which each colored ring represents a range of angular deviation from the central ray. Finally the TV camera is aimed at the heliostat and the color coded heliostat image is displayed on a color monitor.

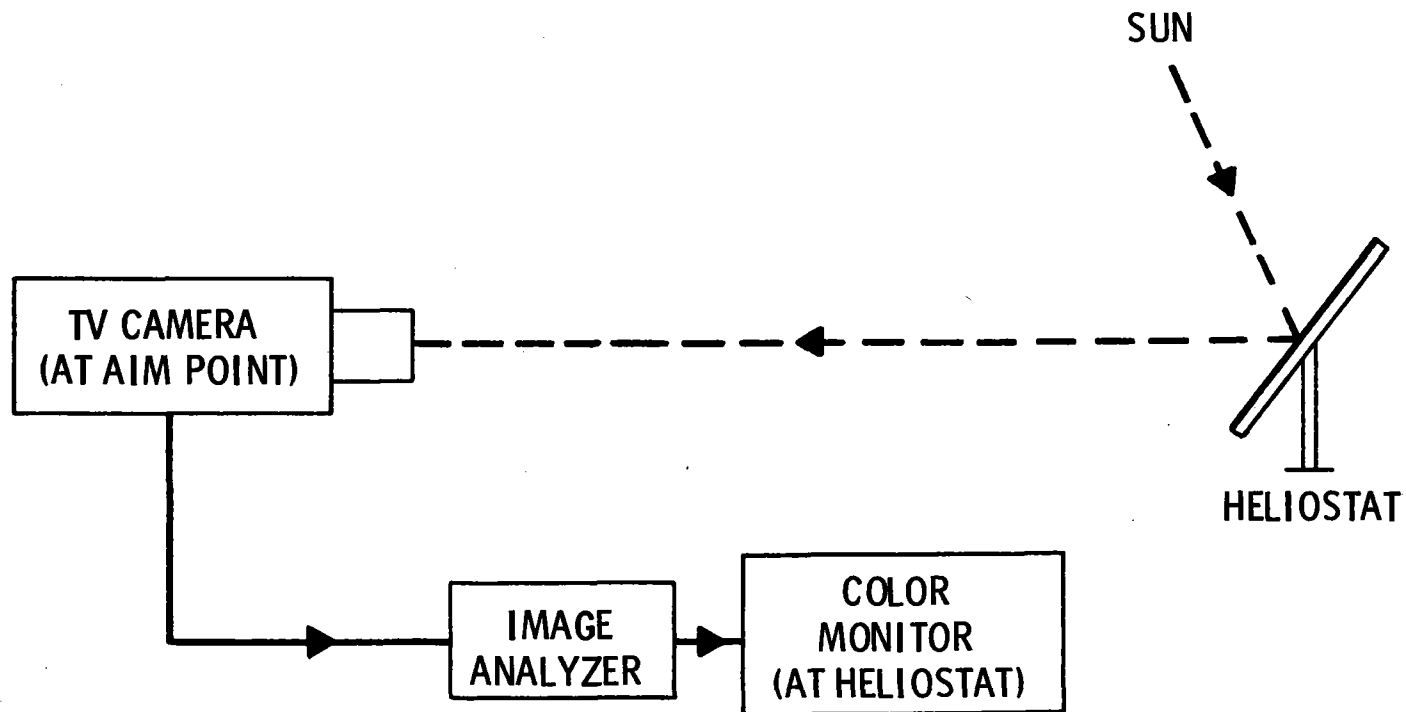


FIGURE 17. Image Characterization System (ICS) (Brumleve, 1979)

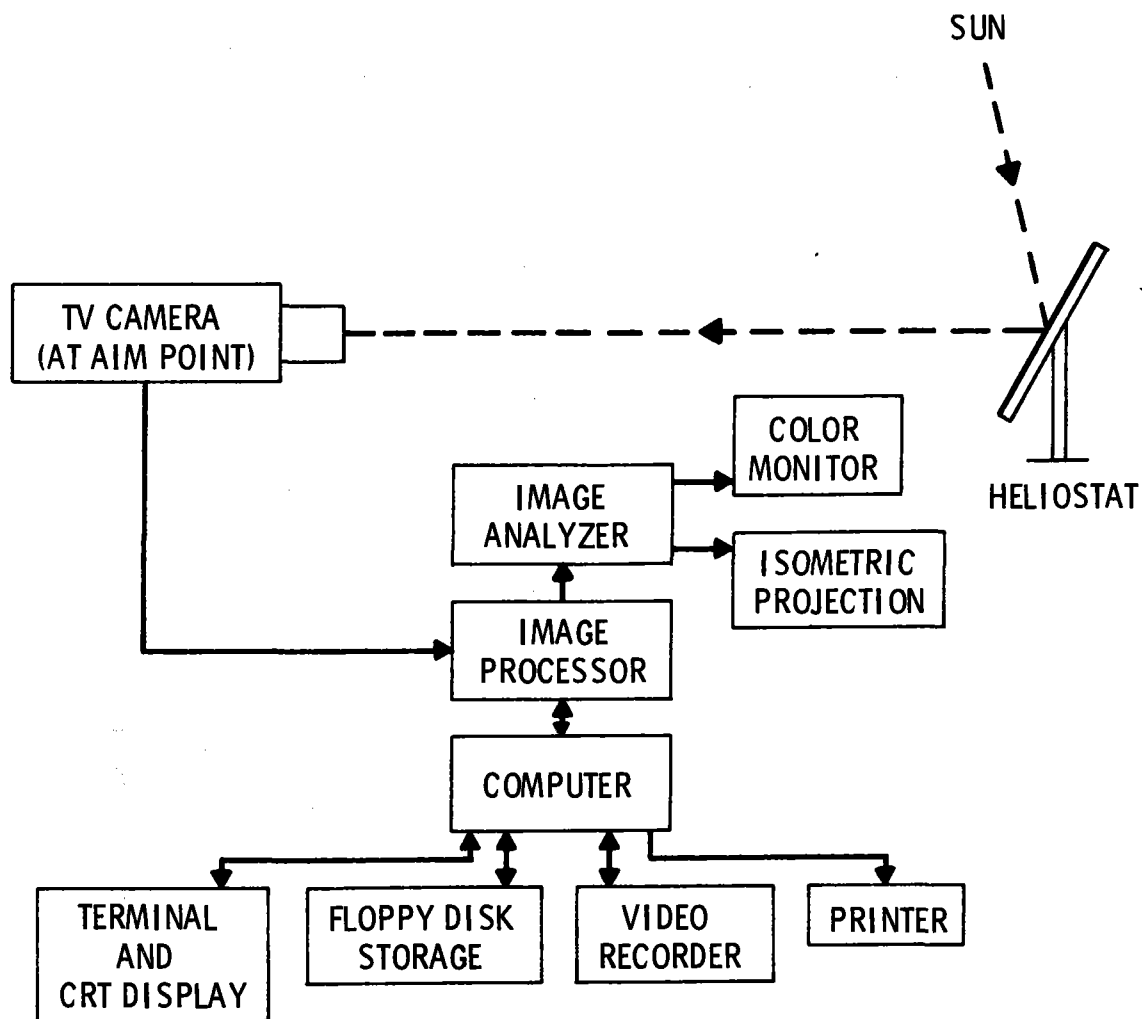


FIGURE 18. Electronic Evaluation System for ICS (Brumleve, 1979)

To compensate for mirror to target atmospheric attenuation and mirror reflectivity losses, the gain of the image analysis unit is adjusted to establish coincidence between the upper edge of the peak color band and the centroid of the direct solar image. The color enhanced heliostat image now represents a visual display of mirror contour, alignment accuracy and specular error, each color indicating a specified deviation of the local mirror normal from perfect. A misaligned, low specularity, or incorrectly focused heliostat is readily apparent.

As in the BCS the ICS may also be used for heliostat alignment. To accomplish this, the heliostat produced solar image is viewed on a color monitor and each facet is oriented to maximize the peak colors (those near the central ray or nearest the center of the sun target). Such an adjustment produces the highest flux density at the camera focal plane and results in the smallest solar beam divergence for the heliostat at that particular sun position.

For quantitative heliostat specularity evaluation additional peripheral instrumentation is required. This equipment is necessary for correction of detector nonlinearity, calibration of the video system, and data processing.

Heliostat characterization is accomplished by acquiring data on mirror deviation from normal at 30,000 points over the heliostat surface area. Typical reduced output is a tabulation of the fraction of heliostat mirror surface which deviates from theoretical by more than a requisite angle in the range of 0 to 2.3 mrad.

The apparent advantage of the ICS, backward gazing system, is that any facet misalignment or specularity anomaly in the heliostat collector field is immediately identifiable and the specific culprit is easily located. The reason for this is that in this technique the optical geometry is conserved in contrast to the BCS examination of the spot of least confusion. Difficulties still exist in unfolding the propagators of the image defects, i.e., separating heliostat mirror error effects from the characteristic aberrations of the optical system and atmospheric induced distortion.

4. Extension of Specularity Assessment Techniques

The optimum scenario for heliostat mirror specularity evaluation depends on the solar facility requirements. The Fourier transform and bi-directional reflectometer techniques are most aptly suited to the screening of small mirror facets for specularity error in a laboratory environment. The extension of these techniques to large plane mirror facets, while seemingly straightforward, encounters spatial resolution difficulties due to diffraction limiting in large transmitting optical elements. In the case of the Fourier technique,

the use of large diameter spherical or parabolic mirrors should be investigated to increase inspection area capability. Likewise, designs incorporating large aperture mirrors might be considered for the bi-directional reflectometer.

For field evaluation of mirror specularity, the beam characterization system (forward gazing) and the image characterization system (backward gazing) present the most feasible and most easily implemented techniques at hand. Both systems are versatile and theoretically will allow simultaneous determination of mirror reflectivity, specularity error, and figure error (to be discussed later) with one instrument. In addition, the systems may be utilized for heliostat alignment algorithms and pointing accuracy confirmation. Implementation of the intensity characterization systems above will require a large theoretical and experimental investigative effort in order to relate solar image intensity to the quantifiable mirror variables. Doubtless further literature and experimental research will unveil additional concepts useful for mirror specularity evaluation and the possibility of modifying the above techniques with these new ideas should not be excluded.

C. Figure

Mirror figure accuracy is largely determined by standard optical shop practices and the experienced eye of the optician. Since the optical shop techniques have proven fruitful in the past, the inclination is to merely develop algorithms for obtaining quantitative figure error information. This is not a straightforward task however and its implementation in general requires sophisticated, delicate optical systems of great expense. The figure error evaluation instrumentation for use on solar facility heliostat mirrors presents an additional complication. Since mirror surface figure error is greatly influenced by the mounting configuration, static and dynamic loading, and extended time materials effects, it is desirable to measure and monitor the figure deformation of the mirror facets on the heliostat structure properly.

The following section constitutes a compendium of candidate concepts and methods for possible solution of the solar facility heliostat figure error analysis problem. The collection is by no means complete as new alternatives appear daily. Indeed the figure evaluation problem is able to draw from a

broad spectrum of optical testing methods, e.g., moiré analysis, interferometry, holography, etc. The eventual method or hybrid method will be determined by practicality, accuracy, and cost of implementation. Before discussing the options available in detail, a definition of figure is appropriate.

1. Definition

Macroscopic or structural mirror deformations are classified as slope or figure errors. Slope errors can be classified into two categories (Sanchez and Saylor, 1979): (1) actual slope error in which the surface normal at a given point deviates from the theoretical normal at that point and (2) sag or bias error in which cumulative slope errors cause the reflector surface to be physically displaced from its expected position. Figure error can be the result of deformation inherent in the mirror forming procedure or mirror loading; for example, due to wind and gravity. The error may be either time dependent or time invariant. The distinction between figure error and specular error is not well defined. However, by convention, figure error refers to variations in mirror surface contour of low spatial frequency (e.g., $>cm$) whereas specular error constituents are of relatively high spatial frequency (e.g., $<cm$) and are a result of microscopic coating and/or substrate structure.

Surface figure error is reported as an angular deviation of the reflected ray from the calculated direction. For example if the assumed angle of reflection is θ , and the experimentally determined angle of reflection is θ' then the defined optical figure error is $|\theta'| - |\theta|$. Note that for a perfect surface (theoretical contour) the error is zero. Pettit, et al. (1979) has suggested the use of a figure error dispersion term, σ_F , to be used in the description of the slope errors of a reflecting solar concentrator. The dispersion term would be utilized with dispersion terms for other image degradation distributions (specularity error, tracking errors) to produce an effective "error cone".

One may use a different variable than the deviation of a reflected ray from the specular direction for slope or figure error quantification. Equally

valid is specification of the mirror surface contour. This method is useful since many optical shop techniques exist for generation of surface contour lines or topographic maps for reflective surfaces. The figure error specification then takes the form (for plane mirrors) of an RMS deviation of reflective surface height or a topographic map indicating contours of equal height for the surface. This information allows calculation of the expected beam divergence of the reflected beam for a given incident beam divergence.

2. Techniques of Figure Error Evaluation

The techniques to be discussed for possible application to figure error evaluation in solar facility heliostat mirrors are for the most part laboratory methods. Only recently has the requirement of a field deployed device for figure assessment appeared.

a. Laser Ray Trace. The collimated high intensity radiation available from a laser lends itself to a very basic solution of the mirror figure error evaluation problem. In the laser ray trace method a laser beam impinges on the mirror surface at some specified incident angle. The deviation of the reflected beam from the specular direction (based on knowledge of the surface normal) is an indication of figure error. The technique may be applied to planar or curved mirror facets, but is most easily implemented when analyzing plane mirrors.

A device for the evaluation of the effective figure of planar float, fusion and rolled glass is reported by Lind and Rusin (1978). The device is illustrated in Figure 19. For analysis a HeNe laser beam illuminates the glass sample surface at an incidence angle of 45° . The reflected beam (from either the first or second surface) is incident on a single axis linear position sensing diode which when interfaced with the associated electronics produces an analog (voltage) output which is directly proportional to the displacement of the laser beam centroid from a predetermined spatial null point. Figure (or figure error) is determined in units of angular deviation from the specular direction by a previous calibration of output voltage versus error angle.

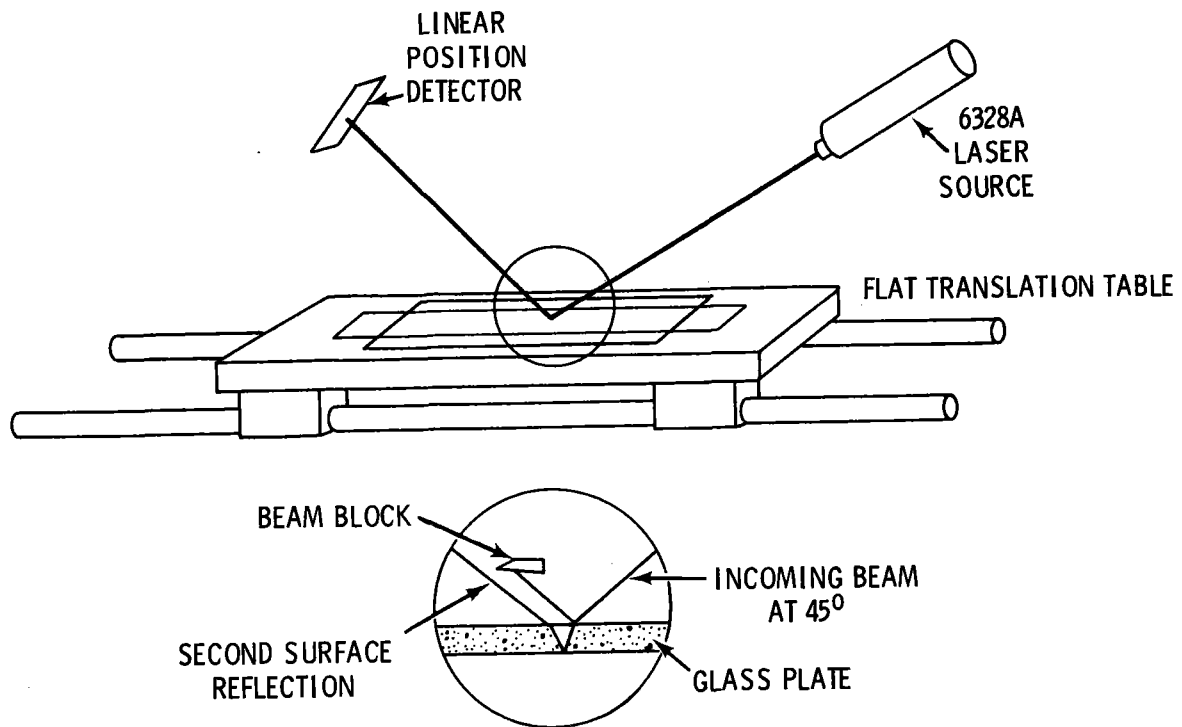


FIGURE 19. Laser Ray Trace Instrument for Glass Flatness Measurements

The test bed consists of a ground flat steel table which is precision translated on linear bearings by a stepping motor driven ball screw. Thus figure error can be determined as a function of beam position on the sample surface. Note that in this configuration the apparent angular error in the optical reflection will be twice the glass sample wedge angle. Computer reduced data output includes a table indicating the fractional glass area which reflects light outside of some requisite angular deviation.

It should be mentioned that the horizontal sample mounting format causes glass conformation to the table contour, i.e., the glass sample deforms slightly to the table shape under its own weight. This situation does not present problems however if the data is corrected for this effect prior to analysis. The correction takes the form of an angular deviation per unit length which must be subtracted from the raw data.

Several alternatives have been suggested for figure error evaluation of parabolic surfaces via the laser ray trace concept. The basic measurement procedure is essentially the same as for planar surfaces except for mirror mounting and translation modes. A typical design described by Pettit and Butler (1977) appears in Figure 20. Details of the operation and data analysis technique are discussed by Butler and Pettit (1977). In this apparatus rather than translating the mirror, the laser is scanned in the horizontal (X) direction across the mirror surface. At the end of the horizontal scan the mirror is displaced in the Z direction and another horizontal scan performed. The resultant raster scan pattern allows data acquisition over the entire reflector area. The location of the reflected ray centroid is ascertained using a position sensitive detector located in the focal plane.

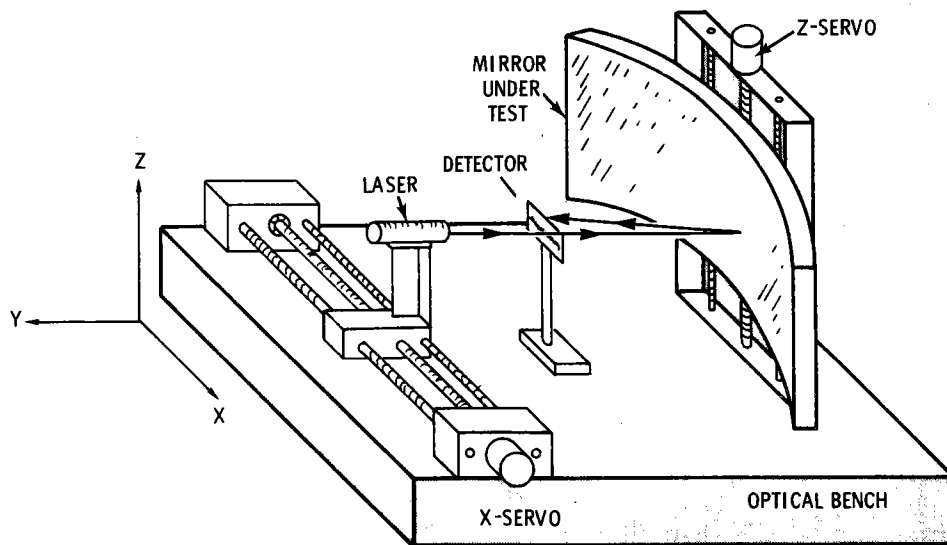


FIGURE 20. Laser Ray Trace Instrument for Analysis of Parabolic Surfaces (Pettit and Butler, 1977)

The reflected beam centroid position is descriptive of the deviation between the slope of the local surface structure being analyzed and a best-fit parabola. The resolution of the apparatus is reported to be a few tenths of a

mrad and the device is capable of determining slope errors up to 90 mrad. The data for each studied parabolic concentrator are analyzed to allow assignment of a "mean" focal length and an RMS deviation (σ_s) of the slope errors about the "mean" focal length.

Sanchez and Saylor (1979) describe a modification of the above method allowing determination of both slope and sag error of a parabolic concentrator. The difference between these two types of figure errors is illustrated in Figure 21. The experimental configuration appears in Figure 22. The method utilizes a HeNe laser as an illumination source and two parallel vertically oriented acrylic sheets. The laser beam is aligned for normal incidence with the acrylic sheets and so that the hypothetical normal to the bottom (i.e., the deepest point) of the collector is parallel to the direction of the incident beam. The laser is then a solar simulation source and the collector is positioned as it would be to collect incident solar radiation.

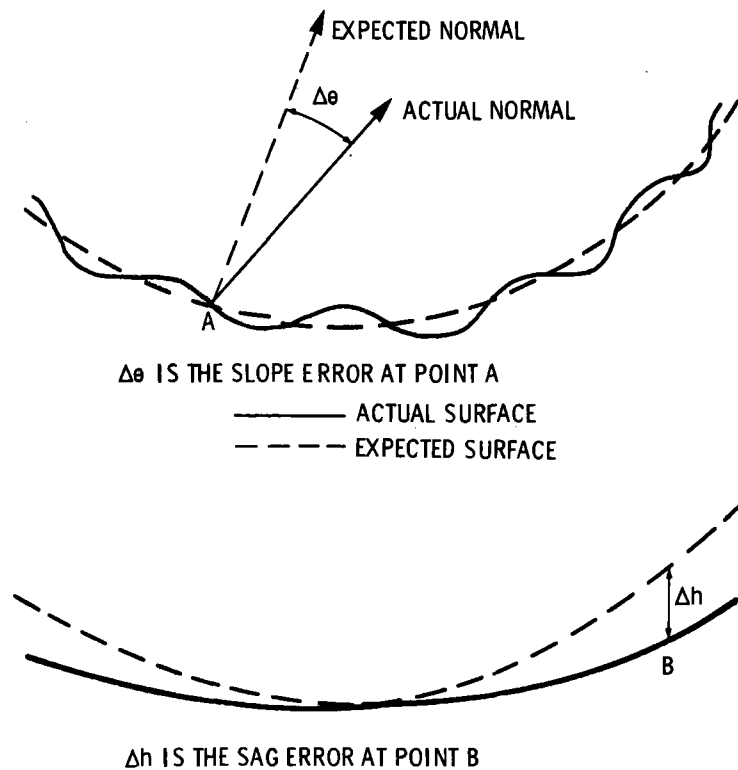


FIGURE 21. Illustration of Slope and Sag Error (Sanchez and Saylor, 1979)

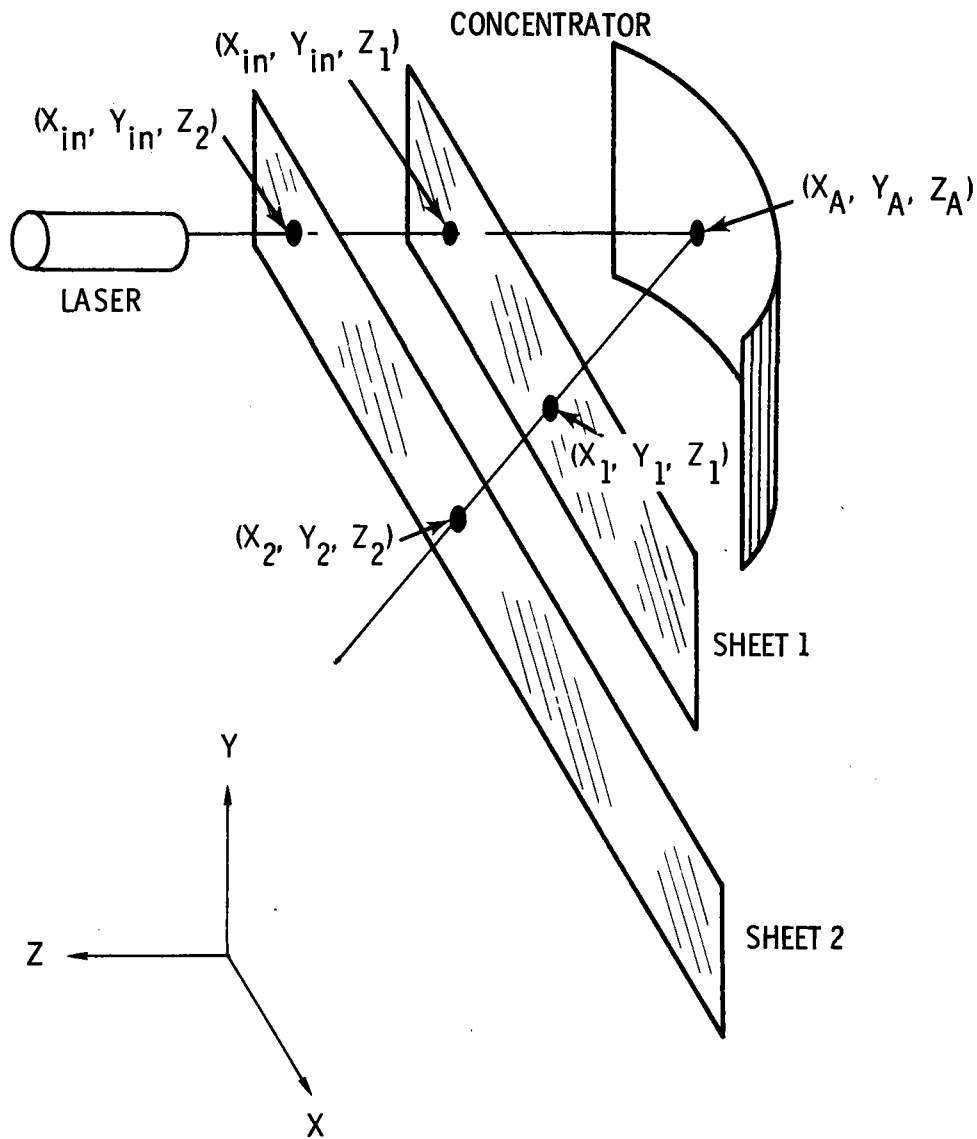


FIGURE 22. Laser Ray Trace Apparatus for Measurement of Slope and Sag Errors in Parabolic Concentrators (Sanchez and Saylor, 1979)

The coordinate system is defined so that the X and Y axes lie in the acrylic sheet planes and the Z ordinate increases in the direction of the laser. The points of incident beam-plane incidence have coordinates (x_{in}, y_{in}, z_2) and (x_{in}, y_{in}, z_1) and the exit beam-plane intersection points are denoted by (x_1, y_1, z_1) and (x_2, y_2, z_2) . The coordinates of the beam-mirror

intersection point, A, are denoted (X_A, Y_A, Z_A) . The geometry of the situation is clarified in Figure 23. Defining $\Delta X_{2A} = X_2 - X_A$, $\Delta X_{21} = X_2 - X_1$, $\Delta Y_{2A} = Y_2 - Y_A$, $\Delta Y_{21} = Y_2 - Y_1$, and $\Delta Z_{21} = Z_2 - Z_1$; the expression for Z_A (via a simple geometrical argument (Sanchez and Saylor, 1979)) is

$$Z_A = Z_2 - \Delta Z_{21} \left((\Delta X_{2A}^2 + \Delta Y_{2A}^2) / (\Delta X_{21}^2 + \Delta Y_{21}^2) \right)^{1/2}. \quad (23)$$

The sag error is then calculated as

$$\Delta h = Z_A - Z_T \quad (24)$$

where Z_T is the theoretical Z coordinate calculated from expressions for the concentrator surface figure. For a parabola, Z_T is given by

$$Z_T = (X_A - X_f)^2 / 4f \quad (25)$$

where f is the mirror focal length and X_f is the coordinate of the focal point. For a paraboloid Z_T is given by

$$Z_T = \left((X_A - X_f)^2 + (Y_A - Y_f)^2 \right) / 4f. \quad (26)$$

The slope error is calculable from the dot product between the expected and actual reflection vectors or

$$\Delta\theta = \frac{1}{2} \cos^{-1} \left[\hat{R}_{\text{actual}} \cdot \hat{R}_{\text{expected}} \right] \quad (27)$$

where $\hat{R}_{\text{expected}}$ for a parabolic surface is given by

$$\hat{R}_{\text{expected}} = \frac{(X_f - X_A, Y_f - Y_A, f - Z_{\text{expected}})}{\left[(X_f - X_A)^2 + (Y_f - Y_A)^2 + (f - Z_{\text{exp}})^2 \right]^{1/2}}. \quad (28)$$

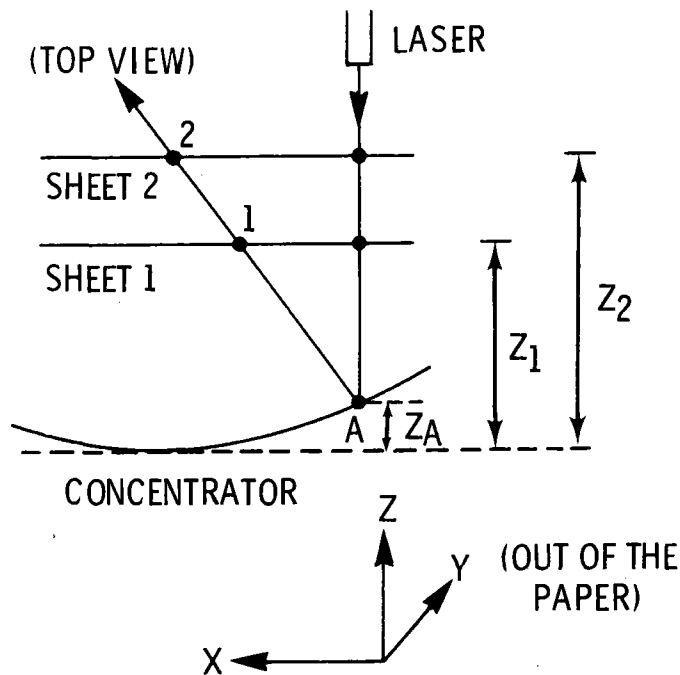


FIGURE 23. Geometry for Sag Error Calculation (Sanchez and Saylor)

The reported experimental error encountered in this technique is reported to be less than 0.10 in. for sag error and the uncertainty in slope error may be maintained at less than approximately 4 mrad. The inherent error in this technique is largely attributable to inaccurate determination of the laser beam intersection point coordinates.

While the technique is conceptually easy to implement, it is sensitive to test mirror misalignment, i.e., rotation. The correction of the acquired data requires operation upon the coordinate system with a rotation matrix specified by the angular rotation error. This correction algorithm is difficult to implement in practice. Details of the procedure are shown by Sanchez and Saylor (1979).

Yet another laser ray trace technique especially suited for evaluation of large (2-3 m) parabolic facets is reported by R. A. Zakhidov, et al. (1977). A schematic of the system appears in Figure 24. The optical system consists of a 25-mW HeNe laser and a 70-mm diameter telescope used as a collimator

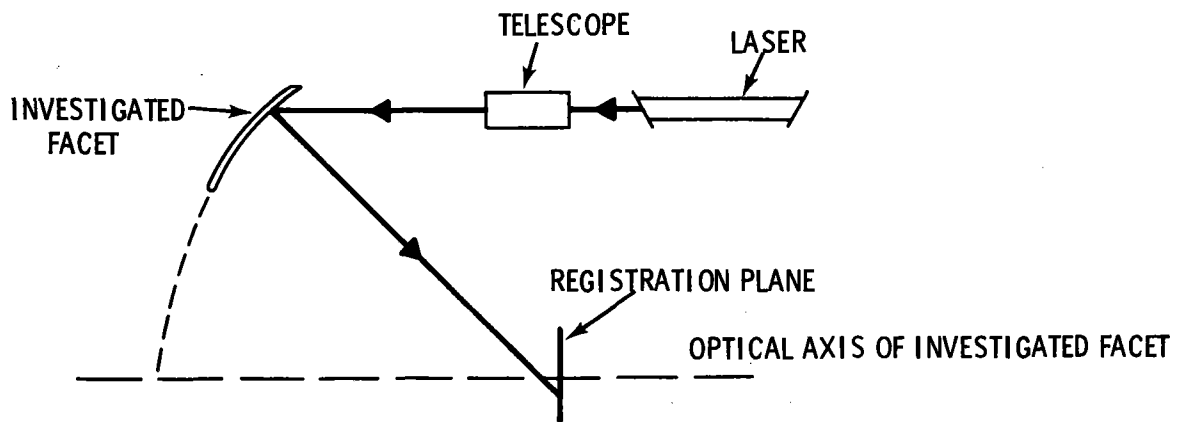


FIGURE 24. Optical Inspection System for Evaluation of Figure Error in Large Parabolic Mirror Facets (Zakhidov et al., 1977)

mounted on a two-dimensional translation stage allowing collinear displacement of the optics over an 800 X 800 mm area. The claimed beam divergence is less than 10 seconds of arc. The beam reflected from the mirror test surface falls incident upon a translatable target cassette where it may be traced and the centroid noted.

The measurement sequence consists of recording the reflected beam profile and brightness maximum coordinate and then translating the probe laser mount to illuminate another mirror area where the process is repeated. The probe beam is apertured with a rectangular stop so that rectangular mirror segments can be inspected in the observation plane. The obtained data is then a distribution of reflected beam cross sections. The position of the reflected cross sections with respect to the cassette baseline coordinates indicates the spatial figure inaccuracy across the entire mirror surface whereas the shape of the reflection spot indicates figure error within a discrete area.

The above technique was applied to characterization of three large mirror facets by drawing an envelope which contained all reflected beam spot contours generated by the entire facet surface. The result of this evaluation is illustrated in Figure 25. Measurements for all three facets were for the same focal distance (1550 mm).

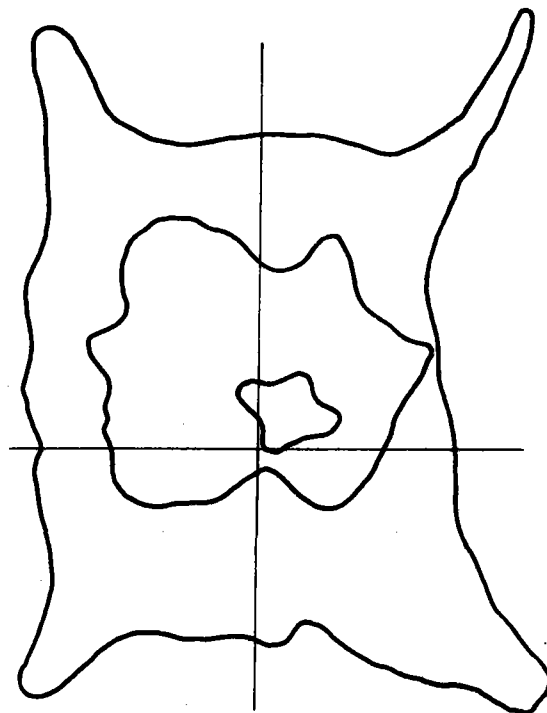


FIGURE 25. Containment Contours for Focal Spots Generated by Three Large Parabolic Facets (Zakhidov et al., 1977)

The above procedure allows localization of figure errors in large parabolic reflectors and in this respect is superior to integral techniques. While the data presented is qualitative, it appears that a straightforward modeling algorithm would allow quantitative error evaluation (i.e., rms slope error).

b. Moiré Fringe Analysis. If two gratings (e.g., Ronchi rulings) of comparable spatial frequency are superimposed, the locus of intersection points of the two line families will form a geometric pattern known as moiré fringes. The extension of this effect has been applied to the study of the topography of flat plates, beams, and other surfaces. In general the procedure for these evaluations consists of illuminating the object under study through a Ronchi grating and observing the fringed surface through the same grating or one matched in spatial frequency. This conventional method is

particularly applicable to nonspecular (diffuse) surfaces, but only if the grating can be placed in close proximity to the surface under test. A modification of the above technique termed the reflected image method (Theocaris, 1966) is utilized for evaluation of specular surfaces. This method is complicated however since a point-to-point topography is required necessitating a rotational specimen mount which would allow a periphery camera to register the translating object image on a single film sheet.

An alternative technique which allows analysis of both specular and diffuse surfaces based on the oblique shadow method has been suggested by Agarwala, et al. (1975). A schematic of the optical arrangement appears in Figure 26. In this arrangement, a collimated image (shadow) of the reference grating G illuminates (via the partially silvered mirror AB) the test surface O. The grating lines when viewed in reflection from the test surface are no longer linear but take on curvature according to the test surface topography. This modulated grating image is incident upon the camera objective and may be focused at C.

To generate the moiré fringes it is necessary to superimpose the original unperturbed grating image onto the modified grating geometry. This is accomplished by reflecting the undeviated grating beam back to the camera image plane where the moiré fringes can be recorded. The spacing between adjacent dark fringes, Δ , is an indicator of the separation of corresponding points on the test surface from the grating plane. The moiré fringe spacing is dependent upon three parameters: 1) the grating pitch P, 2) the angle, θ , at which the test surface is illuminated, and 3) the angle, ϕ , at which observations are made. The connection between the four above quantities, Δ , P, θ , and ϕ is expressed by

$$\Delta = \frac{P}{\tan \theta + \tan \phi} \cdot \quad (29)$$

If the fringes are viewed normal to the test surface, then $\phi = 0$ and the relation becomes

$$\Delta = \frac{P}{\tan \theta} \cdot \quad (30)$$

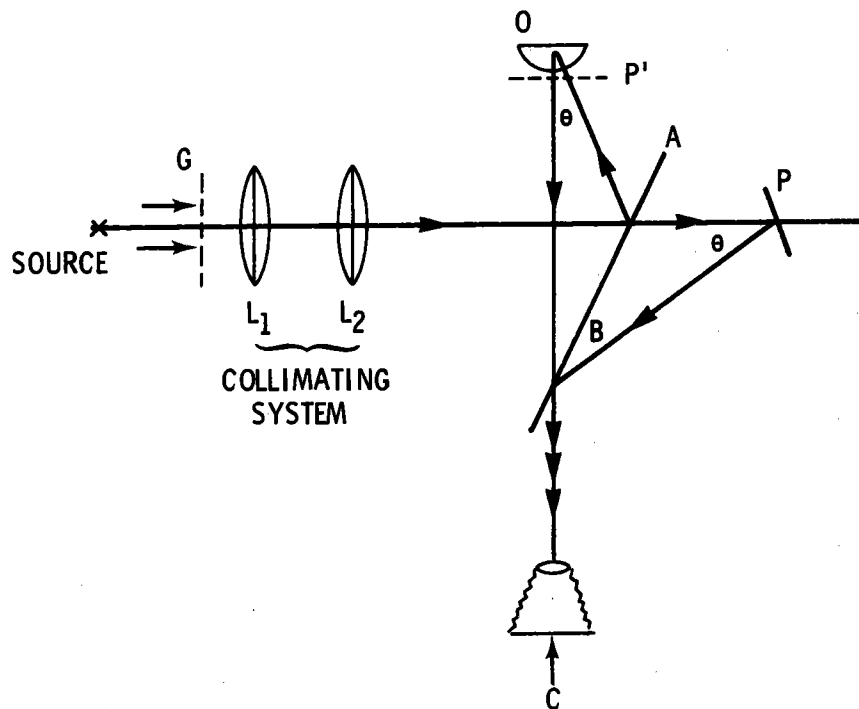


FIGURE 26. Experimental Arrangement for Specular Surface Contour Generation by the Oblique Shadow Method (Agarwala et al., 1975)

The advantages (Agarwala et al., 1975) of the technique are 1) the method may be applied to the study of diffuse or specular surfaces, 2) the moiré fringes (i.e., contour lines) may be generated with relatively large grating to test surface separation, and 3) no errors due to differences in arm optics or magnification need be accounted for since the grating projected on the test surface and the reference grating image are derived from the same beam.

A variation on the above technique with application to diffuse surface inspection is reported by Terada and Ikeda (1979). A schematic of the experimental setup appears in Figure 27. The contour interval Δh is related to the grating pitch S and the illumination incidence angle, θ , by

$$\Delta h = S \times \tan \theta . \quad (31)$$

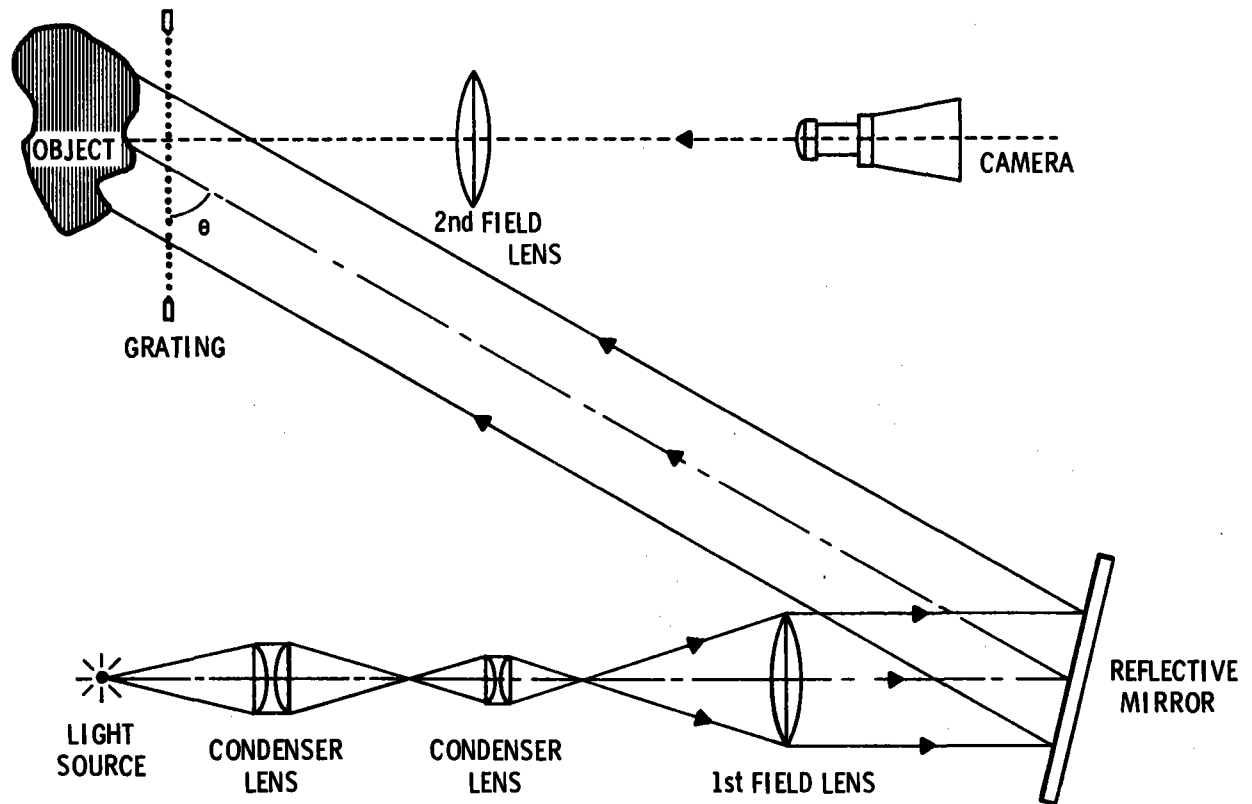


FIGURE 27. Moiré Fringe Apparatus for Generation of Surface Contours on Diffusely Reflecting Objects (Terada and Ikeda, 1979)

The light source utilized in the above apparatus was a Xenon 1 Kw short arc lamp coupled to a collimating lens system. The gratings are constructed of black-coated nylon threads or of printed film interposed between two glass plates. During the time of exposure the grating is horizontally vibrated to wash out spurious moiré fringes. Although the above described method is applied to the analysis of diffusely reflecting objects, it appears that it is possible to extend the technique to mirror figure analysis. If the diffuse object is replaced by a second surface mirror for example, the projected grating image will be transformed upon reflection by the mirror contour and substrate inhomogeneities. Such a modified line set will be evident upon re-transmission through the grating.

The resolution limit to the suggested technique is the minimum achievable contour interval which determines the minimum detectable figure error.

A sample set of contour intervals as a function of grating pitch and incident illumination angle appears in Table 3.

TABLE 3. Contour Intervals for Given Grating Pitches and Illumination Incidence Angles

<u>Pitch of Grating (mm)</u>	<u>Incidence Angle</u>	<u>Contour Intervals (mm)</u>
1.0	63°26'	2.00
	68°11'	2.50
	71°33'	3.00
	75°31'	4.00
0.5	63°26'	1.00
	71°33'	1.50
	75°31'	2.00
0.3	63°26'	0.60
	71°33'	0.90
	75°31'	1.20
0.2	63°26'	0.40
	71°33'	0.60
	75°31'	0.80

As a final note it should be mentioned that data acquisition and analysis for the moiré technique could be expedited by interfacing a TV camera and computer to the experimental system. This would be particularly useful when changes in surface structure are of interest. The generated contours could be stored in memory for future recall or for differencing with previously obtained contours.

c. Image Evaluation. Another class of measurement techniques involves the inspection of a test image upon reflection from the mirror under test. A possible experimental configuration appears in Figure 28. The arrangement consists of a standard test target with well characterized spatial dimensions, an auxiliary imaging mirror, the test mirror, and an instrument to record the

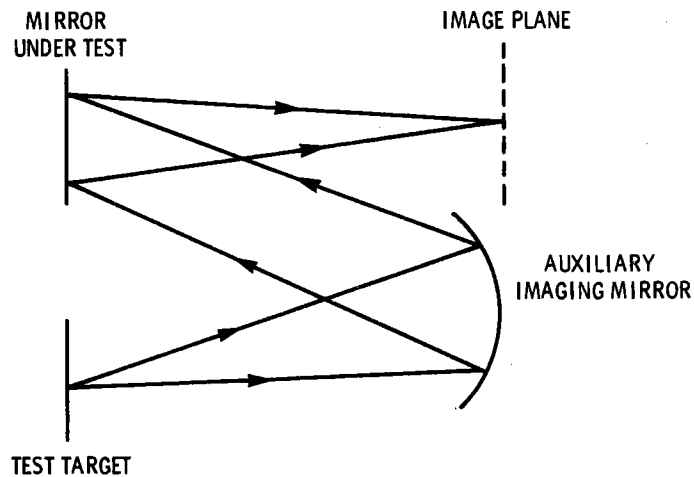


FIGURE 28. Experimental Arrangement for Mirror Figure Analysis by Image Evaluation

intensity distribution at the image plane. The variation in the image dimensions and contrast is an indicator of mirror figure and degree of specularly. Note that before the test mirror error can be evaluated, the contribution of the auxiliary optic (mirror or lens) to the total image degradation must be ascertained.

This technique may be utilized with either collimated or noncollimated target illumination. If the target is illuminated with noncollimated radiation, difficulty is encountered in defining the mirror area which is introducing a particular image defect. This is because the formation of an image point will be the result of additive contributions from different mirror sections. This difficulty may be circumvented by sequential masking of the test surface element.

The auxiliary optic may be removed and the target simply imaged with the facet under test for spherical and parabolic facets. Since the primary aberration introduced with such facets is astigmatism, it must be accounted for when attempting to evaluate figure error. Once again culprit areas can be ascertained by simply masking off adjacent mirror areas and examining target image quality.

A simpler method of image inspection utilizes a collimated light source in lieu of the auxiliary optic. A typical system is depicted in Figure 29. The arrangement projects a mirror modified shadowgraph onto the image plane where it is compared in contrast and dimension to the original target slide. The advantage of this technique is that spatial coordinates are conserved allowing immediate location of defective mirror areas thus eliminating the need for masking. The disadvantage is that evaluation of larger mirror surfaces requires a larger test slide and increased illumination beam diameter which increases system cost significantly.

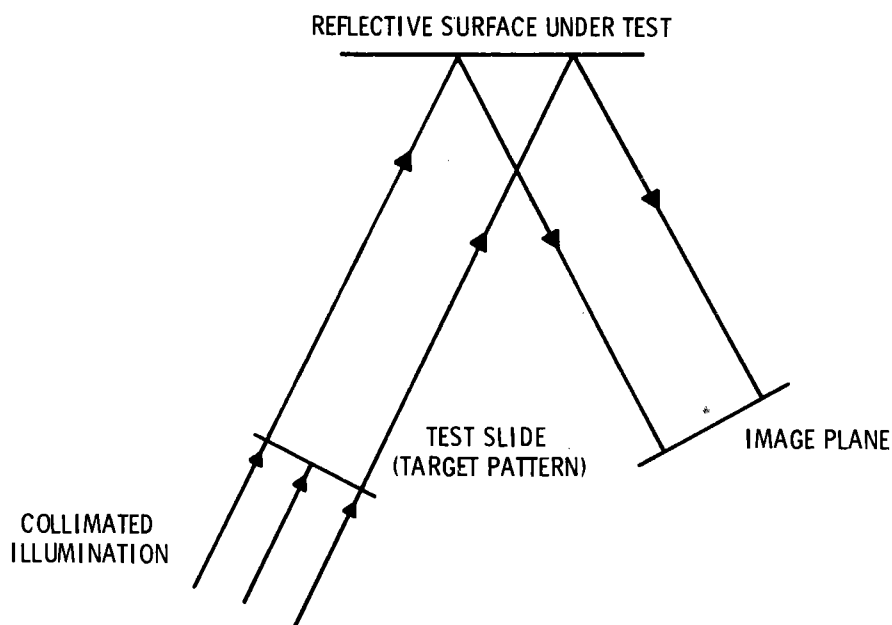


FIGURE 29. Image Evaluation Technique Utilizing Collimated Illumination

Image evaluation has been a popular technique in the past for qualitative evaluation of reflective and/or imaging optical components. The extension of this method to quantitative analysis is not trivial as it requires mathematical definition of intuitive image qualities and expensive computer hardware.

d. Schlieren Method. Schlieren techniques have been used to observe and in some cases quantify inhomogeneities in phase objects. This method can be extended to the evaluation of mirror figure and specularity. A possible Schlieren system for first or second surface mirror inspection appears in Figure 30. The point source is a high intensity Hg or Xe arc which is pinhole apertured to provide illumination at the center of curvature of the spherical mirror. The reflected beam is folded via the test mirror to an adjustable iris diaphragm located in the image plane. The diameter of the iris diaphragm is adjusted for acceptance of a finite angular beam spread determined by the test mirror to aperture interseparation distance. Observation of the illuminated spherical mirror surface through the exit aperture reveals areas of low intensity where the test mirror introduced beam divergence exceeds the limits of the stop. The observed error may be the result of perturbed surface figure in the case of a first surface mirror or a combination of surface figure error and superstrate inhomogeneities in the case of a second surface mirror. Since spatial coordinates are conserved, the defective (out of specification) mirror areas are immediately evident. Data analysis is suited to computer techniques particularly since the figure and specularity quality information are convolved in a spatial intensity distribution.

With appropriate optical component arrangement, the Schlieren method may also be utilized for analysis of curved facets. For the case of spherical facets the auxiliary mirror may be replaced by the facet under test; whereas for parabolic facet analysis the test mirror should be interposed between the spherical auxiliary mirror and the point source image plane.

Intrinsic advantages of Schlieren methods are the minimal apparatus requirement and simplicity of the optical setup and alignment. One drawback is the cost of the video analysis unit required for efficient data analysis. Also, as test mirror dimensions become greater so does the requisite spherical mirror diameter deeming the method impractical for large facets.

e. Mechanical Techniques. Numerous mechanical methods exist for evaluation of materials surface flatness or curvature. The devices generally require physical contact with the surface under test either directly or indirectly (e.g., air jet). The most common type of mechanical device used on

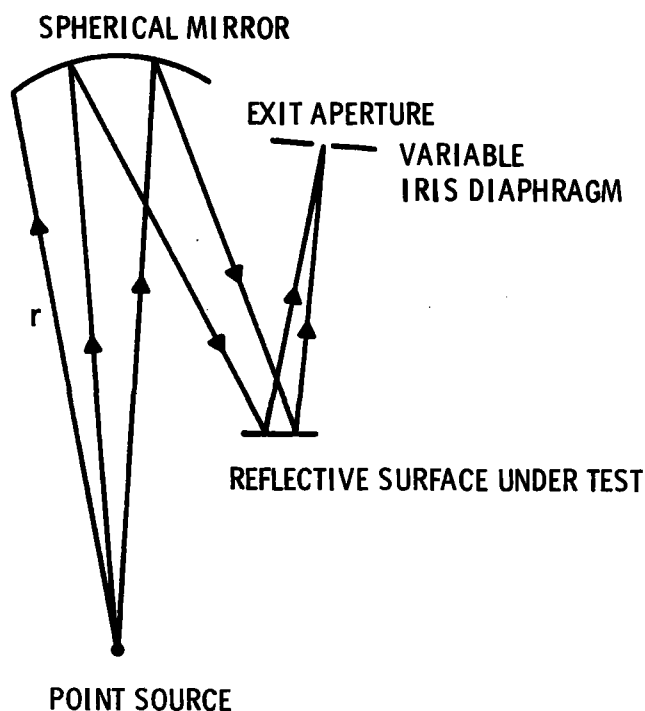


FIGURE 30. Schlieren System for Evaluation of Mirror Figure and Specularity

spherical surfaces is the spherometer illustrated in Figure 31. In its basic form it consists of a micrometer caliper mounted at the vertex of three support legs. The coordinates of the three support leg tips define a plane which intersects the spherical surface being evaluated. The micrometer measures the distance from this plane (normal to both the plane and sphere) to the spherical surface. This distance can then be used with a knowledge of the leg spacing to derive the radius of curvature of the spherical mirror. The same instrument may be used to evaluate flat mirrors ($r \approx \infty$) and parabolic surfaces. For parabolic surfaces care must be exercised since surface curvature is a spatially dependent variable and technically is not a valid parameter for description of paraboloids. The spherometer could be used for pass/fail evaluation of parabolic surfaces as long as the measurement was performed at corresponding points on each reflector.

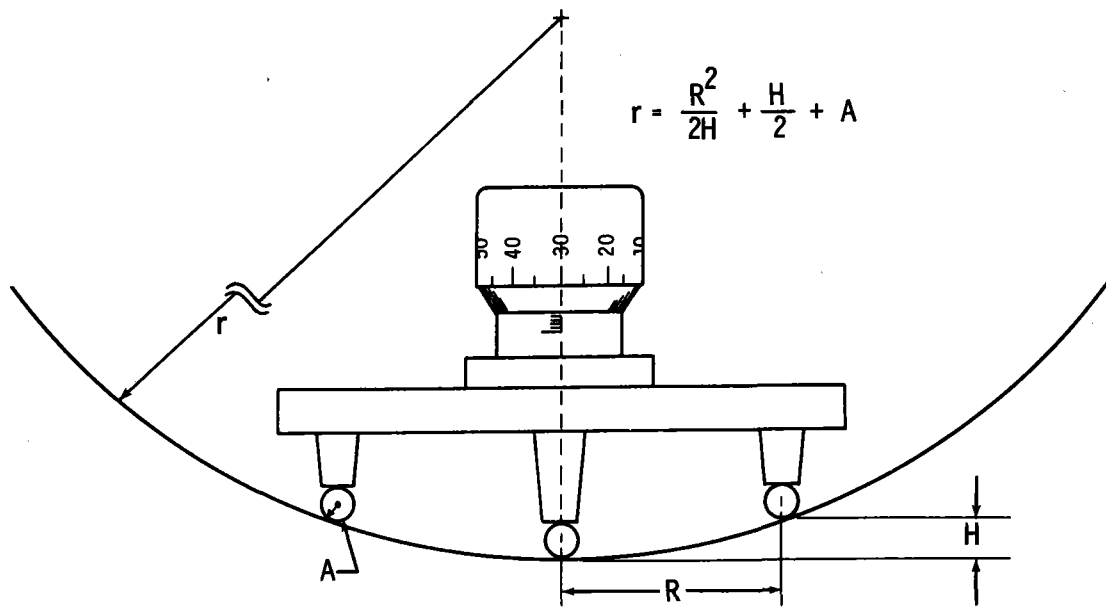


FIGURE 31. Spherometer for Measuring Surface Curvature of Spherical Mirrors

Numerous other types of surface gauges can be pulled across surfaces to generate a one-dimensional substrate or superstrate height distribution. For example, capacitive probes may be used to produce a contactless surface figure indication. Because the probe-glass capacitance is a function of physical separation, gap dielectric properties, and glass surface composition, these parameters must be well characterized before a direct indication of surface figure can be obtained.

The basic shortcoming of mechanical evaluation of mirror surface figure is the requirement of either surface-probe contact or close proximity. Contact usually results in temporary or permanent surface deformation and/or surface damage. Mechanical evaluation of mirror facets in situ (i.e., mounted in the heliostat) is difficult and time inefficient requiring careful and consistent measurement procedures so that results are repeatable (i.e., so that the time dependence of the structural variables can be monitored).

f. Optical Profilometer (Poeth et al., 1979). A number of devices also exist for mechano-optical determination of surface contours of diffusely reflecting objects. The techniques discussed here primarily avail themselves of use in a laboratory environment since in general the optical component alignment is critical.

The most limited of the optical profilometer methods is the fiber-optic probe technique. Schematic representations of two types of fiber-optic proximity gauges appear in Figure 32. The fiber-optics gauge (Menadier et al., 1967) consists of adjacent illumination-detection fibers (contained within one bundle) coupled to a light source/photodetector system. The bundle end is placed in close proximity to the surface under test so that light reflected by the illuminated surface may be coupled back into the detector section fibers. The received intensity is indicative of the bundle face to test surface inter-separation distance. Maximum received intensity results when the fiber acceptance angle is filled and for commercial devices this maximum occurs for approximately 500 μm interseparation distance.

This style of fiber optics gauge finds use as a flat surface proximity gauge. However any variation in surface slope or reflectivity influences the reflected intensity value. Consequently a separate calibration is required for each material type to be evaluated. This gauge would not produce acceptable results for materials exhibiting curvature or reflectivity variation.

A variation on the fiber optic gauge is the fiber-optic lens gauge. The configuration of this instrument is identical to the previous device except for the introduction of an optical imaging element at the termination of the fiber bundle. The detector output of this instrument exhibits a sharp discontinuity when the test surface is located in the lens focal plane as seen in Figure 33. This is a result of illumination light re-entry into the illumination fibers rather than into the detection fibers. The presence of such a sharp null suggests the use of this device in a surface tracking instrument where contour measurements would be derived from a bundle face position encoder. Note that this gauge also suffers from inability to compensate for surface slope and reflectivity variations.

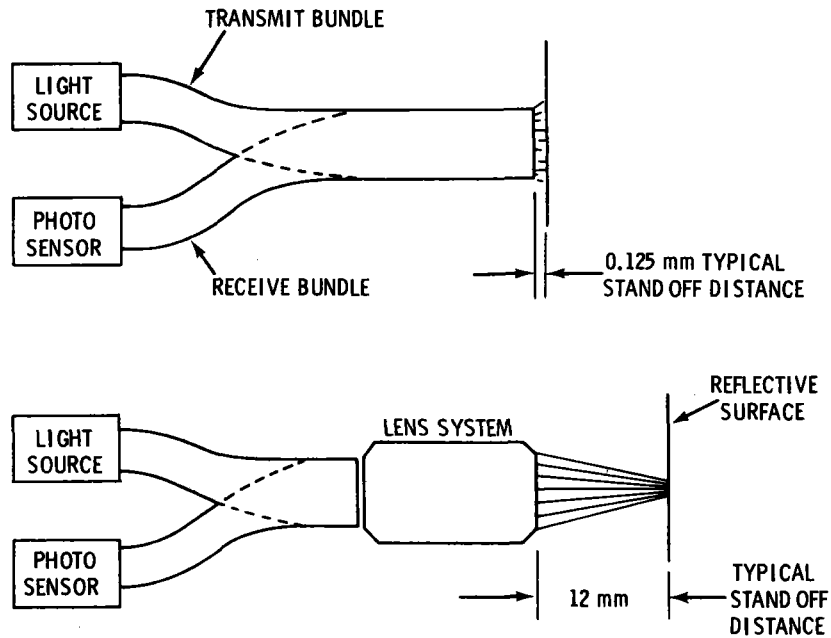


FIGURE 32. Fiber-Optic Proximity Gauges (Menadier et al., 1967)

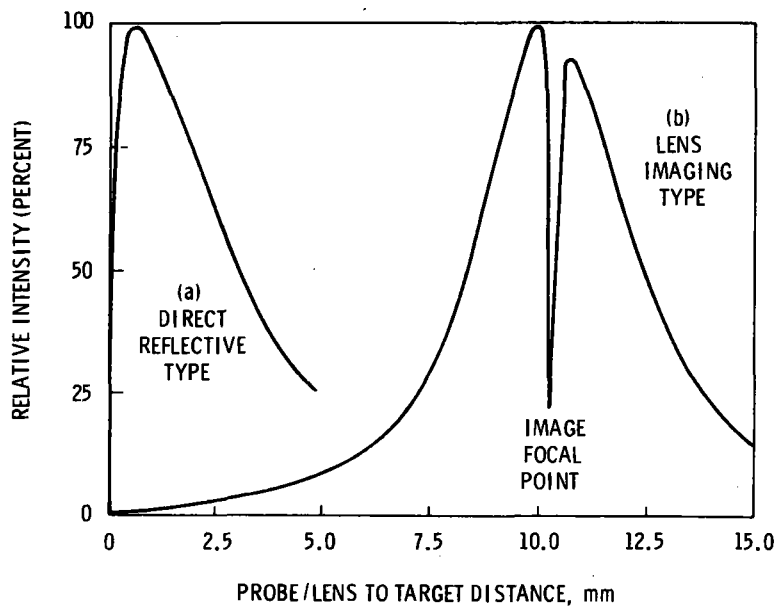


FIGURE 33. Calibration Curves for Fiber-Optic and Fiber-Optic/Lens Proximity Gauges (Poeth et al., 1979)

A technique which surmounts the sensitivity to variations in surface reflectivity (but not the variational slope problem) was suggested by Kelly, et al. (1977). A schematic of the device appears in Figure 34. In the device the surface under test is illuminated by a focused light source. The reflected light is reimaged onto two detectors with differing aperture stops, one allowing wide and another allowing a narrow collection cone angle. The outputs from the two detectors are passed through a divider stage producing a ratio independent of surface reflectivity variation. The prototype optical system is reported to have an accuracy of 0.05 mm over a 14-mm range when an $f/2.6$ imaging lens is incorporated. Use of a slower lens would result in greater accuracy and decreased range.

Another alternative is the technique of optical triangulation. The basis for a triangulation method suggested by Waters (1978) appears in Figure 35. During measurements a light beam is focused onto the test surface and the illumination spot is focused via an auxiliary lens onto a detector located at a deviation angle θ from the illumination axis. For displacement of the test surface along the illumination axis an apparent lateral displacement, ϵ , of the spot image occurs in the focal plane of the objective lens. The displacement of the spot is given by

$$\Delta\epsilon \approx - \left(\frac{f}{L_0 - f} \right) \Delta x \sin \theta \quad (32)$$

indicating that the spot displacement is related linearly to the test surface height variation. The amount of translation may be evaluated with a linear array or linear potentiometric detector. This sensing configuration may also be coupled to a nulling circuit and utilized on a measurement head. The basis of the nulling circuit is a photovoltaic bi-cell detector configured so that both halves experience equal illumination when the test surface is contained in the reference image plane. Displacement of the test surface from this plane results in unequal illumination of the bi-cell components resulting in a difference signal which may be utilized to return the test point (via a translation mount) to the reference plane. Shaft encoders may be used to

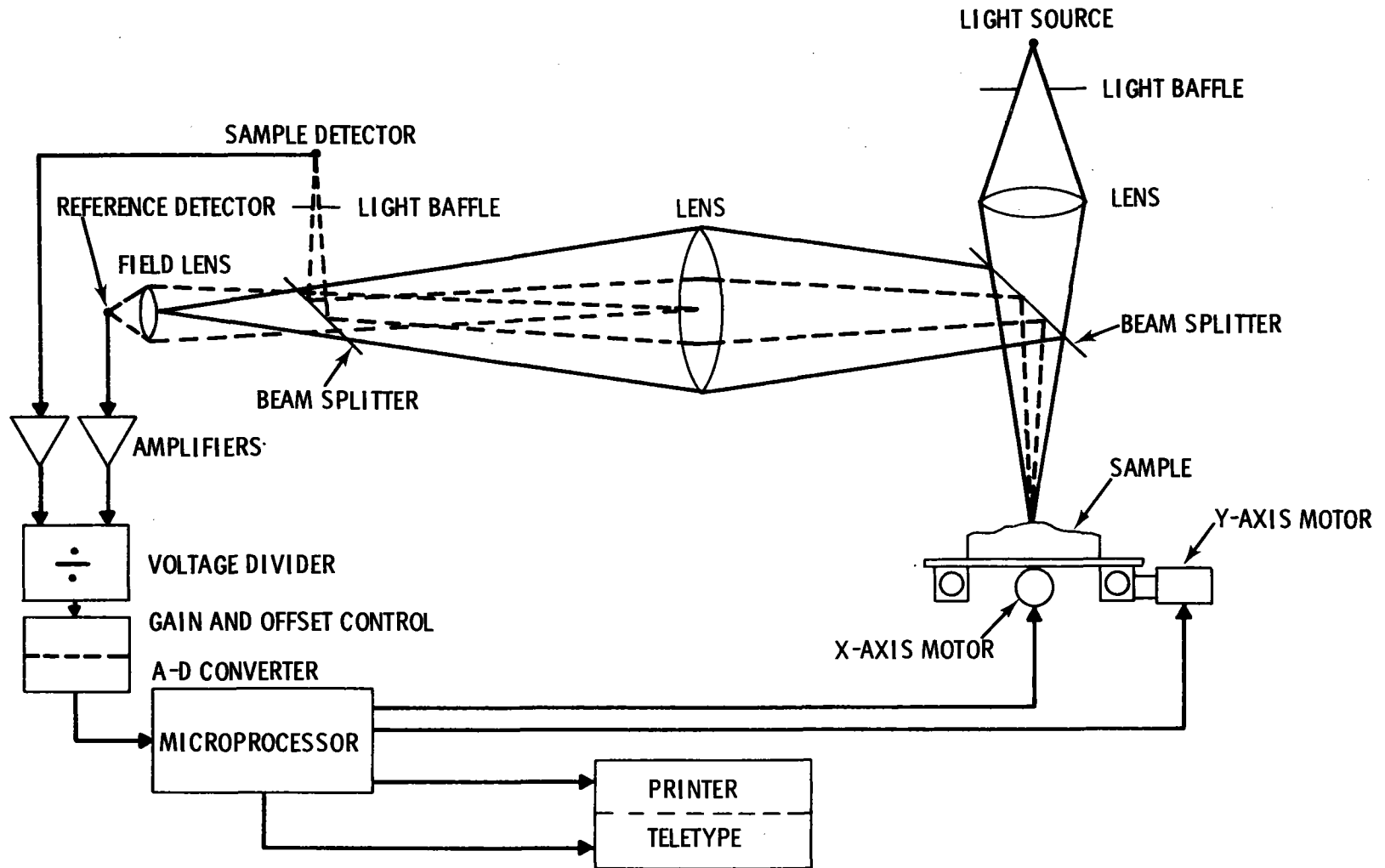


FIGURE 34. Scanning Optical Profilometer (Kelly et al., 1977)

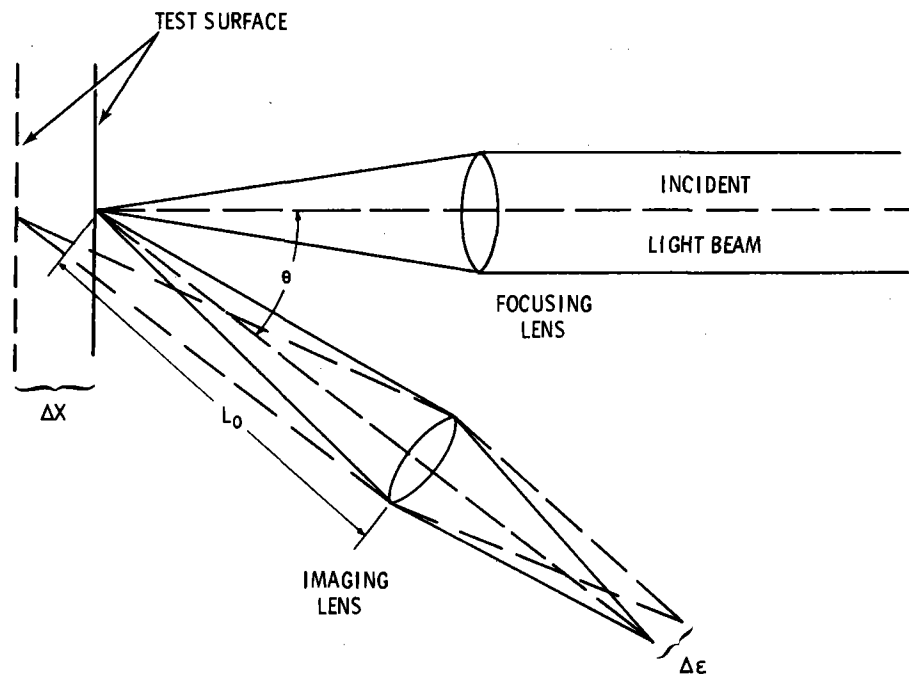


FIGURE 35. Optical Triangulation Profilometer (Spatial Detection Method) (Waters, 1978)

record the necessary mount displacement thereby indicating surface figure. Experimental accuracy of $6 \mu\text{m}$ has been reported for the above system configuration (Waters, 1978).

A modification of the spatial triangulation method discussed above is the temporal technique described by Indebetouw (1979). A schematic of the system appears in Figure 36. In this version a laser beam is scanned across the object while another is swept across a reference surface. The two spots are imaged through a slit onto a detector by an auxiliary lens. As the beams are scanned across the two surfaces their images produce sequential voltage pulses at the detector output. The time lag between these pulses is given by

$$\omega\Delta t = \cotan^{-1} \left[\tan \theta - XP/L \cos \theta (P-Z) \right] - \cotan^{-1} \left[(L \sin \theta - X)/(L \cos \theta - Z) \right]. \quad (33)$$

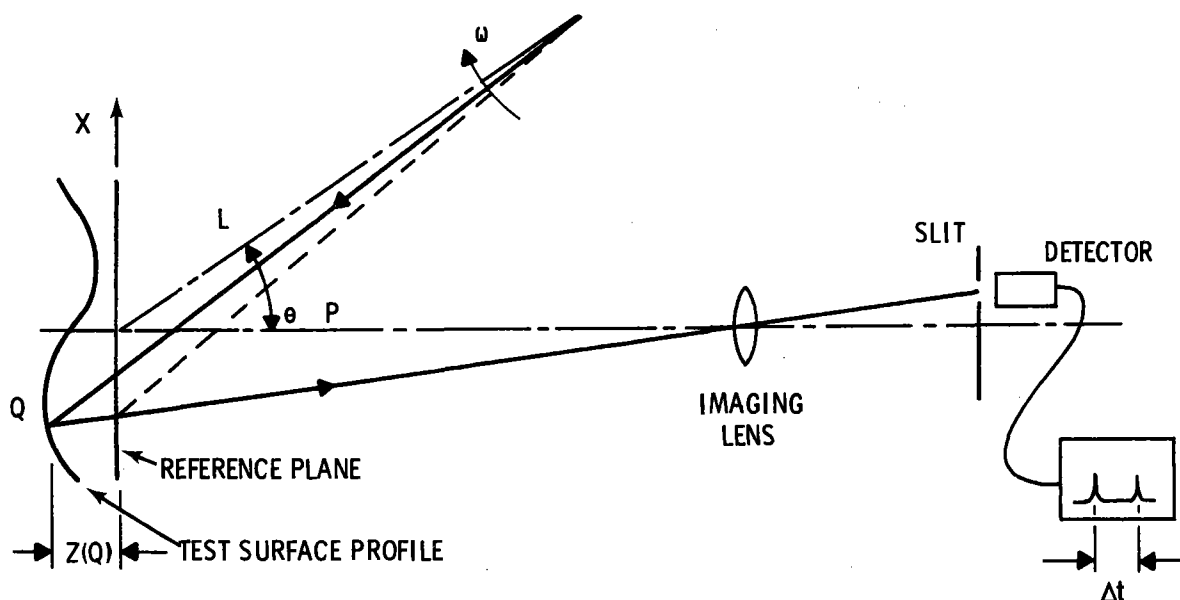


FIGURE 36. Optical Triangulation Profilometer (Temporal Detection Method) (Indebetouw, 1979)

Improvement of the method results if separate detectors view the image spot through a Ronchi ruling thereby producing phase shifted square waves. The time interval between pulses is then obtainable by phase measurement techniques. Theoretical spatial resolution of the above system is $7 \mu\text{m}$; however, experimental usage has indicated $50 \mu\text{m}$ is achievable. Note that if the illumination beam has a large depth of focus, contour measurements are possible without sample translation. For the case of an unfocused laser beam a spatial resolution of 1mm would be realistic.

g. Beam Characterization System. The beam characterization system (BCS) and image characterization system (ICS) have been discussed previously in the context of their use for specularly evaluation. As stated earlier the basis for these techniques is that overall focused beam quality (intensity, distortion, contrast, etc.) or solar image quality is a function of heliostat pointing error, facet reflectivity, facet specularly, and facet figure. The basic unexplored problem is the separation and quantization of figure and specularly independently. Since both figure and specularly error will

generally manifest themselves by producing a statistical spread in beam divergence, assignment of specific error magnitudes is difficult if not impossible. However, in those cases where the combined error is satisfactory, the technique allows nearly instantaneous examination of beam degradation for a given mirror.

h. Interferometry. By far the most elegant method of determining surface figure of reflective surfaces is by interferometric techniques. The variations of the interferometric devices and methods are proliferous requiring a truncation of this discussion after a brief introduction to several options. The discussion which follows is largely a description of laboratory techniques, some of which would require an extensive modification and/or development effort for field use.

1. Newton Interferometer. The most basic of the interferometric techniques for surface figure evaluation utilizes the Newton interferometer. For the purposes of this discussion, two surfaces in contact illuminated by monochromatic light constitute a Newton interferometer. Applied to the evaluation of plane mirrors the procedure produces a comparison between the test surface and a standard optical flat, i.e., this method indirectly displays the interstitial air gap thickness between the reference and test surface. A schematic of the experimental arrangement appears in Figure 37. The monochromatic radiation source is a Na vapor lamp. As an illustration, the fringe pattern produced between two optical flats for a wedge air gap appears in Figure 38. The distance, d , between two consecutive bright or dark fringes is given by

$$d = \frac{\lambda}{2\alpha} \quad (34)$$

where α is the wedge angle between the flats. For a spherical test surface and a planar reference surface the interference pattern takes the form shown in Figure 39. The distance of the n th dark fringe from the center for a mirror of radius of curvature, R is given by

$$x_n = \sqrt{nR\lambda} . \quad (35)$$

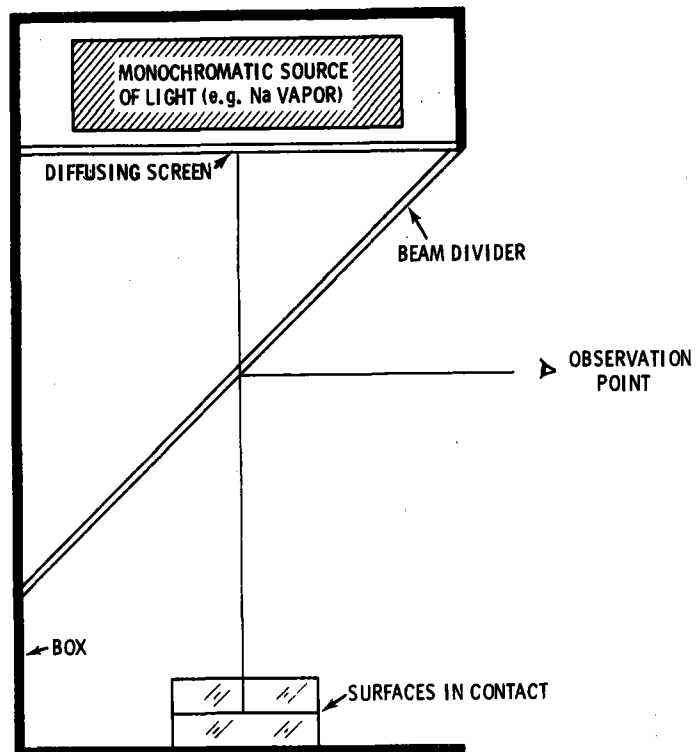


FIGURE 37. Optical Arrangement for Observation of Newton Fringes (Malacara, 1978)

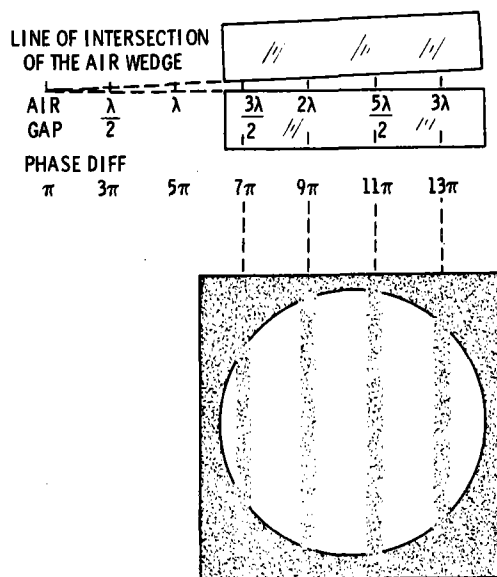


FIGURE 38. Fringe Formation Due to Wedge Air Gap Between Optical Flats (Malacara, 1978)

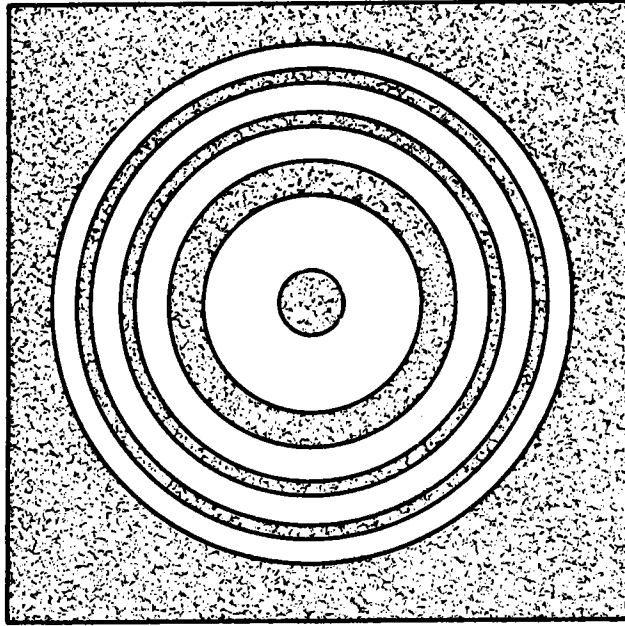


FIGURE 39. Fringes Formed by Air Gap Between Spherical Surface and Optical Flat (Malacara, 1978)

From this it is easily shown that the distance between the $(n+1)^{\text{th}}$ and n^{th} fringe is

$$X_{n+1} - X_n = \sqrt{R\lambda} (\sqrt{n+1} - \sqrt{n}) . \quad (36)$$

A summary of the fringe configuration formed by a reference flat in contact with test surfaces of differing geometries is illustrated in Figure 40.

The fringe visibility is a function of several factors, the most important of which is a reflectivity match between the test and reference surfaces. For this reason, for the evaluation of specular surfaces the reference flat should be coated with a thin evaporated film of chromium or inconel to produce a reflectivity of 30 to 40%. The result is an interferogram with high contrast, high visibility fringes.

Since the fringe spacing is indicative of the air gap spatial thickness variation, this method may be used to generate contours on the test surface.

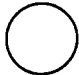

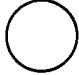












SURFACE TYPE	APPEARANCE OF THE NEWTON'S FRINGES	
	WITHOUT TILT	WITH TILT
PLANE		
ALMOST PLANE		
SPHERICAL		
CONICAL		
CYLINDRICAL		
ASTIGMATIC (CURVATURES OF SAME SIGN)		
ASTIGMATIC (CURVATURES OF OPPOSITE SIGN)		
HIGHLY IRREGULAR		

FIGURE 40. Configuration of Newton's Fringes for Various Test Surface Geometries (Malacara, 1978)

While this is a relatively straightforward display for optical quality surfaces (low fringe spatial frequency) poor surfaces cause rapid spatial phase variation producing fringes of excessive frequency thereby complicating contour interpretation. However this characteristic does allow laboratory determination of time-dependent microscopic figure deformations of heliostat component facets via interferogram comparison. It is important to note that the surface contour being generated is for the top glass surface. While this is satisfactory for first surface mirrors, it will not characterize the reflective surface of back coated mirrors. If the coherence length of the illumination source is sufficient, multiple extraneous contours appear as a result of front and back surface test mirror reflections. Also, any phase variation due to inhomogeneity of the mirror superstrate will be manifested as

a perturbation of the fringe contour. In summary then, the Newton interferometer is an excellent instrument for rapid qualitative evaluation of curved or planar first surface reflectors. The instrument cost is low, being largely comprised of the expense of the reference optical flat.

2. Multiple Beam Interferometers. The basis for the use of multiple beam interferometers for optical component evaluation and testing is that a wavefront upon reflection from an optical element will contain information as to the physical shape of the reflective surface. For example a plane incident wavefront upon reflection from any surface except that of a perfect plane mirror will no longer be planar. The wavefront phase deformation is extracted by addition of an additional well characterized wavefront producing a "fingerprint" intensity distribution in the observation plane. The number of variations (i.e., interferometer types) on the above principle is large and only a few are summarized below.

A typical dual pass interferometer of the Twyman-Green type appears schematically in Figure 41. Note that the compensator plate is not required if laser illumination is utilized. When properly aligned, the interference pattern appears much the same as that for the previously described Newton interferometer. This device is extremely useful for the examination of phase objects (e.g., glass samples proposed for use as mirror super- or substrates) and a sample interferogram of a glass plate appears in Figure 42. The optical path difference, d , introduced by the glass plate can be expressed as

$$d = 2(N-1)t \quad (37)$$

where N is the refractive index of the glass plate and t is its thickness. If the interferometer arms are aligned so as to display a constant intensity profile (no fringes) before introduction of the test glass plate then all fringes which appear after its introduction are due to the plate. If the image field is unaltered it is implied that the quantity $(N-1)t$ is constant

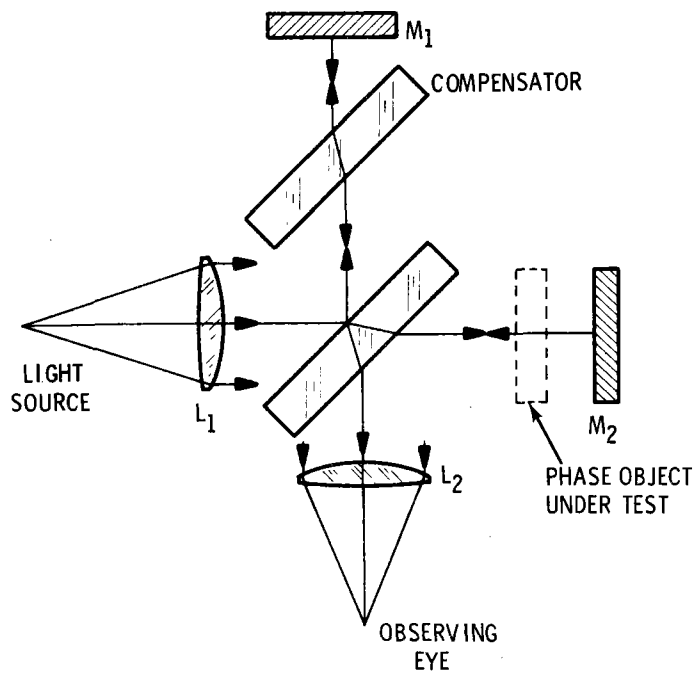


FIGURE 41. Twyman-Green Interferometer (Malacara, 1978)

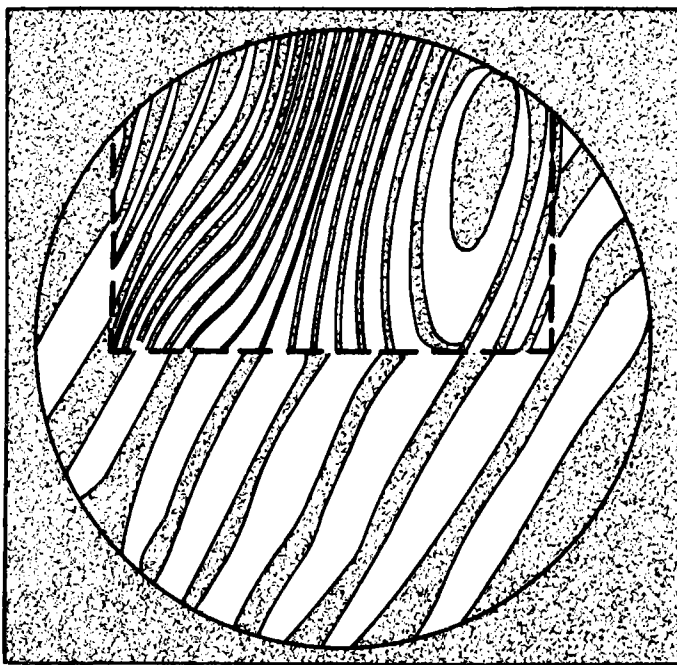


FIGURE 42. Analysis of Glass Plate with Twyman-Green Interferometer (Malacara, 1978)

over the plate. If straight fringes are observed then the glass is homogeneous with a wedge angle ϵ between its two faces. The wedge angle ϵ is given by

$$\epsilon = \frac{\alpha}{2(N-1)} \quad (38)$$

where α is the angle between the two interfering wavefronts given by

$$\alpha = n\lambda \quad (39)$$

where n is the number of observed interference fringes per unit length in the image plane. Distorted fringes are indicative of glass thickness variation and/or variation in the glass index since the only quantity determinable is $(N-1)t$.

To clarify whether the fringe variation is the result of either an index or thickness variance an independent measurement of Nt is required. An interferometer capable of measuring the Nt product for phase objects is the Fizeau interferometer diagrammed in Figure 33. In the arrangement illustrated the device is being utilized for evaluation of the first surface of a test flat or mirror. Instrument alignment is accomplished by adjusting the reference and test surfaces to produce coincidence of the auto-collimated point source images. During fringe observation the diverging lens is inserted to allow expansion and overlap of the reference and test surface reflected wavefronts. For analysis of phase objects the right hand side of the interferometer is modified as shown in Figure 44. It is recommended that to avoid extraneous fringes, the test plate should be sandwiched between two optical flats using an index matching oil. This removes fringe variation due to sample surface flaws. If the spatial deviation of the observed fringes from straightness is denoted as k and the spacing between adjacent fringes is d , then the optical path difference is given by $(k/d)\lambda$. Therefore the optical path difference for an index variation ΔN and thickness t is expressed as $2\Delta Nt$ and

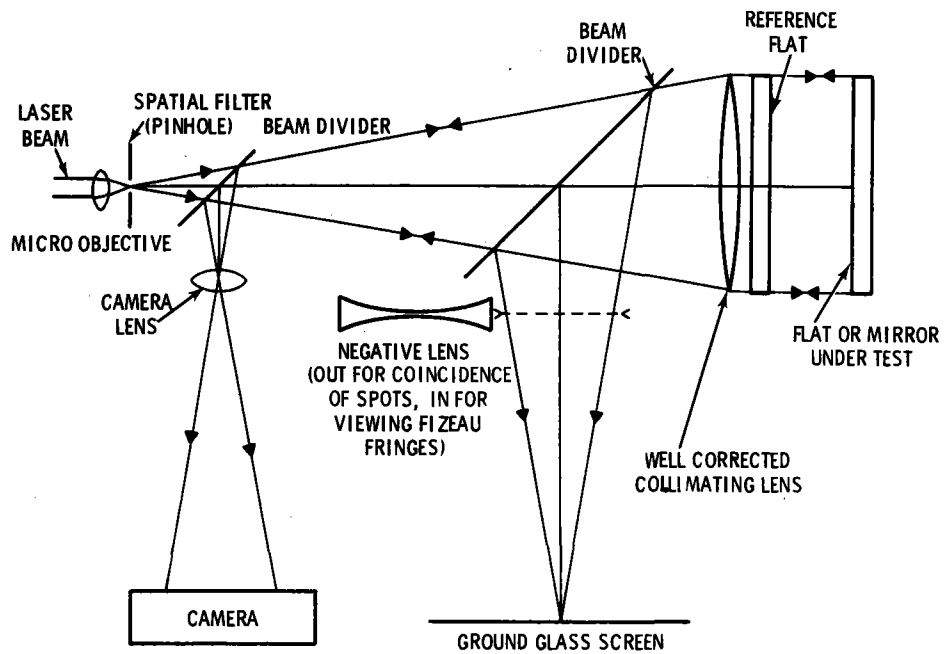


FIGURE 43. Laser Illuminated Fizeau Interferometer (Malacara, 1978)

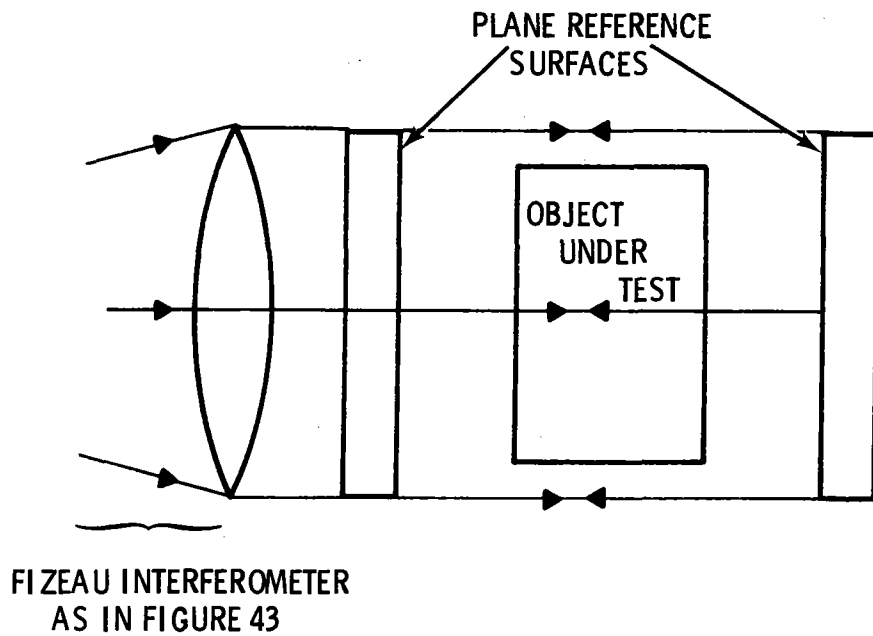


FIGURE 44. Modification of Fizeau Interferometer for Analysis of Phase Objects (Malacara, 1978)

$$\Delta N = \left(\frac{k}{d}\right) \left(\frac{\lambda}{2t}\right) \quad \text{or} \quad \Delta N t = \frac{k\lambda}{2d} . \quad (40)$$

Therefore with this knowledge and the data from a Twyman-Green measurement the varying parameter ΔN or Δt may be ascertained for glass samples.

Another class of interferometer useful for wavefront deformation measurements on either phase or reflective optics is the lateral shearing type. In the lateral shearing interferometer the perturbed sample illumination wavefront is displaced laterally by a small amount and an interferogram is obtained between the original and displaced wavefronts. For nearly planar wavefronts, the lateral shear is produced by displacement of the wavefront in its own plane.

A basic illustration will more clearly demonstrate the principles. Figure 45 depicts the geometries of the original and laterally sheared wavefronts. Since the wavefront is nearly plane the wavefront errors may be expressed as small deviations from this plane, i.e., the wavefront error may be denoted by $W(x,y)$ where x,y are the coordinates of wavefront point P . For a shear displacement s along the x axis, the wavefront error at the same point for the sheared wavefront is $W(x-s,y)$. The path difference ΔW thereby introduced at P between the sheared and original wavefronts is $[W(x,y) - W(x-s,y)]$. This demonstrates that in lateral shearing interferometry the quantity ΔW is the determined parameter. Note that for zero shear (i.e., $s = 0$) no error may be seen no matter how large. The optical path difference is obtainable from discrete points on the wavefront by application of the relation

$$\Delta W = n\lambda \quad (41)$$

where n is the fringe order and λ is the illumination wavelength. Note that Equation 41 may be written as

$$\left(\frac{\partial W}{\partial x}\right) s = n\lambda . \quad (42)$$

This demonstrates that the information obtainable from the lateral shearing interferometer is angular ray aberration.

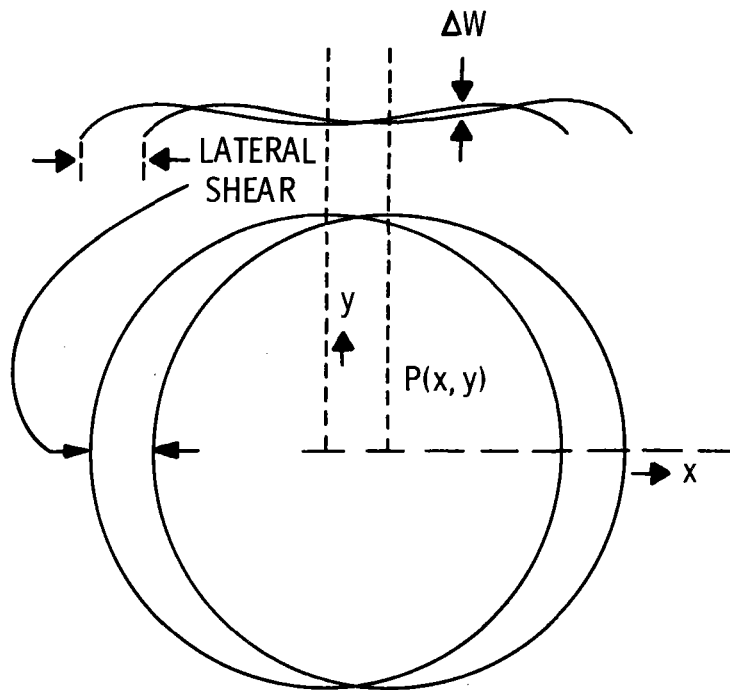


FIGURE 45. Sheared Wavefront Geometry (Malacara, 1978)

A lateral shearing interferometer of the parallel plate type appears in Figure 46. This particular optical arrangement is amenable to figure testing of concave (e.g., spherical) mirrors of varying size. An arrangement for analysis of phase objects (e.g., mirror substrates) is depicted in Figure 47. An interferogram produced by a wavefront exhibiting primary spherical aberration ($W(x,y) = A(x^2 + y^2)^2$) is illustrated in Figure 48.

3. Holographic Interferometry. The ability of a hologram to record phase information for incident wavefronts makes it an important tool for the figure evaluation of optical elements. A brief discussion of two aspects of the holographic technique follows.

The optimum setup for a holographic optical evaluation procedure is essentially the same as that for the analogous interferometer arrangement. Note that so as not to exceed the resolution limit of the recording medium (e.g., photographic film) the included angle between reference and object

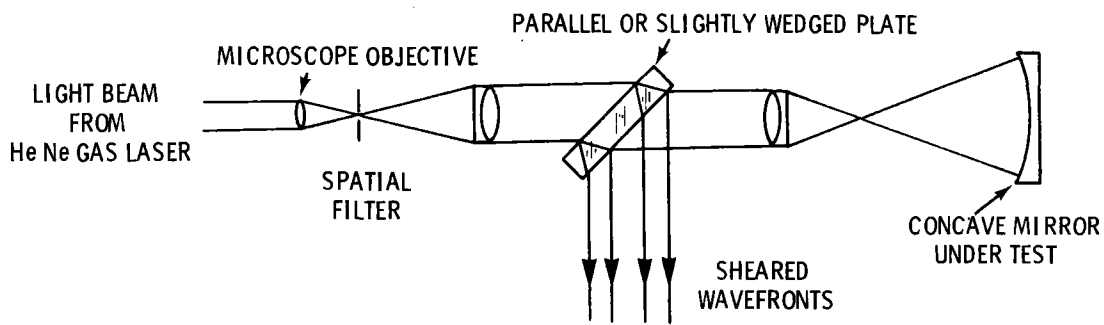


FIGURE 46. Parallel Plate Interferometer for Evaluation of Concave Mirrors (Malacara, 1978)

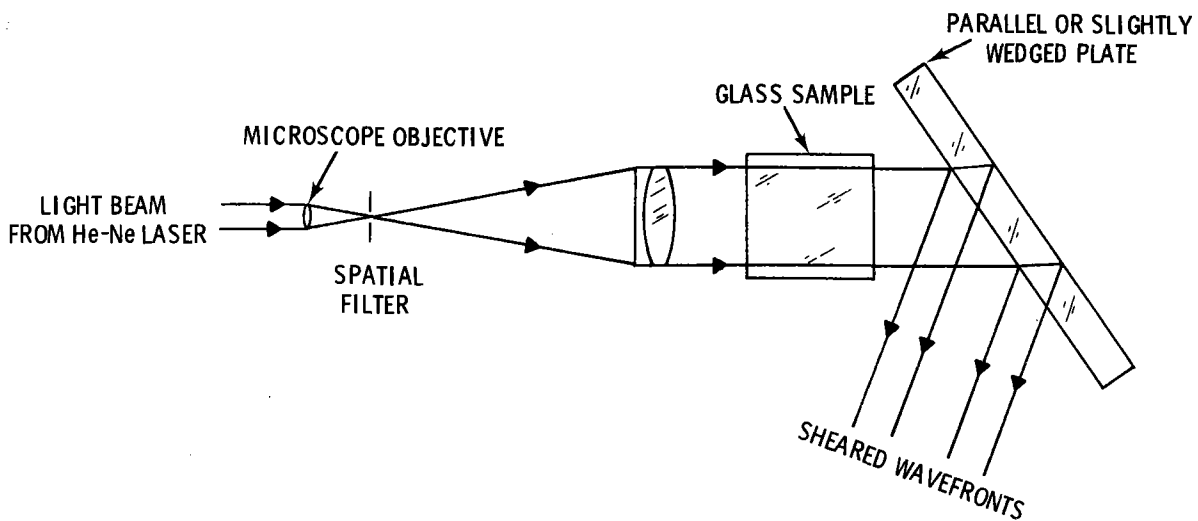


FIGURE 47. Parallel Plate Interferometer for Evaluation of Phase Objects (Malacara, 1978)

beams should be made as small as possible, typically a few degrees. A modified Twyman-Green interferometer for holographic evaluation of concave mirrors appears in Figure 49. A continuous wave laser is used to expose the hologram, although in time variant situations, a pulsed laser may prove advantageous. The information recorded at the hologram is the wavefront intensity and phase variation produced by the laser illuminated mirror. This wavefront can be recorded and analyzed at some later time utilizing the Foucault knife edge

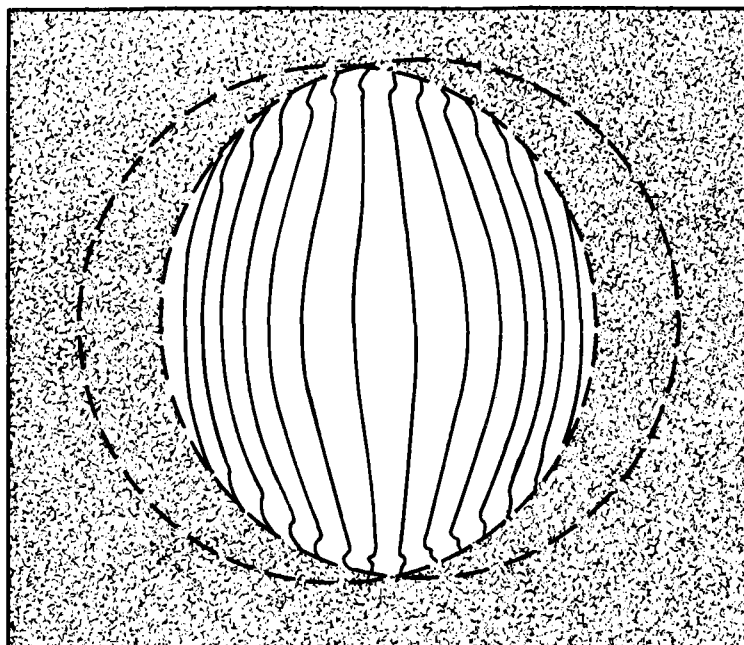


FIGURE 48. Interferogram Produced by a Wavefront Exhibiting Primary Spherical Aberration (Malacara, 1978)

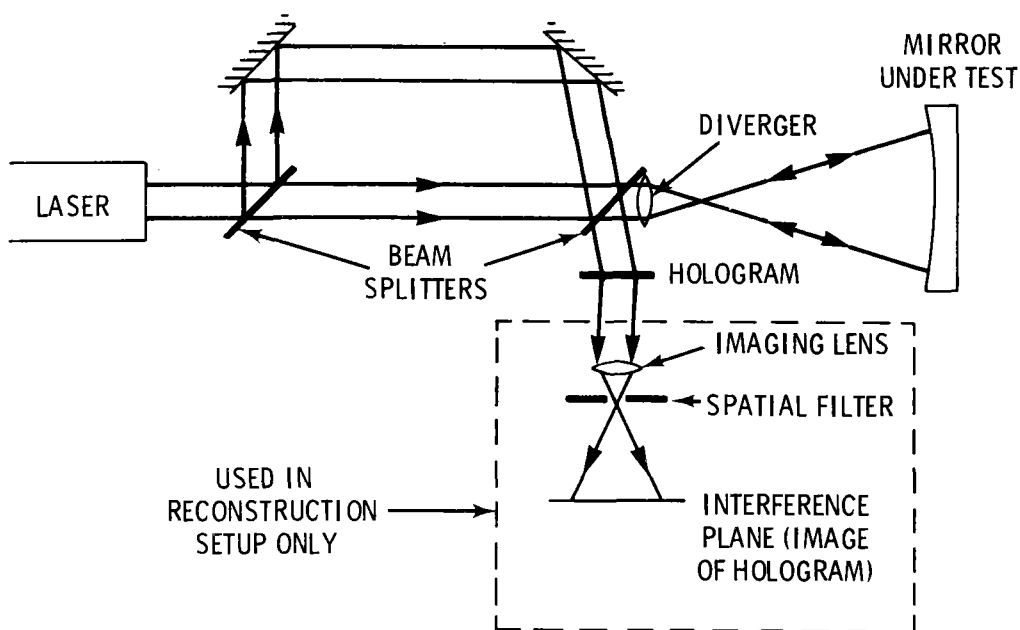


FIGURE 49. Modified Twyman-Green Interferometer for Holographic Evaluation of Concave Mirrors (Malacara, 1978)

test setup depicted in Figure 50 or with the interferometric technique illustrated in Figure 51. The primary sources of error in the holographically reconstructed wavefront technique are a result of 1) differences between the optical recording and reconstruction geometries, 2) deformation of the recording medium, and 3) aberrations introduced by inhomogeneity of the recording material substrate. These problems may be overcome if careful selection of the recording geometry and recording material precede the holographic exposure process.

Variants on the holographic process such as "real-time" and "double-exposure" techniques also find application to the figure evaluation of reflective surfaces. An experimental arrangement for implementation of the "real-time" method appears in Figure 52. In this particular scenario the setup is being utilized to monitor the surface figure of an unworked mirror blank. A hologram is first made of the test surface. After processing, the hologram is

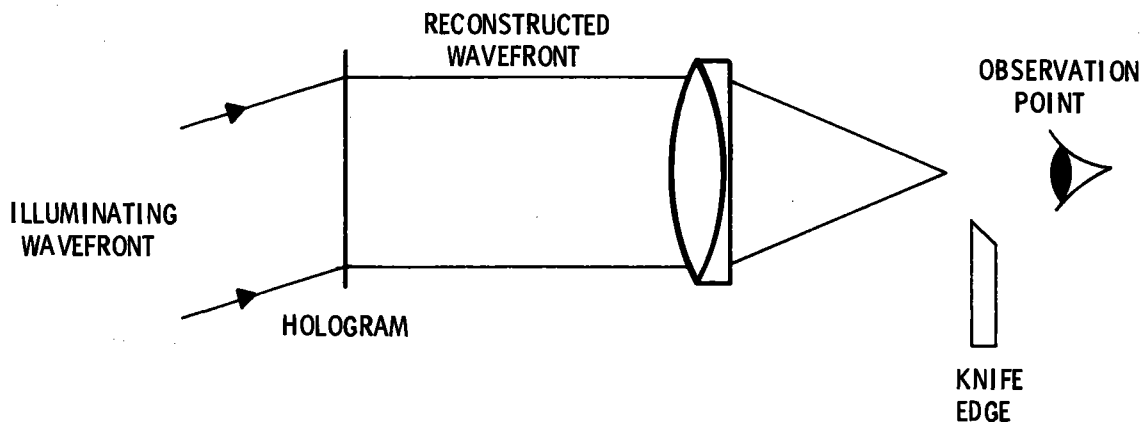


FIGURE 50. Foucault Knife Edge Test for Evaluation of Holographically Reconstructed Wavefront (Malacara, 1978)

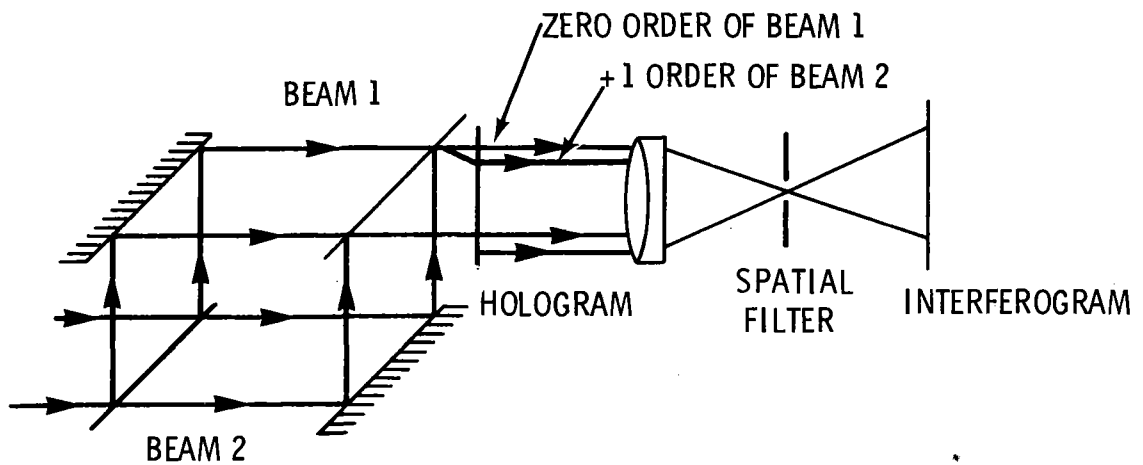


FIGURE 51. Interferometric Evaluation of Holographically Reconstructed Wavefront (Malacara, 1978)

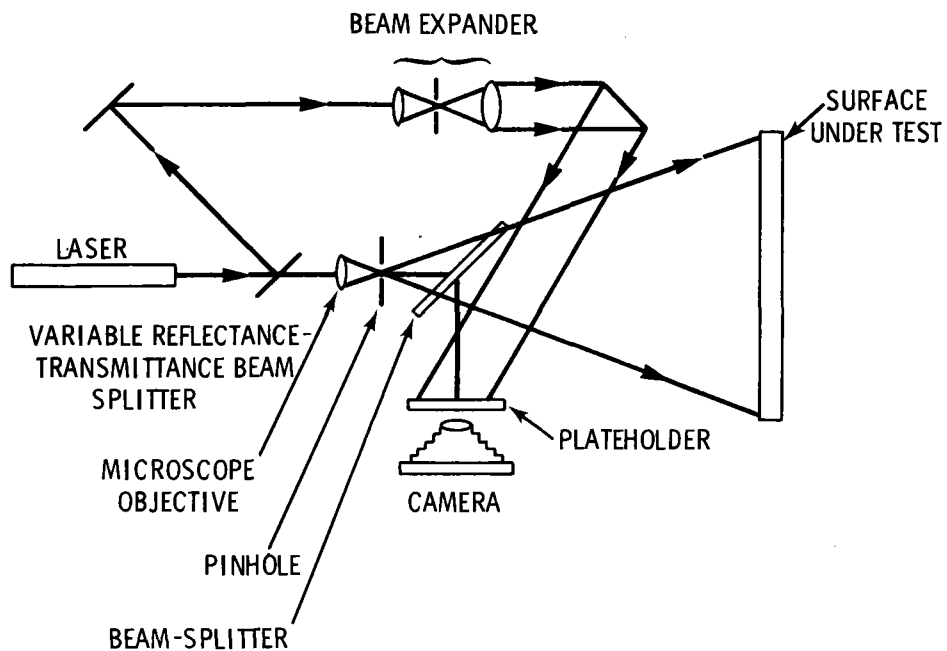


FIGURE 52. Experimental Arrangement for Production of Real-Time Holographic Interferograms (Malacara, 1978)

replaced in its original position. If the test object's shape is unaltered, interference of the real and holographic wavefronts will produce an image of the surface with a single interference fringe across its spatial extent. If the test surface is now deformed, for instance by mechanical loading or temperature gradients, interference fringes will appear which will allow calculation of the perturbed surface shape. For the on-axis arrangement depicted in Figure 52, each interference fringe interval is indicative of a half-wavelength surface deformation in the illumination and viewing direction.

The disadvantage of this test technique is that the surface to be monitored should be a diffuse reflector. While this requisite excludes the method from use as a plane mirror figure evaluation technique, it can be used to monitor substrate deformation under mechanical or thermal loading. For the testing procedure it would be necessary to coat the substrate surface with a retroreflective paint (e.g., Codit reflective liquid).

4. Speckle Techniques. The speckle characteristic of laser illuminated objects is also useful from the standpoint of a possible technique for mirror figure evaluation. Bahuguna, et al. (1979) have studied the effect of spherical aberration in optical elements on the laser speckle distribution in the marginal, least confusion, paraxial, and defocused planes. While their investigation was performed with lens elements (plano-convex), the possibility exists for the use of this technique for reflective elements. The experimental arrangement appears in Figure 53. The illumination spot size on the diffuser is adjustable by varying the beam expander-diffuser separation distance. Observation indicates that for an imaging geometry, the speckle size and shape are aberration dependent, provided the scattering spot dimension is less than the spatial extent of the point-spread function for the optical system. In the presence of spherical aberration the speckle pattern appears radially streaky. A set of photographs taken at various image planes for three spot sizes appears in Figure 54. This technique is easily extended for the evaluation of concave mirrors; however, implementation methods and quantitative evaluation algorithms will require a development effort.

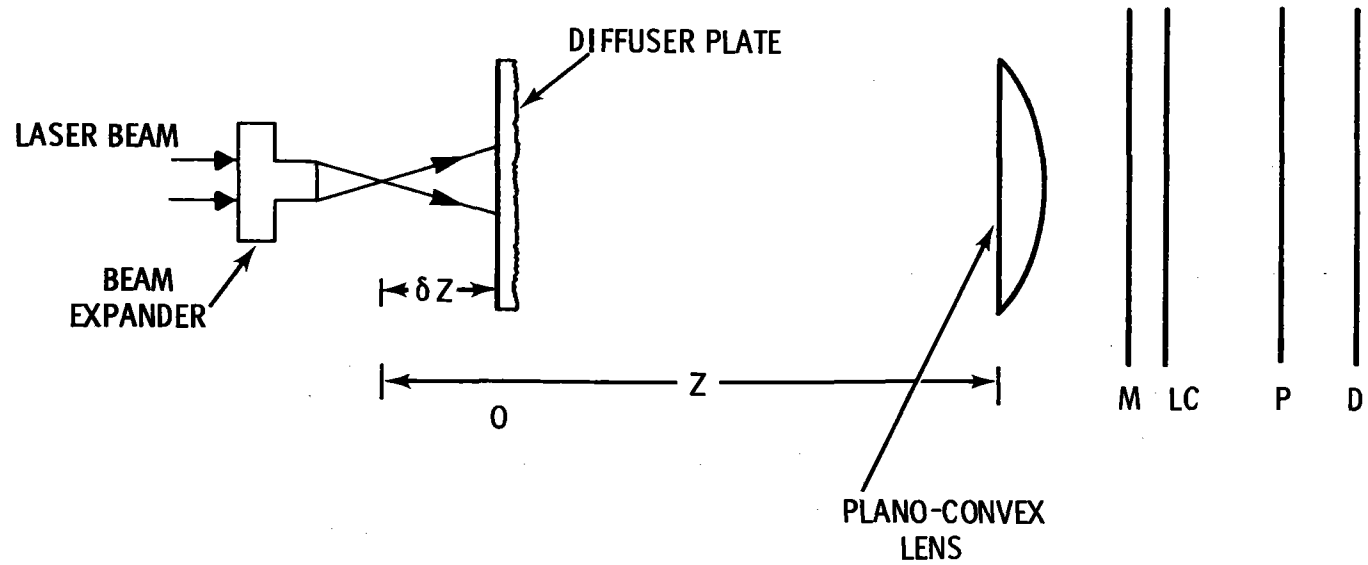
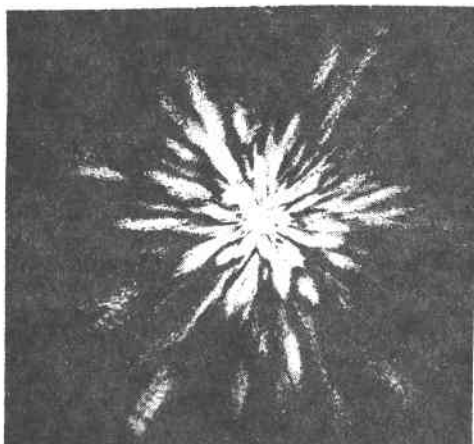
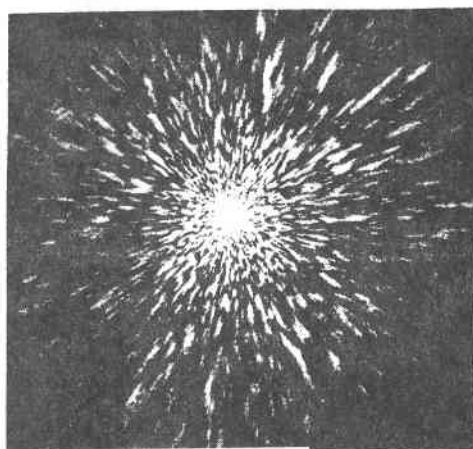


FIGURE 53. Experimental Arrangement for Study of Speckle Distribution in Image Planes of a Plano-Convex Lens (Bahuguna et al., 1979)

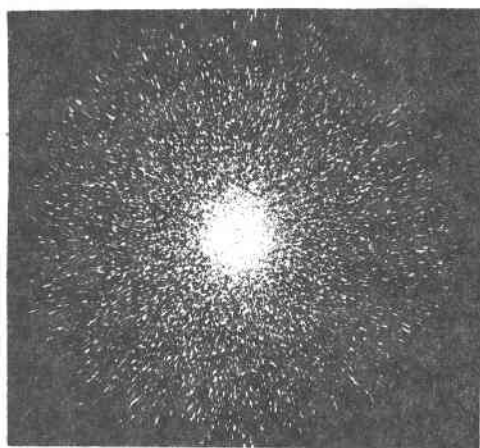
Paraxial Plane:



Angular Size Ω_1

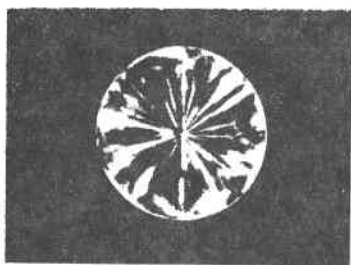


Angular Size Ω_2

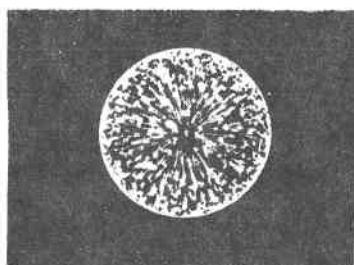


Angular Size Ω_3

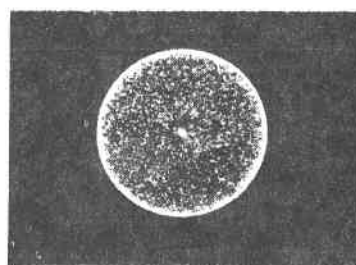
Marginal Plane:



Angular Size Ω_1



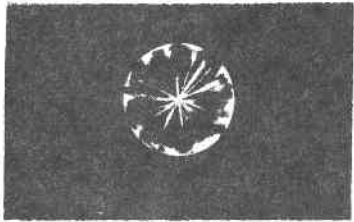
Angular Size Ω_2



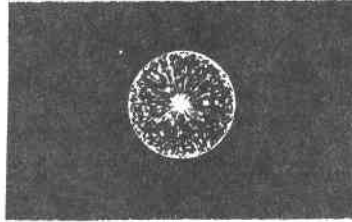
Angular Size Ω_3

FIGURE 54. Speckle Patterns in the Paraxial, Marginal, Least Confusion and Defocused Planes for Three Diffuser Spot Sizes (Angular, Diameters $\Omega_1 = 1.9 \times 10^{-4}$ rad, $\Omega_2 = 4.9 \times 10^{-4}$ rad, $\Omega_3 = 24.7 \times 10^{-4}$ rad)

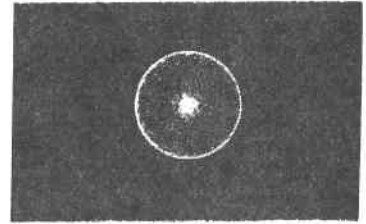
Least Confusion Plane:



Angular Size Ω_1

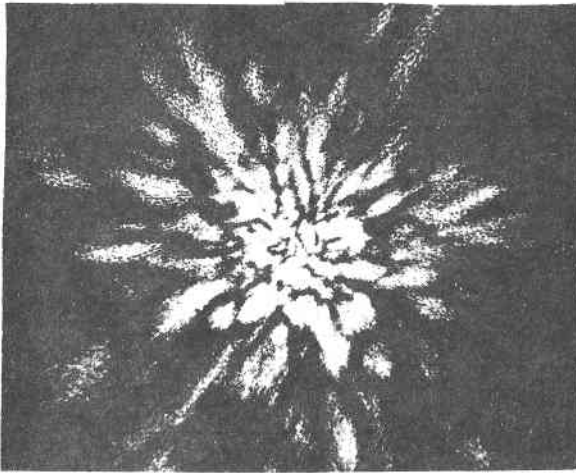


Angular Size Ω_2

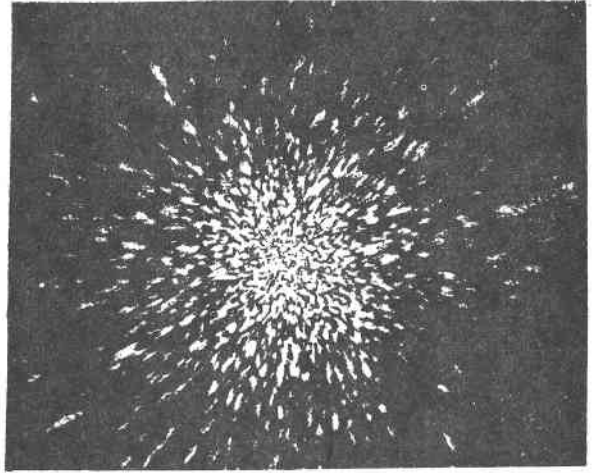


Angular Size Ω_3

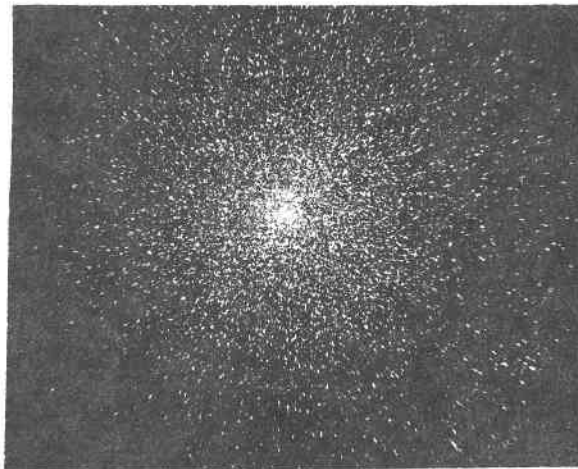
Defocused Plane:



Angular Size Ω_1



Angular Size Ω_2



Angular Size Ω_3

FIGURE 54. (Continued)

Hildebrand^(a) has suggested the use of speckle photography for measurement of the mirror figure of concave facets (e.g., spherical, parabolic). A schematic of the experimental configuration for evaluation of a spherical mirror of radius R appears in Figure 55. A ground glass diffuser (D) and photographic plate (T) are placed in the converging beam of the laser illuminated mirror and an exposure is made. After translation of the diffuser-film packet a distance z, a second exposure is made. The resultant film image is that of an array of laser speckle pairs whose separation is a function of the initial distance from the optical axis. In general the pair separation, δ , is given by

$$\delta = \frac{\rho z}{R} \quad (43)$$

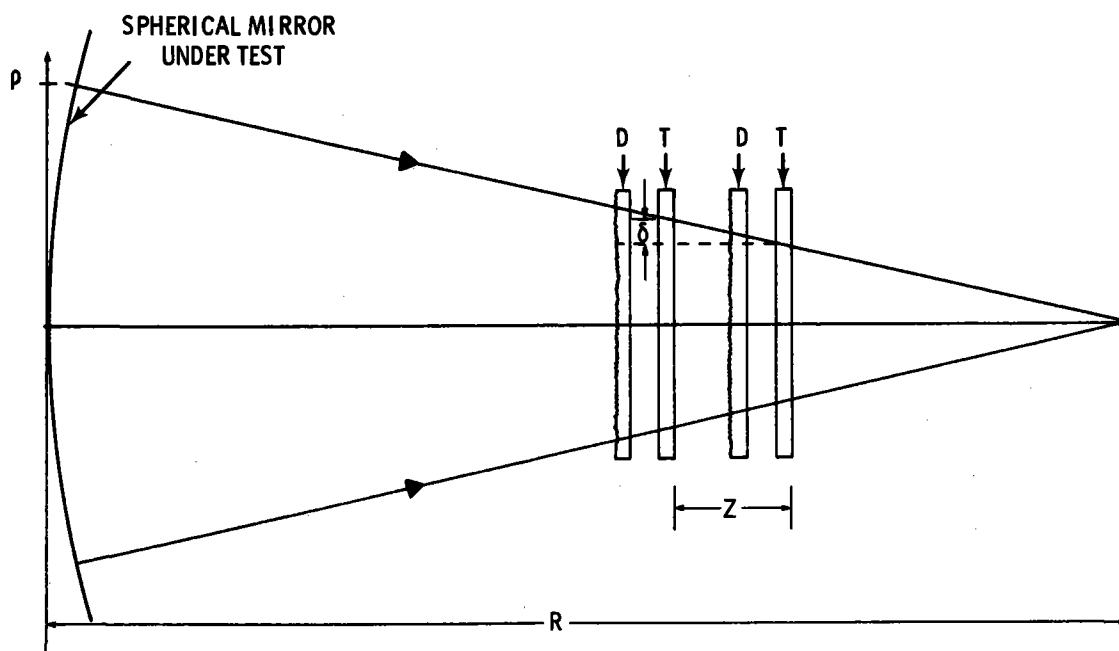


FIGURE 55. Experimental Configuration for Mirror Figure Evaluation by Speckle Photography (Hildebrand, 1979)

(a) Hildebrand, B. P., "Heliostat Mirror Figure Measurement by Speckle Photography", BNW Internal Report, 1979.

where ρ is the radial distance at the plane of the mirror. The speckle photograph is analyzed by projecting a small diameter laser beam through the developed emulsion. The resultant output intensity is that of the fringe distribution attributable to diffraction by adjacent pinhole apertures (Young's fringes). If the double exposure is Fourier analyzed there will be a local ring period, t_o , given by

$$t_o = \frac{1}{\delta} = \frac{R}{\rho z} . \quad (44)$$

The ring pattern is described by the expression for the Fresnel rings

$$|I(\rho)|^2 = 2|T(\rho)|^2 (1 + \cos \frac{\pi z}{R} \rho^2) . \quad (45)$$

If the mirror figure deviates from spherical the observed circular fringe pattern becomes unsymmetric. The deviation from sphericity may be expressed as an error in radius of curvature given by

$$\Delta R = \rho z \Delta t_o . \quad (46)$$

This indicates the possibility of spherical mirror evaluation by this technique. Further development may extend this technique to the evaluation of parabolic and plane mirrors.

The development of speckle techniques for the evaluation of mirror figure warrants further investigation and experimentation. While the above discussion indicates a limited applicability of the method (spherical optics) a minimal research effort may suggest a broader range of implementation scenarios.

3. Extension of Figure Assessment Techniques

The techniques discussed for the evaluation of heliostat mirror figure are largely laboratory techniques. For some cases, further development effort might result in portable apparatus for field mirror inspection. However in their present state of development the techniques described are useful for laboratory pretesting of unmounted mirror facets. The only scenarios at

present exhibiting field capability for evaluation of solar facility heliostat arrays are the Beam Characterization System (BCS) and the Image Characterization System (ICS). Further study is necessary to characterize the effects of figure perturbation on the intensity distribution at the circle of least confusion for the BCS and on the intensity distribution of the solar image for the ICS. If the effects of specularity and figure error are separable with these systems quantitative evaluation of error components would be possible. However, the problem of deconvolution is a nontrivial one.

III. CONCLUSIONS

The selection of the best techniques for general application to the heliostat measurement problem will involve a trade-off between the following four considerations: (1) Feasibility of field implementation of the technique via either a field laboratory or directly to the heliostat-mounted mirror facets, (2) accuracy of measurement method, (3) ease of data reduction, and (4) cost effectiveness of the technique.

Most of the evaluation methods discussed in this report will require a substantial development effort either to make them field worthy or to adapt them specifically to the heliostat mirror facet measurement problem. The present status of the evaluation techniques now available is summarized below.

1. Feasible Techniques for the Field Evaluation of Solar Reflectivity of Solar Facility Heliostat Mirrors
 - a. Portable Bi-Directional Reflectometer - This instrument will require a minimal development effort for field implementation. Field accuracy and reliability have yet to be determined.
 - b. Portable Specular and Hemispherical Reflectance Instruments - These instruments exist. Further investigation is necessary to disclose accuracy and field reliability of these devices.
 - c. Beam Characterization and Image Characterization System - The ability of these techniques to evaluate mirror solar reflectivity is unknown. The evaluation of this ability will require a research effort.
2. Feasible Techniques for the Field Evaluation of the Specularity of Solar Facility Heliostat Mirrors
 - a. Portable Bi-Directional Reflectometer - This instrument will require minimal development effort for field implementation. Field accuracy and reliability have yet to be determined.
 - b. Beam Characterization and Image Characterization Systems - The potential of these systems for in-field mirror specularity evaluation is high, but development of algorithms for

quantitative output will require a substantial experimental and theoretical research effort.

3. Feasible Techniques for the Field Evaluation of the Figure of Solar Facility Heliostat Mirrors
 - a. Laser Ray Trace - This is a possible technique for mirror prescreening and extended mirror deformation studies in a field laboratory environment. Advantages are low cost and ease of implementation.
 - b. Moiré Fringe Analysis - Preliminary investigation indicates the possibility of use of this technique in field laboratory and heliostat facet field applications. Further investigation is necessary to allow quantification of figure error from fringe pattern defects.
 - c. Image Evaluation - Interpretation of image defects requires further investigation. This technique is amenable to field laboratory implementation and with further investigation possibly to heliostat facet field evaluation.
 - d. Schlieren Method - This is primarily a field laboratory technique. Quantification and evaluation of the obtained data requires further development.
 - e. Optical Profilometer - Presently this is primarily a field laboratory technique. Extension of present instrumentation to analysis of specular surfaces will require further development. Variations on the discussed optical profilometry techniques via triangulation or phase modulation should be considered. Indeed extension of current methods may prove promising with a reasonable development effort.
 - f. Beam Characterization and Image Characterization Systems - The potential of these systems for in-field mirror figure assessment is high, but development of algorithms for quantitative output will require a substantial experimental and theoretical research effort.

- g. Interferometry Techniques - These techniques are primarily relegated to the field laboratory environment. With the exception of the Newton Interferometer (i.e., optical flat) the interpretation of the interferograms usually requires a lengthy data acquisition and reduction algorithm.

IV. RECOMMENDATIONS

This report demonstrates the inadequacy of contemporary optical testing methods for providing solutions to the heliostat mirror quality assurance problem. An extensive theoretical and experimental development program is required before routine implementation can be affected. All the techniques summarized in the previous section are basically extensions of routine laboratory procedures, and will require modification for field use. While modification of these techniques may prove fruitful, they should not be pursued to the exclusion of techniques based on different principles and new concepts.

There are at least four major deficiencies in the present analysis techniques. First, two quantities in need of evaluation (specularity and figure), have been only intuitively defined in the past and consequently have lacked quantification. This deficiency should be remedied. Second, the minute magnitude of specularity and figure errors encountered in "good" laboratory optics has resulted in a set of exacting evaluation procedures capable of detecting surface and figure flaws of fractional wavelength extent. However, insurance of the cost effectiveness of the solar power system program excludes such exacting manufacturing tolerances for the mass produced reflective elements. In short, the majority of current optical evaluation methods are too stringent. Third, the physical size of proposed heliostat facets greatly exceeds the dimensions amenable to evaluation by laboratory apparatus. The cost of scaling up the laboratory apparatus to accommodate the large facets is high, thus eliminating practical use of the techniques. Finally, the large reflector area associated with solar thermal power systems dictates the implementation of a high speed inspection system. Such a system for the evaluation of specular surfaces does not exist, either for manufacturing quality assurance or for field implementation. This basic deficiency will require a major development effort.

The development of programs for the quality assurance of solar thermal power facility heliostat facets, should include both conventional techniques and novel concepts. The final solution will most likely be a hybrid composed of contributions from conventional and current optical techniques.

REFERENCES

- Agarwala, B. K., M. M. Bindal, M. Chander and A. Kulshreshtha, 1975, "An Improved Moire Technique to Study the Surface Topography," Indian Journal of Pure and Applied Physics, Vol. 13, June 1975.
- Bahuguna, R. D., K. K. Gupta and K. Singh, 1979, "Study of Laser Speckles in the Presence of Spherical Aberration," J. Opt. Soc. Am., Vol. 69, No. 6, June, 1979.
- Brumleve, T. D., 1979, "Backward Gazing Heliostat Alignment and Evaluation System," Sandia Laboratory, Livermore, CA, Presented at the Heliostat Design Workshop and Second Generation Kickoff Meeting, July 25, 1979.
- Butler, B. L., and R. B. Pettit, 1977, "Optical Evaluation Techniques for Reflecting Solar Concentrators," Proceedings Society of Photo-Optical Instrumentation Engineers, San Diego, CA, August 22-26, 1977.
- Coleman, W. J., M. A. Lind, H. L. Hampton, and N. R. Gordon, 1977, "Research and Development in Solar Mirror Quality Assurance Performance," Pacific Northwest Laboratory, PNL 2427.
- Freese, J. M., 1978, "The Development of a Portable Specular Reflectometer for Field Measurements of Solar Mirror Materials," Sandia Laboratories, Thermophysical Properties Division 5842, SAND 78-1918, October, 1978.
- Hampton, H. L., J. S. Hartman and M. A. Lind, 1978, "Specularity Measurements by Fourier Transform Examination, IES/NBS Solar Seminar on Testing Solar Energy Materials and Systems, Gaithersburg, MD, May 22-24, 1978.
- Indebetouw, G., 1979, "A Simple Optical Noncontact Profilometer," Optical Engineering, 18, pp. 63-66.
- Kelly, W. L., IV, E. E. Burcher, and M. W. Skolant, Jr., 1977, "An Optical Profilometer for Spatial Characterization of Three Dimensional Surfaces," NASA Technical Paper 1012.
- King, D. L., 1979, "Heliostat Evaluation at the CRTF," Sandia Laboratory, Albuquerque, NM, Presented at the Heliostat Design Workshop and Second Generation Kickoff Meeting, July 25, 1979.
- Laity, W. W., 1978, "Assessment of Solar Options for Small Power System Applications," Pacific Northwest Laboratory.
- Lind, M. A., and J. M. Rusin, 1978, "Heliostat Glass Survey and Analysis," Pacific Northwest Laboratory, Richland, WA, PNL-2868, September 1978.

- Lind, M. A., J. S. Hartman and H. L. Hampton, 1978, "Specularity Measurements for Solar Materials," Proceedings SPIE, Optics Applied to Solar Energy IV, August 30-31, 1978, San Diego, CA.
- Lind, M. A., R. B. Pettit, and K. D. Masterson, 1980, "The Sensitivity of Solar Transmittance, Reflectance and Absorptance to Selected Averaging Procedures and Solar Irradiance Distributions," Transactions of the ASME, Journal of Solar Energy Engineering 102: 34-40.
- Menadier, C., C. D. Kissinger, and H. Adkins, 1967, "The Fotonic Sensor," Instruments and Control Systems 40:114-120.
- Moon, P., 1940, "Proposed Standard Solar Radiation Curves for Engineering Use," Journal Franklin Institute, 230:583.
- Pettit, R. B., 1977a, "Evaluation of Portable Optical Property Measurement Equipment for Solar Selective Surfaces," Presented at Winter Annual Meeting ASME, November 27-December 2, 1977, Paper No. 77-WA/SOL-1.
- Pettit, R. B., 1977b, "Characterization of the Reflected Beam Profile of Solar Mirror Materials," Solar Energy, Vol. 19, pp. 733-741, Pergamon Press.
- Pettit, R. B., and B. L. Butler, 1977, "Laser Ray Trace and Bi-Directional Reflectometry Measurements of Various Solar Concentrators," Sandia Laboratory, Albuquerque, NM, SAND-77-1466C.
- Pettit, R. B., 1978, "Summary of Solar Reflector Materials Properties, Sandia Laboratories, Summary Report of the Solar Reflective Materials Technology Workshop, Pacific Northwest Laboratory, PNL 2763, October 1978.
- Pettit, R. B., C. N. Vittitae, and F. Biggs, 1979, "Practical Method for Including Material Scattering Effects in Determining the Amount of Intercepted Sunlight in Solar Concentrators," Sandia Laboratory, Albuquerque, NM, Presented at the 1979 International Solar Energy Society Congress, May 28-June 1, 1979, Atlanta, GA.
- Poeth, D. F., R. E. Schwerzel, R. C. Russell, and B. P. Hildebrand, 1979, "Feasibility Assessment of Autoreplication as Applied to Selected Casting Processes," Battelle Columbus Division, Columbus, OH, August, 1979.
- Sanchez, J., and W. Saylor, 1979, "A Simple Technique for Measuring Slope or Surface Error of a Concentrator," General Electric Valley Forge Space Division, Valley Forge, PA. Presented at 25th ISES Conference, Atlanta, GA., May 26-June 1, 1979.
- Terada, H., and T. Ikeda, 1979, "Photogrammetric Application of Moiré Fringes Produced with a Parallel Beam of Light", Optical Engineering, Vol. 18, No. 4, July-August, 1979.

Theocaris, P. S., 1966, "Moiré Patterns of Slope Contours in Flexed Plates," Experimental Mechanics, 6(4): 212-217.

Waters, J. P., 1978, "Gaging by Remote Image Tracking," Advances in Optical Meteorology, SPIE, Vol. 153.

Zakhidov, Z. A., P. A. Panov, and V. N. Sokolov, 1977, "Using Lasers to Inspect Solar Energy Reflectors," Geliotekhnika, Vol. B, No. 1, pp. 38-41, UDC 621.472.001.

Document Control Page	1. SERI Report No. TR-98366-1	2. NTIS Accession No.	3. Recipient's Accession No.
4. Title and Subtitle Evaluation Techniques for Determining the Reflectivity, Specularity, and Figure of Solar Mirros		5. Publication Date April 1980	
7. Author(s) J. W. Griffin; M. A. Lind; L. D. Philipp		6.	
9. Performing Organization Name and Address Pacific Northwest Laboratory Richland, Washington		8. Performing Organization Rept. No.	
		10. Project/Task/Work Unit No.	
		11. Contract (C) or Grant (G) No. (C) XP-9-8366-1 (G)	
12. Sponsoring Organization Name and Address Solar Energy Research Institute 1617 Cole Boulevard Golden, Colorado 80401		13. Type of Report & Period Covered Technical Report	
		14.	
15. Supplementary Notes SERI Technical Monitor: P. A. Roberts			
16. Abstract (Limit: 200 words) This report is intended as a primer for those persons interested in the optical evaluation of heliostat mirrors. A cursory review of the current options for measuring the reflectance, specularity and figure of mirrors is presented. The extension of both traditional and novel optical laboratory techniques to field applications is also discussed. The authors conclude that while the presently available techniques are invaluable for laboratory testing of moderately sized optical components, they offer no immediate solution to the problem of quality assessment of large solar optics. This is due to the difficulty in altering the techniques to accommodate large optics either because of physical limitation or financial constraints. In general, the spatial resolution capabilities of the available techniques are either too stringent (i.e., interferometry) or too coarse for meaningful results. However, it is felt that eventually viable techniques will evolve based directly or indirectly on concepts presented in this document.			
17. Document Analysis a. Descriptors Mirrors; Solar Reflectors; Optical Properties; Reflection; Reflectivity; Light Transmission; Specularity; Figure; Measuring Methods; Measuring Instruments b. Identifiers/Open-Ended Terms c. UC Categories 62			
18. Availability Statement National Technical Information Service U. S. Department of Commerce 5285 Port Royal Road Springfield, Virginia 22161		19. No. of Pages 110	
		20. Price \$6.50	